NOTICE

The quality of this microform is heavily dependent upon the quality of the original thesis submitted for microfilming. Every effort has been made to ensure the highest quality of reproduction possible.

If pages are missing, contact the university which granted the degree.

Some pages may have indistinct print especially if the original pages were typed with a poor typewriter ribbon or if the university sent us an inferior photocopy.

Reproduction in full or in part of this microform is governed by the Canadian Copyright Act, R.S.C. 1970, c. C-30, and subsequent amendments.

AVIS

La qualité de cette microforme dépend grandement de la qualité de la thèse soumise au microfilmage. Nous avons tout fait pour assurer une qualité supérieure de reproduction.

S'il manque des pages, veuillez communiquer avec l'université qui a conféré le grade.

La qualité d'impression de certaines pages peut laisser à désirer, surtout si les pages originales ont été dactylographiées à l'aide d'un ruban usé ou si l'université nous a fait parvenir une photocopie de qualité inférieure.

La reproduction, même partielle, de cette microforme est soumise à la Loi canadienne sur le droit d'auteur, SRC 1970, c. C-30, et ses amendements subséquents.

TURBULENT FLUID FLOW AND HEAT TRANSFER INDUCED BY SQUARE-RIBBED SURFACE ROUGHNESS IN CONCENTRIC ANNULI

by

Soo W. Ahn

A thesis submitted to the School of Graduate Studies in partial fulfillment of the requirements of the degree of

MASTER OF APPLIED SCIENCE

in the

Department of Mechanical Enginneering
University of Ottawa

ISBN 0-315-60083-7

UNIVERSITÉ D'OTTAWA
UNIVERSITY OF OTTAWA

Abstract

In this study, the asymmetric turbulent fluid flow and heat transfer induced by square-rib roughness elements in concentric annuli are analytically studied in an attempt to investigate the resultant effect of artificial roughness on the heat transfer and friction forces.

In the analysis, a turbulence model based on a modified Prandtl's mixing length theory based on a previous study of the flow in parallel plates with a rough surface on one side is used to determine the velocity distribution and friction. The two velocity profiles in the problem are matched using a force balance. The temperature distribution is then predicted and heat transfer coefficients are calculated.

The results of the velocity profiles and friction factors are in good agreement with the experimental results. The effects of various parameters such as the roughness ratio, the pitch to roughness ratio, the radius ratio, etc. on friction factor and Nusselt number are investigated.

The present study demonstrates that certain artificial roughness elements may be used to enhance heat transfer rates with advantages from the overall efficiency point of view.

Acknowledgement

The candidate is grateful to have had the opportunity to carry out this project under the guidance of Dr. Yung Lee, to whom special thanks are due for supervision, for his invaluable suggestions and for the countless hours he so willingly contributed. The candidate is also grateful to him for financial support he received during the course of my work.

The candidate wishes to express his sincere thanks to his colleague, Dr. Y.P. Lee, for valuable contributions to the general mathematical problem.

Thanks are also due to Mr. G. Toth and his technical staff of the mechanical engineering workshop for construction of the test apparatus.

A special debt of gratitude is due to the author's wife for her understanding and perseverance under the difficult condition.

Contents

List of Tables

List of Figures

Nomenclature

A : cross sectional area of the channel; constant

c : specific heat

C : constant; see Eq. 3.11

De : equivalent diameter; $2(R_o - R_i)$

f : friction factor

f_r : friction factor for the rough core and smooth outer surface

f_s : friction factor for the smooth core and smooth outer surface

F : f_r/f_s

g : gravitational acceleratiion

h : convective heat transfer coefficient

k : mixing length constant

K : thermal conductivity; see Eq. 3.20

l : mixing length

Nu : Nusselt number

Nu_r : Nusselt number for the rough core and smooth outer surface

Nu_s : Nusselt number for the smooth core and smooth outer surface

H : Nu_r/Nu_s

p : pressure

P : pitch, between tips of roughness elements

Pr : Prandtl number

q : heat flux

Q : flow rate

r : radial distance

R : gas constant

R : radius

Re : Reynolds number

S : $R_o - R_i$

t : time

T : temperature

Z_{Ro} : imaginary location where u_i=0

Greek Symbols

α : radus ratio, R_i/R_o

δ_j : $\mid R_m - R_j \mid$

Δ : difference

μ : absolute viscosity

ϵ : roughness height

ν : kinematic viscosity

ρ : density

τ : shear stress

ε : eddy diffusivity

Dimensionless Parameters

A_o^+ : van Driest's constant; see Eq. 3.14

Δ_j : δ_j^+ / R_j^+

R_j^+ : $R_j(\tau_{Ro}/\rho)^{0.5}/\nu$

T_j^+ : $(T_{Ri} - T_j)c\tau_{Ro}/[q_{Ri}(\tau_{Ri}/\rho)^{0.5}]$

u_j^+ : $u_j/(\tau_{Ro}/\rho)^{0.5}$

y_j^+ : $y_j(\tau_{Ro}/\rho)^{0.5}/\nu$

ζ_j : y_j^+/δ_j^+

Superscripts

- : time averaged quantity

+ : non-dimensionalized quantity

Subcripts

b : bulk

H : heat

i : inner

j : i or o

m : corresponding to the location of maximum velocity

M : momentum

o : outer

p : constant pressure

r : rough

R : radius

s : at sublayer boundary; smooth

t : turbulent

Chapter 1

Introduction

The flow in annular ducts has received considerable attention and it appears often in many areas of the thermal process industries and in fluid flow equipment.

An annular geometry has long been recognized as an important flow channel employed for the design of heat exchangers and fuel burners.

In nuclear engineering, it has served as a basic geometry in evaluating the heat transfer performance of various type of reactor elements including, in addition to single ribbed pins in a smooth cylinder, also more complex geometries such as rod bundles in circular or non-circular channels.

Annulus flow is an axisymmetric geometry which, in the limiting cases, is reduced to the circular pipe and plane channel. For this reason, it has attracted the attention of researchers in the hope that its analysis would elucidate some of the evident difference between these two basic flow situations.

In heat exchangers with enhanced heat transfer surfaces, surfaces which are sufficiently rough will have increased heat transfer coefficients because the turbulence setup in the wake of each roughness element will penetrate into the laminar sublayer. Therefore, it is generally expected that the effect would be greater for fluid flow with a higher Prandtl number.

For the completely rough region in duct flow with relatively coarse and tightly spaced roughness elements, the friction factor is shown to be independent of the Reynolds number[1]. Since the roughness of the surface not only increases the heat transfer rate, but also produces additional pressure losses, the heat transfer per unit pumping power expended may not be improved.

Thus, certain roughness elements may be used advantageously from the heat

transfer point of view, but the analytical predictions and experimental studies in the literature are very limited [2]. The pattern and effects of surface roughness on turbulent flow can not be effectively described by any single parameter, such as the average roughness size, ϵ, so that the experimental surface geometry and roughness is apt to become unwieldy.

One approach is to investigate the effect of roughness on one shape of the system, and then to investigate, separately, the effect of shape, using smooth surfaces. In present study, an investigation of the effect of a particular type of artificial roughness element on heat transfer in asymmetric conditions is presented.

Bearing the above consideration in mind the main research objectives are set as follows:

- To predict the friction factor and velocity profiles across the channel flow and compare them with the experimental measurements.
- To predict the local heat transfer characteristics for turbulent fluid flow, fully developed velocity profiles, and constant flux at the rough core tube.
- To find the resultant effect of roughness from a comparison of rough and smooth surfaces with respect to the heat transfer increase relative to the increase of drag forces. This relation is expressed in terms of the non-dimensional parameter:

$$H/F = (Nu_r/Nu_s)/(f_r/f_s) \tag{1.1}$$

Chapter 2

Literature survey

Until recently, the studies of fluid flow and heat transfer in circular and non-circular ducts have been concerned primarily with three groups of problems.

The first group dealt with the development of the velocity profile in the entrance region of a duct with no heat transfer. The fluid is assumed to enter the duct at a uniform velocity. As the fluid moves down the duct, a boundary layer begins forming at the entrance and grows, having a velocity of zero on the wall. The fully developed velocity profile exists when the two edges of the boundary layers coincide.

The second group is concerned with the flow in which the velocity profile of the fluid is already fully developed but enters a section of duct having a wall temperature different from the temperature of the entering fluid. This is the problem of a purely thermal entrance region.

The third group is concerned with the so-called fully developed problems in which the heat transfer and friction parameters do not change along the length of the duct. The result can be applied to long ducts. Therefore, the third group is mainly to study the nature of turbulent flow and heat transfer under the fully developed condition.

Some attention has been given to the effect of the surface roughness on the transport of momentum and heat. In the literature, it seems that very few dealt with the resultant effect of roughness on the heat transfer and drag forces in a concentric annulus.

2.1 Fully developed turbulent fluid flow

As a fluid flows through a duct its velocity profile undergoes a change from its initial entrance form to that of a fully developed profile at an axial location far downstream from the entrance. However, the fully developed flow cases, both laminar and turbulent, have been the subject of many analytical and experimental studies mainly because of their greater simplicity and wider engineering applications.

Since turbulent flow in circular tubes is the type usually encountered in practice, it has been studied extensively. One of most rigorous studies of turbulent flow in a circular pipe was carried out by Diessler[3].

An investigation by Laufer[4] covers the structure of turbulent pipe flow quite thoroughly. Cremers and Eckert[5] measured turbulence correlations with hot-wire anemometer in a triangular duct, and recently Clark[6] also used the hot-wire anemometer to study turbulent boundary layers.

The problems of fully developed turbulent flow in a smooth concentric annulus have been studied experimentally and analytically by Barrow[7], Lee and Barrow [8], Brighton and Jones[9], Rothfus et al.[10], Levy[11], Quarmby[12,13], Michiyoshi and Nakajima[14], Wilson and Medwell[15], and Randhava[16]. In contrast, a small amount of work has been done on the description of fully developed turbulent flow in a rough surface.

In order to describe the patterns and effects of surface roughness on turbulent flow, Schlichting[1] introduced the concept of equivalent sand-grain roughness, k_s, as a means of characterizing different types of surface roughness by referring to the equivalent net effect produced by Nikuradse's experiments, which were carried out in pipes that were artificially roughened with uniform grains of sand.

Some other attempts have been made to set up models of turbulent exchange of flows over rough and smooth surfaces. Allan [17] proposed a description of the distribution of the mean-velocity in two-dimensional or axisymmetric turbulent flow which included the effects of pressure gradients and of the surface roughness. Allan's expression for the distribution of mean velocity is given by

$$u^+ = 2.5 \ln y^+ + 5.1 + k.f_c + C\beta \qquad (2.1)$$

where

k : pressure gradient
f_c: pressure gradient function
C: value of the surface roughness function for fully turbulent flow
β : roughness function

Allan and Sharma [18] used experimental data for a two-dimensional low speed turbulent boundary layer to verify the description of the mean velocity distributions proposed by Allan [17]. They concluded that the effects of pressure gradient and of surface roughness on the mean velocity distribution in the turbulent boundary layer can be treated independently.

Unfortunately, all these models require a prior knowledge of the function to describe a particular set of shapes and arrangements of surface roughness elements. For such cases, there seems to be no reliable prediction for momentum and heat transfer available in the literature.

Drag forces

Drag forces on surfaces having very small roughness such as painted metal plates as well as smooth plates covered with single protuberances, such as rivet heads, welded seams, joints, etc., were measured by Grunow[19].

The effect of artificial roughness on the frictional properties of annuli shape have been studied by Wilkie[20] for various inner surfaces roughened by transverse square and rectangular ribs. Rib heights varied from 0.1% to 1.6% of the equivalent diameter and pitch to height ratio from 2.5 to 50. He concluded that increasing rib width at constant P/ϵ and ϵ/D reduces the friction factor, f. Also slight chamfering of very sharp ribs reduces the friction factor, f, by between 6% and 8%; however, he reported that further chamfering or rounding had no effect.

Roughness function

A critical review was presented by Lewis[21] of the methods used to evaluate the thermohydraulic performance of roughness surfaces. In this study, the fundamental importance of the roughness function is verified and optimization is discussed. Also, Halls' transformation[2], which is used to relate measurements in annuli to circular tubes of rod-bundle flows, is re-examined.

Musker and Lewkowicz[22] proposed an integral method for predicting the development of two-dimensional turbulent boundary layers, which can include the effect of surface roughness. The method based on the energy integral equation is found to give agreement with experimental measurement for both smooth and rough surfaces in an arbitrary pressure distribution.

This method is used to investigate the effect of surface roughness on the separation of a two-dimensional turbulent flow over a flat plate with an external pressure distribution. For the case of annular ducts with rough surfaces, no measurement of eddy diffusivity distribution and turbulence could be found in the published works.

2.2 Asymmetric heat transfer in fully developed region

The nature of turbulent flow and heat transfer under fully developed conditions has been studied extensively by many investigators over the last three decades.

Turbulent heat transfer in smooth circular tubes with variable fluid properties was studied by Deissler[23]. Corcoran et al.[24] measured experimental values of temperature and velocity gradients for the flow between parallel plates.

Labib[25] analytically investigated the resultant effect of artificial roughness on the heat transfer and friction force of the turbulent fluid flow induced by square - rib roughness elements in parallel plates, in which the integral method together with a turbulence model based on the modified Prandtl's mixing length theory for the rough surface was used to determine the velocity distribution and friction.

The results of the velocity profiles and friction factors are in good agreement with Bhuiyan's[26] experimental results. His analytical results represent that the heat transfer increases more than the friction forces for a certain range of Reynolds

numbers and Prandtl numbers for the given roughness structure.

Haberstroh and Baldwin [27], Lawn[28] and Gowen and Smith[29] reported the studies of fully developed turbulent heat transfer in the pipe flow.

Extensive experimental results for air flowing in a smooth annulus with a constant heat flux from the inner core tube under fully developed conditions have been reported by many workers, such as in References[7,8, and 30].

Pickering[31] studied heat transfer experimentally with water flowing in an annulus. He also reviewed and compared the results of the theoretical and experimental works on heat transfer to turbulently flowing fluids in annuli. He concluded that the theoretical prediction of Maloney† exhibited a particularly good correlation with his experimental results. Some more studies on the heat transfer under the fully established turbulent flow condition with uniform internal heat flux in a concentric annulus can be found in such studies as in References [32,33,34,35, and 36].

Turbulent flow and heat transfer in concentric annuli with moving cores was invstigated by Shigechi, Kawae, and Lee[37]. Reynolds et al.[38] tried to generalize the problems of heat transfer in concentric annuli and indicated the possibilities for superposition of their four fundamental solutions. These fundamental solutions were specified by the heat flux or wall temperature boundary conditions of the smooth annuli. Only limited cases such as fully developed heat transfer and the thermal entrance region on problems with arbitrarily prescribed heat flux have been solved.

† : From Reference 31.

Chapter 3

Analytical Studies

3.1 Physical Model

Because of the type of roughness on the rough wall and geometrical characteristic of the annulus, local flow mechanisms in the vicinity of that wall may not fully satisfy any universal velocity profiles. The large scale of roughness may cause a flow recirculation in the wake zone of the roughness elements; thus, the governing equations are broken into smooth and rough sides. For the analysis, we introduce the following assumptions:

1. The annulus is concentric. While the outer wall surface is smooth, the inner core surface is square-ribbed (Fig. 3.1).
2. Velocity and temperature fields in the annulus are fully developed.
3. The location of the maximum velocity coincides with the location of the zero shear stress.
4. For the smooth wall region, the eddy diffusivity for momentum, ϵ_M, by van Driest for the sublayer and that of Reichardt for the fully turbulent region are used.
5. For the rough core wall region, there is a constant heat flux , and a modified logarithmic velocity profile [25] is used. The surface roughness affects the velocity profiles only locally.
6. The turbulent Prandtl number is taken as unity.

7. For Z_{ro} in the modified Prandtl mixing length theory, those obtained in parallel plates are used.

3.2 Velocity and Temperature Distributions

The basic equations governing the transport of momentum and heat can be written as [39]:

$$\frac{\tau_j}{\rho} = (\nu + \varepsilon_M)_j \frac{\partial u_j}{\partial y_j} \tag{3.1}$$

$$-\frac{q}{c\rho} = (a + \varepsilon_H) \frac{\partial T}{\partial r} \tag{3.2}$$

From the equations (3.1) and (3.2), the temperature gradient can be obtained as equation(3.3) in nondimensional parameters [the details of the derivation of the equations (3.3) to (3.5) are given in Appendices A.1 to A.3]:

$$\frac{\partial T_j^+}{\partial \zeta} = \pm \frac{\partial u_j^+}{\partial \zeta} \left(\frac{1 + \varepsilon_M/\nu}{1/Pr + 1/Pr_t \varepsilon_M/\nu} \right)_j \frac{q_j/q_{Ri}}{\tau_j/\tau_{Ro}} \tag{3.3}$$

where +ve is for $j = i$ and -ve for $j = o$. The ratio of eddy diffusivity of heat and momentum, Pr_t, which is often called the turbulent Prandtl number, plays an important role in most analytical studies to predict heat transfer coefficients in turbulent convective heat transfer.

Many investigators assumed this ratio of $\varepsilon_M/\varepsilon_H$ =1 as Prandtl did [40]. But, recent experimental work has shown that those are not equal.

Neverthless, the turbulent Prandtl number, Pr_t, is assumed to be 1 in the present work, for the following reasons: firstly, the lack of an accurate correlation, and secondly for the reason of simplicity.

From a force balance made on the element (Fig. 3.2), we obtain the shear stress distributions as:

$$\frac{\tau_i}{\tau_{Ro}} = \frac{(1-\zeta_i)[2+\Delta_i(1+\zeta_i)](1+\Delta_i Z^+_{ro}/\delta^+_i)}{(1+\Delta_i\zeta_i)[2+\Delta_i(1+Z^+_{ro}/\delta^+_i)](1-Z^+_{ro})} \tag{3.4}$$

$$(0 \le \zeta_i \le 1)$$

$$\frac{\tau_o}{\tau_{Ro}} = \frac{(1-\zeta_o)[1-\Delta_o\zeta_o/(2-\Delta_o)]}{(1-\Delta_o\zeta_o)} \tag{3.5}$$

$$(0 \le \zeta_o \le 1)$$

Since the heating condition is a constant heat flux at the core tube only, the heat flux distributions are obtained from an energy balance made on the element [the details of the derivation of equations (3.6) and (3.7) are given in Appendix A.4] (Fig. 3.3):

$$\frac{q_i}{q_{Ri}} = \frac{[1-a^2(1+\Delta_i\zeta_i)^2](1+\Delta_i Z^+_{Ro}/\delta^+_i)}{[1-a^2(1+\Delta_i Z^+_{ro}/\delta^+_i)^2](1+\Delta_i\zeta_i)} \tag{3.6}$$

$$(0 \le \zeta_i \le 1)$$

$$\frac{q_o}{q_{Ri}} = \frac{a(2-\Delta_o\zeta_o)\Delta_o\zeta_o(1+\Delta_o Z^+_{ro}/\delta^+_i)}{[1-a^2(1+\Delta_i Z^+_{ro}/\delta^+_i)^2](1-\Delta_o\zeta_o)} \tag{3.7}$$

$$(0 \le \zeta_o \le 1)$$

We can obtain the velocity gradient from equation (3.1) [see Appendix A.5 for the derivation of equation(3.8)]:

$$\frac{\partial u^+_o}{\partial \zeta_o} = \delta^+_o\left[\frac{\tau_o/\tau_{Ro}}{1+(\varepsilon_M/\nu)_o}\right] \tag{3.8}$$

$$(0 \le \zeta_o \le 1)$$

Surface roughness can take on many shapes, the name of Nikuradse [41] is indeliably associated with that rational analysis of rough surfaces as a result of his

experiments with turbulent flow in the pipes that were artificially roughened with uniform grain of sand.

Schlichting [42] introduced the concept of equivalent sand-grain roughness as a means of characterizing other types of roughness element by referring to the equivalent net effect produced by Nikuradse's experiments [41]. We develop almost same method as Schlichting's [42].

If the Prandtl mixing-length scheme is used, mixing length, l, and eddy diffusivity for momentum, ε_M, can't go to zero at the wall because of the effect of roughness ; the eddy diffusivity and mixing length must obviously be finite at $y = 0$ for a fully rough surface. This can be readily modeled by a near-wall mixing-length equation:

$$l = k(y + Z_{ro}) \tag{3.9}$$

where Z_{ro} might be expected to be a function of roughness, and k is constant and equal to 0.4. To develop a velocity profile for the fully rough region, we simply replace $l = ky$ with the equation (3.9), this then leads to [39]:

$$\frac{du^+}{dy^+} = \frac{1}{k[y^+ + Z_{ro}^+]}$$

Since there is no sublayer in the fully rough region, the lower limit of integration of this differential equation is at $y^+ = 0$:

$$\int_0^{y^+} du^+ = \frac{1}{k}\int_0^{y^+} \frac{dy^+}{y^+ + Z_{ro}^+}$$

This equation can be obtained as:

$$u^+ = \frac{1}{k}\ln[\frac{y^+}{Z_{ro}^+} + 1]$$

Where Z_{ro}^+ is much smaller than y^+; we can express this as:

$$u^+ = \frac{1}{k}\ln\frac{y^+}{Z_{ro}^+} \tag{3.10}$$

in which Z_{ro} might be obtained from an experimental velocity profile in the annulus; however, we assume that the effect of Z_{ro} is confined to the region very close to the wall and not subjected to the effect of boundary curvature.

Thus, we can use the modified turbulence model for the flat plate. Z_{ro} for the flat plate is obtained as follows [26,43]:

$$Z_{ro} = y_{mr} exp\{-\frac{\tau_{Ro}}{\tau_{Ri}}[\ln(S - y_{mr})u_{\tau_{Ro}}/\nu + Ck_o]\} \tag{3.11}$$

$$y_{mr} = S \times 0.299 Re^{0.066}(S/\epsilon)^{0.14}(P/S)^{0.21}$$

From equation (3.10), the velocity gradient for the inner rough side can be obtained [see Appendix A.5 for derivation of (3.12)]:

$$\frac{\partial u_i^+}{\partial \zeta_i} = \frac{u_{\tau_{Ri}}}{u_{\tau_{Ro}}} \frac{1}{k_i \zeta_i} \tag{3.12}$$
$$(\frac{Z_{ro}^+}{\delta_i^+} \leq \zeta_i \leq 1)$$

3.3 Eddy Diffusivity for Momentum

Accuracy of description of the eddy diffusivity for momentum along and across the duct is required for a solution of velocity and temperature profiles.

The most interesting feature of the study on turbulent fluid flow in a concentric annular duct is the complete failure in application of the conventional universal velocity profile or the law of the wall [44].

Since the assumption of an eddy diffusivity of zero at the pipe center line is not realistic, we postulate that Reichardt's expression [45] for the eddy diffusivity of momentum can be applicable to the entire turbulent flow regions on the outer smooth wall region of the concentric annulus with proper modification for the region

remote from the outer wall. Thus, using the dimensionless parameters, we can obtain as follows[44]:

$$(\varepsilon_M/\nu)_o = [(k_o\delta_o^+/6][1-(1-y_o^+/\delta_o^+)^2][1+2(1-y_o^+/\delta_o^+)^2] \tag{3.13}$$

$$(y_{os}^+ \leq y_o^+ \leq \delta_o^+)$$

For the region very close to the outer wall, simulating the sublayer by introducing a damping function into the mixing-length equation, $l = ky$, we retain van Driest's dimensionless expression [46] for the eddy diffusivity given by:

$$(\varepsilon_M/\nu)_o = k_o^2 y_o^{+^2}[1-exp(-y_o^+/A_o^+)]^2 \mid \frac{\partial u_o^+}{\partial y_o^+} \mid \tag{3.14}$$

$$(0 \leq y_o^+ \leq y_{os}^+)$$

For the inner rough region, we use the Prandtl mixing length theory to evaluate the eddy diffusivity for momentum, ε_M.

Eddy diffusivity for momentum from Prandtl's mixing length theory is obtained as:

$$(\varepsilon_M/\nu)_i = k_i^2 y_i^{+^2} \mid \partial u_i^+/\partial y_i^+ \mid \tag{3.15}$$

$$(Z_{ro}^+ \leq y_i^+ \leq \delta_i^+)$$

3.4 Reynolds Number, Friction Factor, and Nusselt Number

Now that the eddy diffusivities, $(\varepsilon_M/\nu)_j$, are known for the entire fluid region, the velocity and temperature profiles can be derived. The Reynolds number, friction factor, heat transfer coefficient and Nusselt number can be obtained in the usual way as:

Reynolds Number

Reynolds number is defined as:

$$Re = \frac{2u_b(R_o - R_i)}{\nu} = 2u_b^+(R_o^+ - R_i^+) \tag{3.16}$$

The average velocity, u_b, can be expressed from the definition in dimensionless parameters as [see Appendix A.6 for the derivation of equation(3.17)]:

$$u_b = \frac{\nu}{R_o}\left(\frac{2\alpha}{1-\alpha^2}\right)\left[\delta_i^+ \int_{\frac{z_{R_o}^+}{\delta_i^+}}^{1} (1+\Delta_i\zeta_i^+)u_i^+ d\zeta_i + \frac{1}{\alpha}\delta_o^+ \int_0^1 (1-\Delta_o\zeta_o)u_o^+ d\zeta_o\right] \tag{3.17}$$

Substituting equation(3.17) into equation(3.16), we obtain:

$$Re = \frac{4\alpha}{(1+\alpha)}\left[\delta_i^+ \int_{\frac{z_{R_o}^+}{\delta_i^+}}^{1} (1+\Delta_i\zeta_i)u_i^+ d\zeta_i + \frac{1}{\alpha}\delta_o^+ \int_0^1 (1-\Delta_o\zeta_o)u_o^+ d\zeta_o\right] \tag{3.18}$$

Friction Factor

The friction losses occurring in turbulent flow are proportional to the kinetic energy of the fluid unit volume and the area of the solid surface in contact with the fluid. The friction factor is generally defined as:

$$f = \frac{\overline{\tau}}{0.5\rho u_b^2}$$

The friction factor for the whole annulus is defined in the following dimensionless form [see Appendix A.7 for derivation of equation (3.19)]:

$$f = \frac{8(1-\alpha)^2[1+\alpha(\tau_{jRi}/\tau_{jRo})]}{(1+\alpha)}(R_o^+/Rc)^2 \tag{3.19}$$

Nusselt Number

From the definition, Nusselt number is:

$$Nu = 2(R_o - R_i)h/K = \frac{2(R_o^+ - R_i^+)Pr}{T_b{}^+} \tag{3.20}$$

where the heat transfer coefficient, h, is defined as:

$$h = q_{Ri}/(T_{Ri} - T_b) \tag{3.21}$$

The bulk temperature, T_b^+, can be expressed from the definition in dimensionless parameters as:

$$T_b^+ = \frac{4}{(1+\alpha)}(\frac{1}{Re})[\alpha\delta_i^+ \int_{\frac{z^+_{Ra}}{\delta_o^+}}^{1}(1+\Delta_i\zeta_i)u_i^+T_i^+d\zeta_i + \delta_o^+\int_0^1(1-\Delta_o\zeta_o)u_o^+T_o^+d\zeta_o] \tag{3.22}$$

The details of derivation of equation (3.22) are given in Appendix (A.8).

3.5 The Ratio of H/F

The roughness made artificially on the wall surface enhances turbulence in the flow; thus, the effect of turbulence causes an increase in heat transfer as well as friction factor.

However, the more the increase in the friction loss in terms of roughness becomes, the more pumping power must be supplied; therefore, it is desirable that the ratio of the increase in heat transfer and the increase in friction loss be discussed in consideration of the heat exchanger design.

Ratio of friction factor, F

The normalized friction factor, F, is defined as ratio of f_r/f_s, in which f_r is the friction factor in the annulus having the roughness element on the core tube, and f_s is the friction factor due to the smooth annulus; therefore, the normalized friction factor, F, means the increase in the friction loss for the roughness.

Ratio of Nusselt number, H

The normalized Nusselt number, H, is defined as the ratio of Nu_r/Nu_s, in which Nu_r is the Nusselt number in the annulus having the roughness element on the core tube, and Nu_s is the Nusselt number in the smooth annulus; therefore, the normalized Nusselt number, H, means the increase in the heat transfer due to the roughness.

The resultant effect of artificial roughness is determined from a comparison of rough and smooth surface with regard to the heat transfer increase relative to the increase in pressure loss. This is expressed in terms of a non-dimensional parameter, H/F, which is defined as:

$$H/F = (Nu_r/Nu_s)/(f_r/f_s) \tag{3.23}$$

$H/F > 1$ suggests that the increase in the heat transfer due to roughness is greater than the increase in pressure loss due to roughness and therefore it is advantageous to have the particular roughness elements from the overall efficiency point of view.

3.6 Matching Conditions

The turbulent fluid flow and heat transfer in the concentric annulus with a roughness on the core tube have two different velocity and temperature distributions cross the flow channel; however, the velocity and temperature profiles should be matched at the point of maximum velocity.

Shear Stresses

From the force balance made on an element (Fig. 3.2), we can obtain:

$$\frac{\tau_{Ri}}{\tau_{Ro}} = \frac{R_o}{(R_i + Z_{ro})}\left[\frac{R_m^2 - (R_i + Z_{ro})^2}{R_o^2 - R_m^2}\right] \tag{3.24}$$

Relationship between k_i and k_o

It is well established that the standard universal velocity is not fully adequate for the inner velocity distribution of a concentric annulus [47], [48]; therefore, while a fixed value of 0.4 for k_o is taken in the analysis, the value of k_i should be calculated from the appropriate boundary conditions in the analysis of a concentric annulus with a smooth wall [49].

However, in the present study with the high roughness density, it may be assumed that the turbulent induced by the surface roughness on the core surface is such that the effect of the curvature on the value of k_i is negligible small; therefore, it is assumed that:

$$k_i = k_o \tag{3.25}$$

Velocity

The dimensionless velocities, u_o^+ and u_i^+ are nondimensionalized with $u_{\tau_{Ro}}$, and as the velocities at the points of the maximum velocities are continuous, we can obtain:

$$u_{om}^+ = u_{im}^+$$

Relationship between T_{im} and T_{om}

From the equality of temperature at the positions of maximum velocities ($r = R_m$ or $\zeta_o = \zeta_i = 1$), we obtain:

$$T_{om}^{+} = T_{im}^{+}$$

and

$$\frac{\partial T_{im}^{+}}{\partial \zeta_i} = -\frac{\partial T_{om}^{+}}{\partial \zeta_o}\frac{\delta_i^{+}}{\delta_o^{+}}$$

Once the matching conditions are established, the dimensionless temperature distributions in the inner and outer regions can now be obtained by substituting equations (3.4), (3.5), (3.6), (3.7), (3.8), and (3.12) into equation (3.3).

3.7 Method of Calculations

To solve the equations given above, the following input and fixed parameters are provided for the calculation, and the calculation is done as the following procedure:

Input parameters

α =0.2, 0.4, 0.5, and 0.8.

R_o^{+} = in terms of Re: 10^4 to 10^5.

Pr = 0.1, 0.72, 1.0, 10., and 30.

P/ϵ =2, 4, and 8.

S/ϵ = 9.7, 19.4, and 25.

Fixed parameters

$Pr_t = 1$

A_o^+ =26 (van Driest damping parameter)

y_{os}^+ =26 (sublayer thickness)

Procedure of calculation

To obtain results for a given Reynolds number, first of all, a Reynolds number should be given; however, the Reynolds number is actually obtained from the velocity profile, and the velocity profile is obtained from the given Reynolds number.

Therefore, a two-dimensional iteration method [50] is used: one is for the velocity profile, and the other is for the Reynolds number.

For the initial guess, a dimensionless sublayer thickness (ζ_{sub}) is used:

$$\zeta_{sub} = \frac{y_{sub}^+}{\delta_o^+} = \frac{26}{R_o^+(1 - R_m^+/R_o^+)}$$

in which ζ_{sub} is the number between 0 and 1, R_o^+ and $\frac{R_m^+}{R_o^+}$ are the variables of the Reynolds number.

With the guessed $\frac{R_m^+}{R_o^+}$, the velocity profiles in the smooth and rough parts are obtained, where we use the 5 point Gaussian quadrature integration method.

At the maximum velocity position, we check the equality of velocity. With the condition that velocities of both parts are equal, the Reynolds number is calculated with the velocity profile obtained, from Simpson's integration method with the number of nodes equal to 5000.

If the velocities are not equal, we guess the value of R_m^+/R_o^+. If the calculated Reynolds number ($Re1, Re2$) is equal to the given Reynolds number (Re^*)(Fig. 3.4), the velocity profile will be calculated. If it will not equal, we reguess the variable, ζ_{sub}.

Finally, the friction factor, temperature profile, bulk temperature, and Nusselt number are calculated.

The computation was carried out numerically on the University of Ottawa computer, IBM, AMDAHL 5880. A simplified flow chart of the program is given in Appendix B

Chapter 4

Experimental studies

In the previous chapter, the theoretical analysis was presented and the predicted velocity profiles, local friction factors, temperature profiles, and Nusselt numbers for the developed regions of concentric annulus with a roughness on the core tube were evaluated

The experimental programme undertaken in the present study is designed to meet some of research objectives described before, i.e., velocity profile and friction factor. The working fluid is chosen as air in atmospheric conditions due to purposes of economical construction of test facilities and also availability of information on physical properties.

The main experimental programme consists of providing detailed measurements of static pressure drop along the developed channel length, velocity profiles, and velocity gradient profiles. The static pressure measurements are made with a MKS pressure transducer and the calibration of which is checked against a micromanometer at frequent intervals.

Velocities are measured with a single pitot tube and velocity gradients are measured with a double pitot tube. The traverses are made manually.

4.1 Apparatus

The main experimental and the auxiliary apparatus are shown schematically in Fig. 4.1 and a photograph of the channel assembly is given in Figure 4.2. The

essential dimensions of the test section are included in Table 4.1. The major part of the apparatus was used by Park [44] previously for his study.

Surface roughening of the core tube is done by machining rectangular grooves on the core tube surface in the transverse direction on a milling machine. The height of the grooves, shown in Fig. 4.3, is 1.5 mm. The pitch to height ratios (P/ϵ) for the present study are 2, 4, and 8 (Fig. 4.3). Air is drawn through a flow measuring orifice [51] into a settling chamber by a centrifugal fan driven by a 1.5 HP, 1710 RPM A/C motor.

The settling chamber consists of filters, screens, and flow straighteners (Fig. 4.1). The control of flow rate of air is done with the movable gate located on the side of the diffuser box. The bell-mouthed section is machined from a 305×305×203 mm plexiglas block and the blower fan is rated 8.5 cu. m/min at 510 mm of water. The total dimension of the main apparatus is about 7980 mm in length (Fig. 4.1). The annular test section consists of a 97.4 mm I.D. outer tube with a 39.2 mm O.D. core tube having the roughness height, ϵ, of 1.5 mm (Fig. 4.4).

Provisions are made for the measurement of the position of the core tube relative to the outer tube and pressure drops, and for the detailed exploration of the velocity field at the measuring station (78.9 equivalent diameters). The core tube is supported at three locations by 3-point carriers which provide radial adjustment of the core tube.

The position of the core tube relative to the outer tube is determined by a depth micrometer gauge through several openings along the length and around the circumference of the test sections. In this way, the maximum eccentricity of the annulus is less than 3 %. To minimize axial misalignment, all the flanges are clamped together and then drilled and reamed simultaneously during the manufacturing stage.

The assembled test section is mounted horizontally on several supports. Provision is made on the feet of these supports to provide a fine adjustment of height by screws. Thus, the horizontal alignment of the whole assembly could be easily accomplished by adjusting these screws. The horizontal alignment is checked by a surveying level.

The maximum misalignment is 3.2 mm per 5.5 m. To minimize the pressure loss and the vibration effect from the blower, a conical diffuser and a flexible tube is used to connect the assembly annulus to the blower.

4.2 Instrumentation

Pitot tube and pressure measurement system

The mean velocity profiles across the test section are measured by means of the pitot tube made of a hypodermic stainless steel tube, 1.1 mm O.D. and 0.5 mm I.D.. For flow field investigation, it is desirable to make the total probe tube diameter small with regard to the annulus passage dimensions in order to minimize flow interference.

However, at low velocities viscosity causes an error in the total pressure reading [52, 53] which is difficult to correct for. Taking these facts into consideration the above dimensions are chosen.

The static pressure holes were connected to the pressure measuring network of tubes through 3.2 mm I.D. pressure connectors. These were made by drilling through the wall from the outside and by carefully removing the burrs on the inside. A short length (9.5 mm) of about 6.4 mm O.D. brass tubing is then carefully soldered over the each hole.

Jayflex-180 plastic tubing of 9.5 mm O.D. and 6.4 mm I.D. is used for this purpose. The MKS differential pressure transducer (Baratron type 77)[54] and differential micro-manometer depending on the heads of the pressures are used for pressure measurement. The specific gravity of the manometer fluid in the present study is 0.8185. All pressure measurements were made relative to the atmosphere, i.e. one of the transducer inputs is open to the ambient.

Double pitot tube

The position of maximum velocity is found by means of a double pitot tube consisting of two tip pitot tubes 1.5 mm apart[55, 56]. No appreciable difference is found between the two pitot tubes when placed in a uniform stream during the calibration stage.

Data recording system

All the measurements are automatically recorded. For this purpose, a Hewlett-Packard HP-5050B digital recorder is used in conjunction with a HP 2901A Input

scanner and a HP 2401C Integrating digital voltmeter (Fig. 4.5).

Flowrate meter

The flow rate meter to measure the flow rate in the channel and in turn to calculate the average velocity is an orifice plate placed before the settling chamber(Fig. 4.2). The orifice plate is designed according to ISO recommendation R541 with vena contracta taps[57, 58].

4.3 Calibration of instruments

Orifice plate

The calibration of the orifice plate is done by a numerical integration of the velocity profiles, using a single pitot tube, measured at test sections to give the flow rate for a given pressure drop across the orifice plate[59]. A traversing mechanism located at 78.9 equivalent diameters from the bell-mouthed entrance to the tube facilitated the measurement of velocity profiles throughout the cross section of the annular tube.

Pressure drop data are obtained over the entire accessible Reynolds number range, whose upper limit is restricted by the blower capacity. The results of calibration [flow rate (Q) versus pressure difference at orifice ($\Delta P_{orifice}$)] are shown in Figs. 4.6, 4.7, and 4.8.

4.4 Experimental procedure

Before any experimental measurement is carried out, the electronic instruments are turned on for at least two hours to attain steady state conditions and to avoid drift due to warm up. Then the necessary adjustments on the anemometer system and the pressure measuring meter are made.

The apparatus is run for at least 30 minutes which is found to attain steady state conditions in the flow, and the flow chart of measurement is shown in Fig.

4.9.

The main experimental variables for the present study are the pitch of the roughness, P, and the height of roughness,ϵ. For each roughness pitch the following measurements are taken:

1. Static pressure drop versus channel length, x.
2. Static pressure drop at fully developed conditions versus Reynolds number
3. Velocity profiles versus y using pitot tube at 78.9 equivalent diameters from the inlet of test tube
4. Double pitot tube reading ΔP_{dp} versus y at fully developed conditions.

The range of Reynolds number covered is from 15,000 to 62,000 approximately. The pressure and temperature of the ambient are also recorded before each run. The room temperature is able to be kept nearly constant with $\pm 0.5°C$ during each test. All the measurements are carried out only at late in the night to avoid disturbances on the main power supply.

Static pressure and velocity profiles measurements

Due to rapid random fluctuations in the pressure readouts from both the electronic meter and the inclined micromanometer, an estimate of the average readout has to be made. The error introduced in this manner is estimated to be less than $\pm 0.5\%$ considering the maximum and minimum values of the instantaneous readouts.

The velocity profiles are recorded either manually or through the data acquisition system. The velocity profiles in accordance with Re and P/ϵ are shown Figs. 4.10 - 4.12, in which the asymmetry of the flow are already seen. The velocity profiles obtained from the annulus throughout the experiment are numerically integrated, and used for calculating Reynolds numbers and also for the calibration of the orifice as discussed in Section 4.3.

To investigate the effect of the roughness geometry on a core tube, the velocity patterns at different position are measured (Figs. 4.13 and 4.14). The developed region can be known from the measurement of static pressure drop versus channel length, x, (Fig. 4.15), and at the developed region from $x/De = 42.27$, dp/dx values are calculated as a function of x by fitting a straight line into the data points taken

five at a time and taking the slope of this line as the dp/dx in the middle of the range of the five points (Figs. 4.16, 4.17, and 4.18).

The average friction factors are obtained by using the following relation derived from the momentum balance for a fully developed flow as shown in Appendix A.7 (Fig. 4.19).

$$f = \frac{R_o f_o + R_i f_i}{R_o + R_i} \tag{4.1}$$

where

$$f_i = \frac{2\tau_i}{\rho u_b^2}, \; and \; f_o = \frac{2\tau_o}{\rho u_b^2} \tag{4.2}$$

Determination of the probe position relative to the walls

The starting position of the probe relative to the channel walls is determined by advancing the probe toward the core tube wall until the probe just touches the wall and this point is taken as the reference point for the y-coordinate.

The touching of the probe is checked through the outer tube by electrical contact. The relative radial displacement of a probe is measured with 0.025 mm. The repeatability of the position of the probe is given as ± 0.2 mm for the manual drive.

Maximum mean velocity points

The maximum mean velocity points are found by making double pitot tube traverses in the y direction and recording the pressure differences between the pitot tubes. The reading is a measure of the velocity gradient and the place where the curve cuts the ΔP_{dpitot}=0 line corresponding to the maximum velocity point (Fig. 4.20).

This procedure is repeated 9 times every Reynolds number, and each maximum mean velocity point is taken an average at which all the standard deviations are less than 0.2 % (Fig. 4.21-32).

Physical properties

The values of dynamic viscosity(μ) are taken from Reference[60] corresponding to the ambient temperature. The ideal gas equation of state $p = \rho RT$ is used to calculate the density of air(ρ), corresponding to the ambient conditions.

The accuracy of p and T measurements is estimated to be ± 0.1 mmHg and $\pm 0.5°C$ respectively. In view of the higher accuracy in measurements of geometrical

parameters, it can be concluded that the uncertainty involved in the u_b and Re largely depends on the flow rate measurement.

A list of mean flow parameters considered, together with a summary of the expressions relating them, is given in Appendix C. These expressions constitute a system of 16 equations. To solve these equations, 15 parameters can be considered in three groups:

1. Geometrical parameters: A, $D\epsilon$, S, ϵ, P, R_i, R_o, α
2. Physical properties of working fluid: ρ, μ,
3. Experimental flow variables: dp/dx, r, R_m, Q, y

A closer examination of the 9 inputs mentioned above and a consideration of dimensional analysis technique will reveal that the effects of all of these parameters can be incorporated in the effects of the following five main dimensionless groups:

$$P/\epsilon,\ \alpha,\ \frac{S}{\epsilon},\ Re,\ f$$

The first three are geometric parameters. Re and f are used to relate the geometric properties, fluid properties, and flow variables. The major engineering interest from the type of experiments undertaken in the present study is to find the correlations among P/ϵ, Re, f.

The rest of the parameters considered are mainly for further understanding of the physical flow.

Chapter 5

Experimental Results and Discussions

Results from both the analytical and experimental studies described in the previous chapters enable us to evaluate the various characteristics of the turbulent flow and heat transfer in the developed region of a concentric annulus with a rough core tube.

In the present experimental study, the mean velocity profiles and the locations of maximum mean velocities are the most important parameters. Thus, it is essential to investigate in detail the local flow mechanism with particular emphasis on the velocity distributions and the locations of maximum mean velocities, because this will be a check on the nature of the underlying assumptions used in the analysis.

Maximum mean velocity point

As shown in Figs. 4.21 to 4.32, the variation of maximum velocity positions indicates strong dependence on Re and P/ϵ.

With the increases of Re and P/ϵ, the maximum mean velocity positions get proportionately closer to the smooth wall. The variation with Re indicates stronger diffusion of turbulent eddies from the rough towards the smooth side as the velocity indicates and the momentum exchange near the rough wall becomes more vigorous. These points deviate more from the center-line of the channel towards the smooth wall with increase of P/ϵ (up to P/ϵ=8) i.e., for a lower roughness density at the same S/ϵ ratio (Figs. 4.10 - 4.12).

This may seem unexpected since a higher roughness density would imply a more vigorous momentum exchange than a lower roughness density. A closer examination of vortex patterns between roughness elements of different pitches[61, 62, 63, and 64] reveals the possibility that at a higher roughness the flow will tend to skip over the tips of the elements; however, at a lower density, the flow will find some time to re-attach, and when it faces a new element it will be thrown into the stream creating vigorous eddies. Therefore, the points under consideration are even further displaced from the rough wall.

In the present analysis, the radius of maximum velocity for the fully developed turbulent flow is predicted from Eq. (3.24). It is often assumed, without any justification, that the position of zero shear coincides with the radius of maximum velocity. This can not be accepted immediately for general case although, of course, it must be true for some duct geometries for reasons of symmetry. It has been shown[8, 65] that the assumption, viz.: the position of zero shear coincides with the radius of maximum velocity is not necessary true for turbulent flow in the annulus.

The experimental results of Kjellstrom and Hedberg[65] show that, for partially roughened annuli, there is a small but significant difference between the radius of the maximum velocity and the point of zero shear. However, in the present study, it is assumed that the radius of maximum velocity coincides with the position of zero shear.

Mean velocity distributions

The predicted velocity profiles [Table 5.1(a), (b), and (c)] are compared with the experimental measurements in Figs. 4.10 -4.12 [Table 5.2(a), (b), and (c)]. In general the theoretical velocity profiles obtained through [46, 44, and 39] agree reasonably well with the experimental data, except near the walls. For calculation, a value of k, von Karman's constant, should be assigned, and here k =0.4 is chosen. The results are shown in Table 5.2(a), (b), and (c). Between the sublayers near the walls and the maximum velocity points, the velocity profiles are in good agreement with the theoretical results of [44].

Thus, as far as the mean flow properties are concerned, the fluid particles within these regions are unaware of the nature of the opposite surface. The velocity profiles

illustrate that the velocity profiles in the outer region vary little with radius ratio and are similar to the circular tube. Meanwhile, the velocity field in the inner region deviated with changes in roughness density (P/ϵ) and radius ratio (α). The deviation of the inner portion from the outer is greater with high roughness density and larger radius ratio.

This deviation of the velocity profiles for the inner regions from those for the outer regions could be explained as a result of the increase in the radius ratio and the roughness density. The effects of the roughness geometry on the velocity patterns are shown in Figs. 4.13 and 4.14, in which the flow patterns in the vicinity of a core tube is a function of relative rib spacing (P/ϵ).

At a higher value of P/ϵ (lower roughness density), the flow tends to reattach, and in the face of a new element it will be ejected into the stream, producing more turbulence[63, 64].

Friction factor

The predicted friction factors calculated from Eq. (3.19) are compared with the experimental friction factors in Fig. 4.19. The agreement between the analyses and the experiments is rather good. In the same figure, a comparison is made with the friction factor taken from the classical Moody diagram corresponding to the same relative roughness. The differences, which might be significant in certain critical applications, are due to the following reasons:

- Though the friction factor depends on velocity, diameter, density, viscosity, roughness, and radius ratio, the Moody diagram predicts a constant friction factor in the Reynolds number range considered for the rough side, since the flow is completely rough in this range [1, 66]. The present study indicates a transition range type flow between the completely smooth and completely rough regimes.

  This is due to the asymmetry of the roughness distribution on the channel walls. The combination of completely rough flow on one side and smooth flow on the other in the annulus produces this type of observed behavior, namely, the variation of total friction with Re, S/ϵ, α, and P/ϵ.

- The Moody diagram does not recognize the effects of roughness density and radius ratio on the friction factor as shown in Fig. 4.19. For different

values of roughness density and radius ratio for a given S/ϵ and α, the friction factor is the same for the given Reynolds number.

The effect of P/ϵ and α on the non-dimensional ratio $F(f_r/f_s)$ can be shown in Figs. 5.1- 5.7. In general this ratio increases with increase of P/ϵ and decrease of α at the Reynolds number range of $10^4 - 10^5$. This is possibly due to increase in momentum exchange at lower roughness density and radius ratio [61, 62]. However, as shown in Figs. 5.6 - 5.8, it is interesting to note that as the radius ratio is decreased at a lower roughness density and high Reynolds number, the normalized friction factor (F) decreases.

- Also, if the test channel had different shapes of roughness (i.e. rectangular ribs, triangular ribs, etc.) with the same height, one would still tend to use the same relative roughness value used above in order to calculate the friction factor from the Moody diagram.

  This in turn would predict exactly the same friction factor for all of the cases. The problem arises because the Moody diagram is evaluated for a particular type of roughness. To be able to use the Moody diagram, an equivalent sand roughness should be defined for every particular roughness structure on a wall. This sand roughness should also be a function of Reynolds number in the case of asymmetric roughness distribution. The use of the parameter, Z_{ro}, which is connected to be the equivalent sand roughness, is introduced in the present study to provide a step in the theoretical analysis of the behavior of the flow near a rough wall.

usselt number

The predicted Nusselt numbers in the developed region of the annular duct having a core with rough surface are shown in Figs. 5.8 - 5.9, and they clearly indicate that the values of Nusselt numbers are always greater than that of the channel with smooth surfaces.

This tendency is obvious from the fact that the rough surface develops considerably larger values of heat transfer coefficient for the given flow conditions mentioned in the previous section. This increase in the heat transfer coefficient can also be

deduced from other aspects of the turbulent flow in a concentric annulus. It can be shown for the present geometry by a force balance that the shear stress on the rough core wall, τ_{wr}, is always greater than the shear stress on the smooth outer wall, τ_{ws}.

This greater shear stress on the rough wall is understandable, because a part of the turbulent shearing stresses can be transmitted to the wall through pressure forces exerted on the roughness elements. The large value of shear means a larger value of ε_M. At the same time, the larger value of ε_M indicates vigorous thermal diffusion and hence a higher rate of heat transfer. Therefore, it is not surprising to see from Figs. 5.8 -5.9 that there are increases in the heat transfer coefficient.

Fig. 5.9 shows the effect of relative height of roughness on the heat transfer coefficient. In general, the heat transfer decreases with increasing values of S/ϵ. This is possibly due to the effect of roughness on the exchange mechanism and is confined to the regions located in proximity of the wall[67]. When S/ϵ approaches infinity, the heat transfer coefficient will have the value that associated with the smooth surface.

The effect of P/ϵ on the normalized Nusselt number, $H(Nu_r/Nu_s)$, are shown in Figs. 5.10 and 5.11. The non-dimensional ratio, H, increases with an increase in P/ϵ, Prandtl number and Reynolds number. However, the ratio, H, decreases with an increase in α and a decrease in Reynolds number as shown in Figs. 5.12 -5.14.

Ratio of H/F

It has been demonstrated that the heat transfer coefficient increases with the introduction of roughness on the channel wall. On the other hand, rough surfaces develop considerably larger values of friction coefficient than a channel with smooth walls. To determine whether the percentage increase in the rate of the heat transfer will be offset by the increase in the pressure losses, the non-dimensional ratio H/F has been used. If H/F is less than unity, the increase in the rate of heat transfer will be offset by an increase in pressure losses, which requires higher pumping power.

Conversely, if H/F is greater than unity, then the heat transfer will increase more rapidly than the drag, resulting in a more effective system.

In present investigation it has been found that H/F ratio is affected by the parameters, P/ϵ, S/ϵ, α, Pr, and Re. The values of H/F are not constant, and the parametric effects are discussed in the following:

- Effect of P/ϵ:

  Figs. 5.15 - 5.17 show that the ratio H/F plotted against P/ϵ for Prandtl number = 0.72 and radius ratio(α) = 0.4, and Reynolds number from 10,000 to 100,000.

  As clearly shown from the Figs. 5.15 - 5.17, the ratio of H/F increases with increase of P/ϵ. This trend is expected, since a part of the turbulent shearing stresses can be transmitted to the wall through pressure forces exerted on protuberances. No analogue exists for this mechanism in heat transfer.

- Effect of S/ϵ:

  As shown Figs. 5.15 - 5.17, in general, a small increase in H/F with a decrease in S/ϵ is noticed. This is due to the fact that the effect of roughness on the exchange mechanism is confined to the regions located in the proximity of the wall.

  Similar observations have been reported by Owen and Thomson [67], who made measurements of different values of Prandtl number in a rough tube.

- Effect of α:

  Fig. 5.19 shows the variation of H/F versus α for Prandtl number=0.72, relative height of roughness, S/ϵ=19.4. As clearly indicated in Figs. 5.18 and 5.19, the ratio of H/F increases with a decrease in α. This is because as α increases, the ratio of the normalized friction factor increment becomes larger than that of the normalized Nusselt number increment. The physical geometry of radius ratio (α) shows that α= 0 and α= 1 mean the pipe without a core tube and the parallel plate, respectively.

- Effect of Prandtl number(Pr):

  It is well known that at very low Prandtl numbers where the predominant mechanism is molecular diffusion, roughness would be expected to have less influence on the turbulent heat transfer process. The heat transfer conductance increases substantially at high Prandtl numbers

due to any small disturbance of the laminar sublayer which represents a high thermal resistance. This trend can be shown in Figs. 5.20 and 5.22 where the ratio H/F increases with an increase in Prandtl number.

- Effect of Reynolds number:

  As indicated in Figs. 5.10 - 5.14, heat transfer increases with an increase in Reynolds number. It is also shown in Figs. 5.1 - 5.7 that normalized friction forces increase with increase in Reynolds number. However, since the normalized heat transfer increases more rapidly than the normalized friction factor, one would expect that the ratio, H/F, will increase with increase of Reynolds number.

  Typical variations of H/F with Re are represented in Figs. 5.15 - 5.19. It should be noted that the effect of Reynolds number on H/F is significant at its high values. At high Reynolds number, a greater influence of roughness is expected due to the thinner laminar sublayer.

From the above-mentioned discussion, in order to design an efficient system of heat transfer, it is advantageous to

a) decrease the relative height of roughness (S/ϵ),

b) decrease the radius ratio(α),

c) increase the pitch between the roughnes elements, i.e., relative rib spacing (P/ϵ),

d) increase Reynolds number(Re), and

e) increase Prandtl number(Pr)

Chapter 6

Conclusion

The following conclusions are derived from the analytical and experimental investigation on the drag force and heat transfer characteristics in the developed region of fluid flow flowing turbulently in a concentric annulus with a uniformly heated core tube having square-ribbed surface roughness elements:

1. A good agreement is obtained between the analytical results for velocity profiles and friction factors and the experimental results.
2. The effects of roughness density, relative roughness height, Reynolds and Prandtl numbers on the ratio H/F are identified.
3. The normalized friction factor (F) decreases with an increase in S/ϵ and increases with an increase in P/ϵ.
4. The normalized heat transfer coefficient (H) increases with an increase in P/ϵ, and decreases with an increase in S/ϵ.
5. Certain artificial roughness elements can be used to enhance heat transfer rates with advantages from the overall efficiency point of view and the required pumping power per unit heat transfer rate decreases with increasing values of P/ϵ, decreasing values of S/ϵ and α, and increasing Reynolds and Prandtl numbers for the ranges of parameters studied.

Reference

1. H. Schlichting, "Boundary Layer Theory", McGraw Hill Book Co., Inc., 6th Edition (1968).

2. W.B. Hall, "Heat Transfer in Channels Having Rough and Smooth Surfaces", J. of Mech. Eng. Science, 4, No. 3, (1962).

3. R.G. Deissler, "Analytical Investigation of Turbulent Flow in Smooth Tubes with Heat Transfer with Variable Fluid Properties for Prandtl Number of 1", NACA, TM 2242, (1950).

4. J. Laufer, "The Structure of Turbulrnce in Fully Developed Pipe Flow", NACA Rept. 1174, (1954).

5. C.J. Cremers and E.R.G. Eckert, "Hot-Wire Measurements of Turbulence Correlations in a Triangular Duct", J. of Applied Mech., 609-614, (1962).

6. J.A. Clark, "A Study of Incompressible Turbulent Boundary Layers in Channel Flow", J. of Basic Eng., Trans. ASME, 90, 445-468, (1968).

7. H. Barrow, "Fluid Flow and Heat Transfer in an Annulus with a Heated Core Tube", Proc. Inst. Mech. Eng., 56, 1113, (1955).

8. Y. Lee and H. Barrow, "Turbulent Flow and Heat Transfer in Concentric and Eccentric Annuli", Proceedings, I. Mech. E., 178, 1-16, (1964).

9. J.A. Brighton and J. B. Jones, "Fully Developed Turbulent Flow in Annuli", J. of Basic Eng., Trans. ASME, Sec. D, 86, 835-844, (1964).

10. R.R. Rothfus, W.K. Sartory and R.I. Kermode, "Flow in Concentric Annuli at High Reynolds Numbers", A.I.Ch.E. Journal, 12, 1086-1091, (1966).

11. S. Levy, "Turbulent Flow in An Annulus", J. of Heat Transfer, ASME, 89, 25-31, (1967).

12. A. Quarmbly, "An Experimental Study of Turbulent Flow Through Concentric Annuli", Int. J. Mech. Sci., 9, 205-221, (1967).

13. A. Quarmbly, "An Analysis of Turbulent Flow in Concentric Annuli", Appli. Sci. Res., 19, 250-273, (1968).

14. I. Michiyoshi and T. Nakajima, "Fully Developed Turbulent Flow in a Concentric Annulus", J. of Nuclear Sci. and Tech., 5, 354-359, (1968).

15. N.W. Wilson and J.O. Medwell, "An Analysis of Heat Transfer for Fully Developed Turbulent Flow in Concentric Annuli", J. of Heat Transfer, Trans. ASME, 90, 43-50, (1968).

16. S.S. Randhave, "An Analysis of Turbulent Flow in Concentric Annuli", A.I.Ch.E. Journal, 15, 132-133, (1969).

17. W.K. Allan, "Velocity Distribution in Turbulent Flow", J. Mech. Eng. Sci., 12, 391, (1970).

18. W.K. Allan and V. Sharma, "An Investigation of Low Turbulent Flows Over Smooth and Rough Surface", J. Mech. Eng. Sci., 16, 71-78, (1974).

19. F. Schultz-Grunow, "Der hydraulische Reibungswiderstand von Platten mit Maβig Rauher Oberflache", Insbesondere von Schiffsoberflachen, Jb. Schiffbautechen Ges., 39, 176-198, (1938).

20. D. Wilkie, "Forced Convection Heat Transfer from Surface Roughened by Transverse Ribs", Third International Heat Transfer Conference, Chicago, Illinois, 1, 19, (1966).

21. M.J. Lewis, "Roughness Functions, the Thermohydraulic Preformance of Rough Surfaces and the Hall Transformation - An Overview", Int. J. Heat Mass Transfer, 17, 809-814, (1974).

22. A.J. Musker and A.K. Lewkowicz, "The Effect of Ship Hull Roughness on the Development of Turbulent Boundary Layers", Int. Symposium on Ship Viscous Resistance, SSPA, Goteborg, (1978).

23. R.G. Deissler, "Investigation of Turbulent Flow and Heat Transfer in Smooth Tubes, including the Effects of Variable Fluid Properties", Trans. ASME, 73, 101-107, (1951).

24. W.H. Corcoran, F. Page, Jr., W.G. Schlinger and B. H. Sage, "Temperature Gradients in Turbulent Gas Streams", Industrial and Eng. Chem., 44, (1952).

25. R. M. Labib, "Asymmetric Turbulent Heat Transfer in the Thermal Entrance Region", Master of App. Sci., Dept. of Mech. Eng., University of Ottawa (1979).

26. A. Bhuiyan, "An Asymmetric Turbulent Fluid Flow Induced by Rectangular Ribbed Surface Roughness", Master of App. Sci., Dept. of Mech. Eng., Univ. of Ottawa, (1977).

27. R.D. Haberstroh and L.V. Baldwin, "Application of a Simplified Velocity Profile to the Prediction of Pipe - Flow Heat Transfer", Paper No. 67-HT-25, Trans. ASME, Sept., (1967).

28. C.J. Lawn, "Turbulent Heat Transfer at Low Reynolds Numbers", J. of Heat Transfer, Trans. ASME, 96, 532-536, (1969).

29. R.A. Gowen and J.W. Smith, "Turbulent Heat Transfer from Smooth and Rough Surfaces", Int. J. of Heat Mass Transfer, 11, 1657-1674, (1969).

30. A. Quarmbly, "Some Measurements of Turbulent Heat Transfer in the Thermal Entrance Region of Concentric Annuli", Int. J. Heat Mass Transfer, 10, 267-276, (1967).

31. A.R. Pickering, "Forced Convective Heat Transfer to Water in an Annulus", United Kingdom Atomic Energy Authority, AEEW-R 295, (1964).

32. W.A. Sutherland and W.M. Kays, "Heat Transfer in an Annulus with Variable Circumferential Heat Flux", Int. J. Heat Mass Transfer, 7, 1187-1194, (1964).

33. A.J. Ziegenhagen, "Approximate Eigenvalues for Heat Transfer to Laminar or Turbulent Flow in an Annulus", Int. J. Heat Mass Transfer, 8, 499-505, (1965).

34. I. Michiyoshi and T. Nakajima, "Heat Transfer in Turbulent Flow with Internal Heat Generation in Concentric Annulus, (I) Fully Developed Thermal Situation", J. of Nuclear Sci. and Tech., 5, 476-484, (1968).

35. A. Quarmbly and R.K. Anand, "Fully Developed Turbulent Heat Transfer in Concentric Annuli with Uniform Walls Heat Fluxes", Chem. Eng. Sci., 24, 171-187, (1969).

36. J.C. Han, L.R. Glicksman, and W.M. Rohsenow, "An Investigation of Heat Transfer and Friction for Rib-roughened Surfaces", Int. J. Heat Mass Transfer, 21, 1143-1156, (1978),

37. T. Shigechi, N. Kawae, and Y. Lee, "Turbulent Flow and Heat Transfer in Concentric Annuli with Moving Cores", in Press, Int. J. Heat Mass Transfer.

38. W.C. Reynolds, R.E. Lundberg and P.A. McCuen, "Heat Transfer in Annular Passages. General Formulation of Problem for Arbitrarily Pre-

scribed Wall Temperatures or Heat Fluxes", Int. Jour. Heat Mass Transfer, 6, 483-493, (1963).

39. W. M. Kays and M. E. Crawford, "Convective Heat and Mass Transfer", 2ed., McGraw-Hill, New York, 187, (1980).

40. L. Prandtl and Z. Angew, Math. U. Mech., 5, 136 (1952); see also NACA, TM 1231, (1949).

41. J. Nikuradse, NACA, TM 1292, (1933).

42. H. Schlichting, "Experimental Investigation of the Problem of Surface Roughness", NACA, TM 823, (1936).

43. Y. Lee, M. A. Bhuiyan and R. M. Labib, " Asymmetric Turbulent Fluid Flow Induced by Square Ribbed Surface Roughness", 7th CANCAM Conf., Sherbrooke, (1979).

44. S. D. Park, "Developing Turbulent Flow in Concentric Annuli : An Analytical and Experiment Study", Ph. D. Thesis, Department of Mechanical Engineering, University of Ottawa, (1971).

45. H. Reichardt, "Vollstandige Darstellung der turbulenten Geschwindigkeitsverteilung in glatten Leitungen", Z. angew. Mathematik und Mechanik, 31, 208-219, (1951).

46. E. R. van Driest. "On Turbulent Flow near a Wall", J. of Aero. Sci, 23, 485, (1956).

47. J. A. Brighton and J. B. Jones, "Fully Developed Turbulent Flow in Annuli", Trans. ASME, J. Bas. Eng., 86, 835-844, (1964).

48. V. K. Jonsson and A. Sparrow, "Experiments on Turbulent Flow Phenomena in Eccentric Annular Ducts", J. Fluid Mech., 25, 65-86, (1965).

49. H. Barrow, Y. Lee and A. Roberts, "The Similarity Hypothesis Applied to the Turbulent Flow in an Annulus", Int. J. Heat and Mass Transfer, 8, 1499-1505, (1965).

50. D. D. McCracken and W. S. Dorn, "Numerical Methods and Fortran Programming", New York, Wiley, (1964).

51. British Standard Code, "Orifice Plate with Corner Tappings", B. S. 1042: Part 1, 107, (1964).

52. A. D. Young and J. N. Mass, "The Behaviour of a Pitot Tube in a Traverse Pressure Gradient", A.R.C., R & M 1770, (1937).

53. F. Homann, "The Effect of High Viscosity on the Flow Around a Cylinder and a Sphere", NACA, TM 1344, (1952).

54. Instrumentation Manual, MKS Baratron Type 77, MKS Instruments Inc., Burlington, Massachusetts, (1967).

55. F. R. Hama, "Boundary Layer Characteristics for Smooth and Rough Surfaces", Trans. of Soc. of Naval Arch. and Marine Eng., 62, 333-358, (1954).

56. C. J. Lawn and M. J. Hamlin, "Velocity Measurements in Roughened Annuli", RD/B/N1278, Central Electricity Generating Board, Research & Development Department, Berkeley Nuclear Lab., (1969).

57. ISO Recommendation R 540, "Measurement of Fluid Flow by Means Orifice Plates and Nozzles", 1st Edition, (1967).

58. R. L. Spiller, "The Art and Practice of Orifice Flow Metering", Instrumentation Technology, 18, 52-56, (1971).

59. B. S. Massey, "Mechanics of Fluids", Van Nostrand Reinhold Co., London, (1971).

60. E. R. G. Eckert and R. M. Drake, "Heat and Mass Transfer", McGraw Hill Book Co. Inc., Appendix of Property Values, (1959).

61. H. Famf and G. Feuerstein, "Warm eibergamg und Druckverlust in Ringspaltstromung", 4th Int. Heat Transfer Conf., FC5.3, Paris, (1970).

62. F. Williams and J. Watts, "The Development of Rough Surface with Improved Heat Transfer Performance and a Study of the Mechanism Involved", 4th Int. Heat Transfer Conf., FC5.5, Paris, (1970).

63. R.L. Webb, E.R.G. Eckert, and R.J. Goldstein, "Heat Transfer And Friction in Tubes with Repeated-Rib Roughness, Int. J. Heat Mass Transfer, 14, 601-617, (1971).

64. R.W. Benodekar, A. J. H. Goddard, and R.I. Issa, "Numerical Prediction of Turbulent Flow over Surface-Mounted Ribs", AIAA Journal, 23, 358-366, (1985).

65. B. Kjellstrom and S. Hedberg, "On Shear Stress Distributions for Flow in Smooth or Paritally Rough Annuli", AE-243, Aktiebolaget Atomenergi, Stockholm, Sweden, (1966).

66. M. Tennekes and J.L. Lumley. "A First Course in Turbulence", The M.I.T Press, Cambridge. Massachusetts. and London, England, (1972).

67. P.R. Owen and W.R. Thomson. "Heat Transfer Across Rough Surfaces", JFM, 15, 321-334, (1943).

Appendix A

Derivation of Equations

A.1 Derivation of equation(3.3)

We have to consider two cases of momentum and energy equations: for $j = i$ and for $j = o$:

First for $j = i$

Dividing equation(3.2) by equation(3.1),

$$\frac{\partial T_i}{\partial y_i} = -\frac{q_i/\rho c(1+\varepsilon_M/\nu)\frac{\partial u_i}{\partial y_i}}{\frac{\tau_i}{\rho}(\frac{1}{Pr}+\frac{1}{Pr_t}\varepsilon_M/\nu)} \tag{A.1}$$

Using the dimensionless parameters,

$$\frac{\partial u_i}{\partial y_i} = \frac{\partial u_i^+}{\partial \zeta_i}\frac{1}{\delta_i^+}\frac{u_{\tau_{Ro}}^2}{\nu} \tag{A.2}$$

Using the definition of dimensionless temperature,

$$\frac{\partial T_i}{\partial y_i} = -\frac{\partial T_i^+}{\partial \zeta_i}\frac{q_{Ri}u_{\tau_{Ro}}^2}{\delta_i^+\nu}\frac{1}{c\times\tau_{Ro}} \tag{A.3}$$

Substituting equation (A.2) and (A.3) into (A.1),

$$\frac{\partial T_i^+}{\partial \zeta_i} = \frac{\partial u_i^+}{\partial \zeta_i} \frac{(1+\varepsilon_M/\nu)_i q_i/q_{Ri}}{(1/Pr + \frac{1}{Pr_t}\varepsilon_M/\nu)_i(\tau_i/\tau_{Ro})} \tag{A.4}$$

Second, for $j = o$

Using the same method with that of $j = o$.

$$\frac{\partial T_o^+}{\partial \zeta_o} = -\frac{\frac{q_o}{q_{Ri}}(1+\varepsilon_M/\nu)_o}{\frac{\tau_o}{\tau_{Ro}}(1/Pr + \frac{1}{Pr_t}\varepsilon_M/\nu)_o} \frac{\partial u_o^+}{\partial \zeta_o} \tag{A.5}$$

Adding equation (A.5) to (A.4),

$$\frac{\partial T_j^+}{\partial \zeta_j} = \pm \frac{\partial u_j^+}{\partial \zeta_j} \frac{(1+\varepsilon_M/\nu)_j}{(\frac{1}{Pr} + \frac{1}{Pr_t}\varepsilon_M/\nu)_j} \frac{(q_j/q_{Ri})}{(\tau_j/\tau_{Ro})} \tag{A.6}$$

A.2 Derivation of equation (3.4)

Using a momentum equation,

$$u\frac{\partial u}{\partial x}+v\frac{\partial u}{\partial r}-\frac{1}{r}\frac{\partial}{\partial r}[(\mu+\varepsilon_M)r\frac{\partial u}{\partial r}]+\frac{1}{\rho}\frac{dp}{dx}=0$$

Using these concepts: $\frac{\partial u}{\partial x}=0$ at fully developed flow and $u \gg v$,

$$\frac{\partial}{\partial r}[(\mu+\varepsilon_M)r\frac{\partial u}{\partial r}]=\frac{1}{\rho}\frac{dp}{dx}r \tag{A.7}$$

Assuming that the maximum velocity point(R_m) becomes the zero shear stress point ($R_{m\tau}$), and integrating with respect to r, we obtain:

$$R_{m\tau}(\nu+\varepsilon_M)\frac{\partial u}{\partial r})\,|_{R_{m\tau}}-(Z_{ro}+R_i)(\nu+\varepsilon_M)\frac{\partial u}{\partial r}\,|_{Z_{ro}+R_i}=\frac{1}{\rho}\frac{dp}{dx}[\frac{{R_{m\tau}}^2-(R_i+Z_{ro})^2}{2}] \tag{A.8}$$

Using the boundary condition,

$$\tau_{R_i+Z_{ro}}=-\frac{dp}{dx}[\frac{{R_{m\tau}}^2-(R_i+Z_{ro})^2}{2}]\frac{1}{Z_{ro}+R_i} \tag{A.9}$$

Integrating equation (A.7) using the boundary conditions,

$$-\frac{\tau_i}{\rho}=\frac{1}{\rho}\frac{dp}{dx}(\frac{{R_{m\tau}}^2-r^2}{2})\frac{1}{r} \tag{A.10}$$

Dividing equation (A.10) by equation (A.9),

$$\frac{\tau_i}{\tau_{Ri+Z_{ro}}}=\frac{(R_{m\tau}^2-r^2)(R_i+Z_{ro})}{[{R_{m\tau}}^2-(R_i+Z_{ro})^2]r} \tag{A.11}$$

Using dimensionless parameters, we can obtain:

$$\frac{\tau_i}{\tau_{Ri+Z_{ro}}}=\frac{(1-\zeta_i)\{2+\Delta_i(1+\zeta_i)\}(1+\Delta_i\frac{Z_{ro}^+}{\delta_i^+})}{(1+\Delta_i\zeta_i)[2+\Delta_i(1+\frac{Z_{ro}^+}{\delta_i^+})](1-\frac{Z_{ro}^+}{\delta_i^+})} \tag{A.12}$$

Multiplying (A.12) by the equation nondimensionized from equation (3.24), the following equation is obtained:

$$\frac{\tau_i}{\tau_{Ro}} = \frac{(1-\zeta_i)[2+\Delta_i(1+\zeta_i)](1+\Delta_i\frac{Z^+_{Ro}}{\xi^+_i})}{(1+\Delta_i\zeta_i)[2+\Delta_i(1+\frac{Z^+_{Ro}}{\xi^+_i})](1-\frac{Z^+_{Ro}}{\xi^+_i})} \tag{A.13}$$

A.3 Derivation of equation (3.5)

Integrating equation (A.7) using the boundary conditions, we obtain:

$$\tau_{Ro} = \frac{dp}{dx}\left(\frac{R_o{}^2 - R_{m\tau}{}^2}{2}\right)\frac{1}{R_o} \tag{A.14}$$

$$\tau_o = \frac{dp}{dx}\left[\frac{(R_o - y_o)^2 - R_m^2}{2}\right]\frac{1}{(R_o - y_o)} \tag{A.15}$$

Dividing equation (A.15) by (A.14),

$$\frac{\tau_o}{\tau_{Ro}} = \frac{R_o}{(R_o - y_o)}\frac{[(R_o - y_o)^2 - R_m^2]}{R_o^2 - R_m^2} \tag{A.16}$$

Using the dimensionless parameters,

$$\frac{\tau_o}{\tau_{Ro}} = \frac{(1 - \zeta_o)(2 - \Delta_o - \Delta_o\zeta_o)/(2 - \Delta_o)}{(1 - \Delta_o\zeta_o)} \tag{A.17}$$

A.4 Derivation of equations (3.6) and (3.7)

Derivation of equation (3.6)

Conditions:

1. The core wall has constant heat flux.
2. The outer wall is insulated.

From the energy balance made on the control volume (Fig. 3.3).

Inflow of heat - outflow of heat =an increase in internal energy

(A.18)

Using an energy balance,

$$Inflow\ of\ heat\ = 2\pi r dx q_r^{''} \tag{A.19}$$

$$Outflow\ of\ heat\ = 2\pi(r+dr)dr(q_r^{''} + \frac{\partial q_r^{''}}{\partial r}dr) \tag{A.20}$$

$$An\ increase\ in\ internal\ energy\ = 2\pi r dr dx \times \rho u c_p \frac{\partial T}{\partial x} \tag{A.21}$$

Substituting equations (A.19), (A.20) ,and (A.21) into equation (A.18), and arranging,

$$-\frac{\partial}{\partial r}(q_r^{''} r) = r\rho u c_p \frac{\partial T}{\partial x} \tag{A.22}$$

From the boundary conditions, we also assume:

$$\frac{\partial T}{\partial x} = \frac{dT}{dx} = \frac{dT_b}{dx}, u = u_b$$

Because the turbulent flow is fully developed, the heat flux is already very small in the channel, the assumption concerning the velocity field is not critical to the evaluation of $q(r)$. Therefore, it is assumed that $u = u_b$.

Integrating the equation (A.22) and applying the boundary conditions,

at $r = R_o$, $q_r = 0$

$$q_r^{''} . r = \rho u_b c_p \frac{dT_b}{dx} \frac{(R_o{}^2 - r^2)}{2} \tag{A.23}$$

at $r = R_i + Z_{ro}$, $q_r = q_{Ri} = constant$

$$q_{Ri}(R_i + Z_{ro}) = \rho u_b c_p \frac{dT_b}{dx}\{\frac{{R_o}^2 - (R_i + Z_{ro})^2}{2}\} \tag{A.24}$$

Dividing Equation (A.24) by (A.23),

$$\frac{q_r}{q_{Ri}} = \frac{(R_i + Z_{ro})({R_o}^2 - r^2)}{r[{R_o}^2 - (R_i + Z_{ro})^2]} \tag{A.25}$$

Using dimensionless parameters,

$$\frac{q_i}{q_{Ri}} = \frac{(1 + \Delta_i \frac{{Z_{ro}}^2}{\delta_i^+})[1 - \alpha^2(1 + \Delta_i \zeta_i)^2]}{(1 + \Delta_i \zeta_i)[1 - \alpha^2(1 + \Delta_i \frac{Z_{ro}^+}{\delta_i^+})]}$$

Derivation of equation(3.7)

Equation (A.25) becomes:

$$\frac{q_r}{q_{Ri}} = \frac{R_i(1 + \frac{Z_{ro}}{R_i})[1 - (\frac{r}{R_o})^2]{R_o}^2}{r[{R_o}^2 - {R_i}^2(1 + \frac{Z_{ro}}{R_i})^2]} \tag{A.26}$$

Substituting $r = R_o - y_o$ and using the dimensionless parameters,

$$\frac{q_i}{q_{Ri}} = \frac{\alpha(2 - \Delta_o \zeta_o)\Delta_o \zeta_o (1 + \Delta_i \frac{Z_{ro}^+}{\delta_i^+})}{[1 - \alpha^2(1 + \Delta_i \frac{Z_{ro}^+}{\delta_i^+})](1 - \Delta_o \zeta_o)} \tag{A.27}$$

A.5 Derivation of equations (3.8) and (3.12)

Derivation of equation (3.8)

Equation (3.1) for $j = o$ becomes:

$$\frac{\tau_o}{\rho} = \nu(1 + \varepsilon_M/\nu)\frac{\partial u_o}{\partial y_o} \tag{A.28}$$

Dividing this by τ_{Ro}, and using $u^2_{\tau_{Ro}} = \frac{\tau_{Ro}}{\rho}, \delta_o^+ = u_{\tau_{Ro}}\delta_o/\nu, \zeta_o = \frac{y_o^+}{\delta_o^+} = \frac{y_o}{\delta_o}$,

$$\frac{\partial u_o^+}{\partial \zeta_o} = \delta_o^+[\frac{\tau_o/\tau_{Ro}}{1 + (\varepsilon/\nu)_o}] \tag{A.29}$$

Derivation of equation(3.12)

Differentiating equation (3.9) with respect to y_i,

$$\frac{\partial u_i}{\partial y_i} = \frac{u_{\tau_{Ri}}}{k_i}\frac{1}{y_i} \tag{A.30}$$

using dimensionless notation, $u_i^+ = \frac{u_i}{u_{\tau_{Ro}}}$, $y_i^+ = \frac{u_{\tau_{Ro}}}{\nu}$, and $\zeta_i = \frac{y_i}{\delta_i} = \frac{y_i^+}{\delta_i^+}$,

$$\frac{\partial u_i^+}{\partial \zeta_i} = \frac{u_{\tau_{Ri}}}{u_{\tau_{Ro}}}\frac{1}{k_i\zeta_i} \tag{A.31}$$

A.6 Derivation of equation (3.17)

$$u_b = \frac{1}{\pi(R_o^2 - R_i^2)}\left(\int_{R_i+Z_{ro}}^{R_m} u_i 2\pi r dr + \int_{R_m}^{R_o} u_o 2\pi r dr\right) \qquad \text{(A.32)}$$

First term in equation (A.32) becomes,

$$\frac{\int_{R_i+Z_{ro}}^{R_m} u_i 2\pi r dr}{\pi(R_o^2 - R_i^2)}$$

Changing the range of the integration.

$$\frac{\int_{Z_{ro}}^{R_m-R_i} 2u_i(R_i + y_i)dy_i}{R_o^2[1 - (R_i/R_o)^2]} \qquad \text{(A.33)}$$

Using the following notations, $\zeta_i = \frac{y_i}{\delta_i} = \frac{y_i^+}{\delta_i^+}$,

at $y_i = Z_{ro}, \zeta_i = \frac{Z_{ro}^+}{\delta_i^+}$,

at $y_i = R_m - R_i, \zeta_i = 1$,

Equation (A.33) becomes,

$$\frac{\nu 2\alpha}{R_o(1-\alpha^2)}\delta_i^+ \int_{\frac{Z_{ro}^+}{\delta_i^+}}^{1} u_i^+(1 + \Delta_i\zeta_i)d\zeta_i \qquad \text{(A.34)}$$

Second term in equation (A.32) is,

$$\frac{\int_{R_m}^{R_o} u 2\pi r dr}{\pi(R_o^2 - R_i^2)} = \frac{2\pi}{\pi R_o^2[1 - (R_i/R_o)^2]}\left(\int_{R_m}^{R_{sub}} u r dr + \int_{R_{sub}}^{R_o} u r dr\right) \qquad \text{(A.35)}$$

$r = R_o - y_o; dr = -dy_o$

changing the range of integration,

$$\frac{2}{R_o^2[1 - (R_i/R_o)^2]}\left[\int_0^{R_o-R_{sub}} u_o(R_o - y_o)dy_o + \int_{R_o-R_{sub}}^{R_o-R_m} u_o(R_o - y_o)dy_o\right]$$

Using these notations, $\zeta_o = \frac{y_o}{\delta_o}$, $\zeta_{sub} = \frac{R_o-R_{sub}}{\delta_o}$, and $\frac{y_o}{R_o} = \frac{\delta_o}{R_o} \times \frac{y_o}{\delta_o} = \Delta_o\zeta_o$,

$$\frac{\nu}{R_o}\frac{2\alpha\delta_o^+}{(1-\alpha^2)\alpha}\left[\int_0^{\zeta_{sub}} u_o^+(1 - \Delta_o\zeta_o)d\zeta_o + \int_{\zeta_{sub}}^{1} u_o^+(1 - \Delta_o\zeta_o)d\zeta_o\right] = \qquad \text{(A.36)}$$

$$\frac{\nu}{R_o}\frac{2\alpha\delta_o^+}{(1-\alpha^2)\alpha}[\frac{\delta_o^+}{\alpha}\int_0^1 u_o^+(1-\Delta_o\zeta_o)d\zeta_o]$$

Summing equations (A.34) and (A.36)

$$u_b = \frac{\nu\alpha}{R_o(1-\alpha^2)}[\delta_i^+\int_{Z_{ro}/\delta_i^+}^1(1+\Delta_i\zeta_i)u_i^+d\zeta_i + \frac{\delta_o^+}{\alpha}\int_0^1(1-\Delta_o\zeta_o)u_o^+d\zeta_o] \qquad (A.37)$$

A.7 Derivation of equation (3.19)

The friction factor for entire range of annulus is:

$$f = \frac{f_i R_i + f_o R_o}{R_i + R_o} = \frac{\frac{\tau_i}{0.5\rho u_b^2} R_i + \frac{\tau_o}{0.5\rho u_b^2} R_o}{R_i + R_o} \tag{A.38}$$

Substituting $u_b = \frac{Re\nu}{2(R_o - R_i)}$.

$$f = \frac{8(1-\alpha)^2[1 + \alpha(\tau_{jRi}/\tau_{jRo})]}{(1+\alpha)} (R_o^+/Re)^2 \tag{A.39}$$

A.8 Derivation of equation (3.22)

From the definition of bulk temperature in the annulus, we obtain,

$$T_b = \frac{2\pi \int_{R_i}^{R_o} urTdr}{2\pi \int_{R_i}^{R_o} urdr} = \frac{\int_{Z_{ro}+R_i}^{R_m} urTdr + \int_{R_m}^{R_o} urTdr}{\int_{Z_{ro}+R_i}^{R_m} urdr + \int_{R_m}^{R_o} urdr} \tag{A.40}$$

We can express the denominator as follows.

$$u_b \pi R_o^2[1 - (\frac{R_i}{R_o})^2] = 2\pi(\int_{Z_{ro}+R_i}^{R_m} urdr + \int_{R_m}^{R_o} urdr)$$

Using $u_b = \frac{Re\nu}{2R_o(1-\alpha)}$,

$$T_b = \frac{\int_{Z_{ro}+R_i}^{R_m} urTdr + \int_{R_m}^{R_o} urTdr}{\frac{Re\nu R_o(1+\alpha)}{4}} \tag{A.41}$$

The first term in the numerator of equation (A.41) is,

$$\int_{Z_{ro}+R_i}^{R_m} urTdr = \int_{Z_{ro}}^{R_m-R_i} (R_i + y_i)uTdy_i = R_i \int_{Z_{ro}}^{R_m-R_i} (1 + \frac{y_i}{R_i})uTdy_i \tag{A.42}$$

Using the dimensionless parameters,

$$\int_{Z_{ro}+R_i}^{R_m} urTdr = R_i\nu\delta_i^+ \int_{Z_{ro}^+/\delta_i^+}^{1} (1 + \Delta_i\zeta_i)u_i^+ Td\zeta_i$$

Substituting $T = T_{Ri} - \frac{T_o^+ q_{Ri} u_{\tau_{Ro}}}{c\tau_{Ro}}$,

$$\int_{Z_{ro}+R_i}^{R_m} urTdr = -R_i\nu\delta_i^+ \int_{Z_{ro}^+/\delta_i^+}^{1} (1 + \Delta_i\zeta_i)u_i^+ \frac{T_i^+ q_{Ri} u_{\tau_{Ro}} d\zeta_i}{c\tau_{Ro}} + \tag{A.43}$$

$$R_i\nu\delta_i^+ T_{R_i} \int_{Z_{ro}^+/\delta_i^+}^{1} (1 + \Delta_i\zeta_i)u_i^+ d\zeta_i$$

The second term in the numerator of equation (A.41) is,

$$\int_{R_m}^{R_o} urTdr = R_o\nu\delta_o^+ \int_0^1 (1 - \Delta_o\zeta_o)u_o^+ Td\zeta_o \tag{A.44}$$

$$= -R_o\nu\delta_o^+ \int_0^1 (1 - \Delta_o\zeta_o)u_o^+ \frac{T_o^+ q_{R_i} u_{\tau_o} d\zeta_o}{c\tau_{R_o}} + R_o\nu\delta_o^+ T_{Ri} \int_0^1 (1 - \Delta_o\zeta_o)u_o^+ d\zeta_o$$

Substituting equations (A.43) and (A.44) into equation (A.41).

$$T_{Ri} - T_b = \frac{4[\alpha\delta_i^+ \int_{Z_{To}^+/\delta_i^+}^1 (1+\Delta_i\zeta_i)u_i^+ \frac{T_i}{u_{\tau_{Ro}}} d\zeta_i + \zeta_o^+ \int_0^1 (1-\Delta_o\zeta_o)u_o^+ \frac{\tau_o^+ q_{Ro} u_{\tau_o}}{c\tau_{Ro}} d\zeta_o]}{Rc(1+\alpha)}$$

The bulk dimensionless temperature becomes.

$$T_b^+ = \frac{4}{(1+\alpha)} \frac{1}{Rc} [\alpha\delta_i^+ \int_{Z_{To}^+/\delta_i^+}^1 (1+\Delta_i\zeta_i)u_i^+ T_i^+ d\zeta_i + \delta_o^+ \int_0^1 (1-\Delta_o\zeta_o)u^+ T_o^+ d\zeta_o]$$

Appendix B

Flow chart of calculation

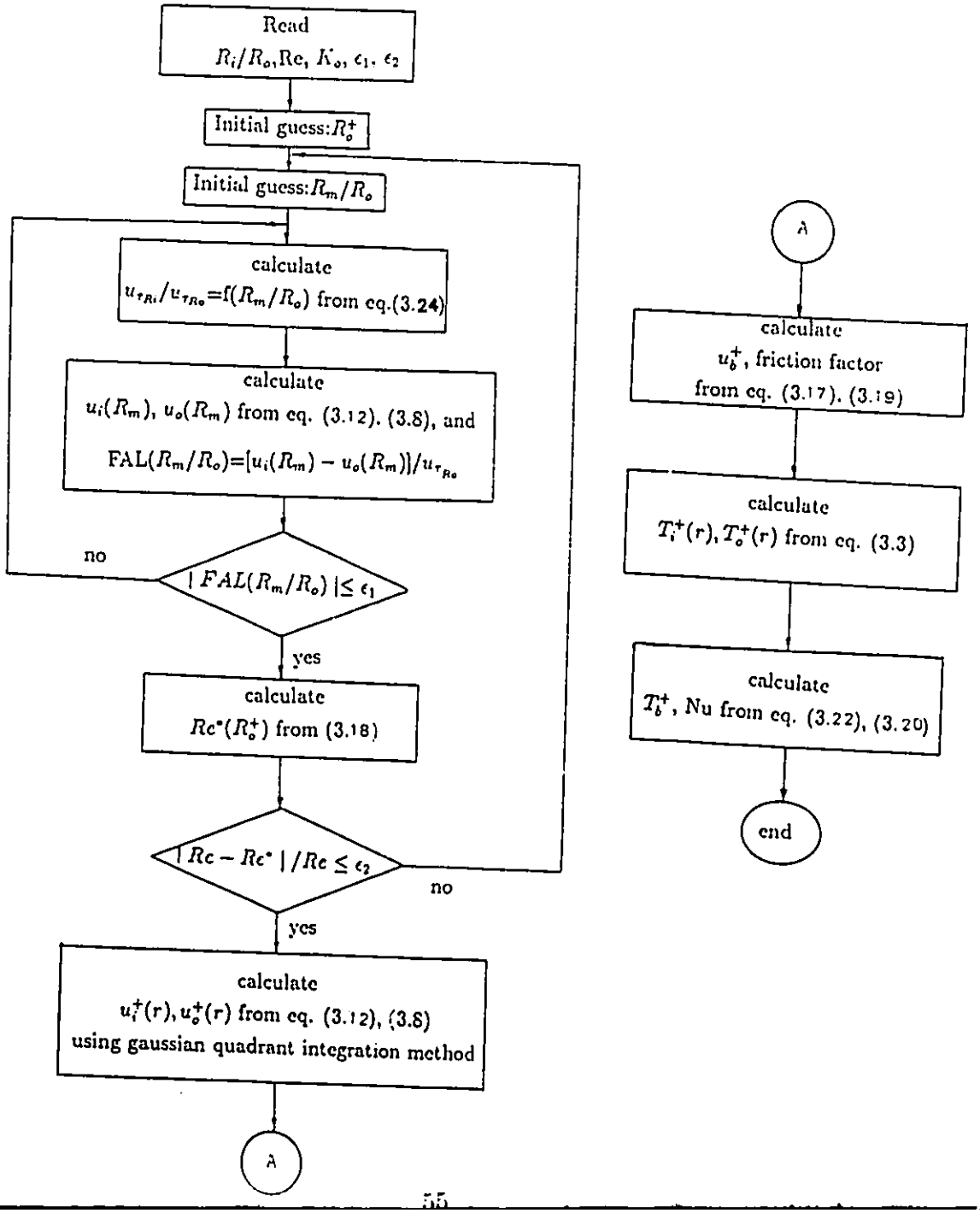

Appendix C

Summary of relations between mean flow parameters

$$u_{\tau_{Ro}} = (\tau_{Ro}/\rho)^{0.5} \qquad \text{(Definition)}$$

$$u_b = \frac{Q}{A} \qquad \text{(Definition)}$$

$$u_b = \frac{1}{\pi(R_o^2 - R_i^2)}\left(\int_{R_i+Z_{ro}}^{R_m} u_i 2\pi r dr + \int_{R_m}^{R_o} u_o 2\pi r dr\right) \qquad \text{(Definition)}$$

$$Re = \frac{u_b De}{\nu} \qquad \text{(Definition)}$$

$$f_i = \frac{\tau_i}{0.5\rho u_b^2} \qquad \text{(Definition)}$$

$$f_o = \frac{\tau_o}{0.5\rho u_b^2} \qquad \text{(Definition)}$$

$$f = \frac{f_i R_i + f_o R_o}{R_i + R_o}$$

$$\tau_{Ri+Zro} = -\frac{dp}{dx}[\frac{{R_{m\tau}}^2 - (R_i + Z_{ro})^2}{2}]\frac{1}{Z_{ro} + R_i} \qquad \text{(Eq. A.9)}$$

$$-\frac{\tau_i}{\rho} = \frac{1}{\rho}\frac{dp}{dx}(\frac{{R_{m\tau}}^2 - r^2}{2})\frac{1}{r} \qquad \text{(Eq. A.10)}$$

$$\tau_{Ro} = \frac{dp}{dx}(\frac{{R_o}^2 - {R_{m\tau}}^2}{2})\frac{1}{R_o} \qquad \text{(Eq. A.13)}$$

$$\tau_o = \frac{dp}{dx}[\frac{(R_o - y_o)^2 - R_m^2}{2}]\frac{1}{(R_o - y_o)} \qquad \text{(Eq. A.14)}$$

$$S = y_o - y_i$$

$$Z_{ro} = y_{m\tau} exp\{-\frac{\tau_{Ro}}{\tau_{Ri}}[\ln(S - y_{m\tau})u_{\tau_{Ro}}/\nu + Ck_o]\} \qquad \text{(Eq. 3.11)}$$

$$y_{m\tau} = S \times 0.299 Re^{0.066}(S/\epsilon)^{0.14}(P/S)^{0.21}$$

$$(\varepsilon_M/\nu)_o = [(k_o\delta_o^+/6][1 - (1 - y_o^+/\delta_o^+)^2][1 + 2(1 - y_o^+/\delta_o^+)^2] \qquad \text{(Eq. 3.13)}$$
$$(y_{os}^+ \le y_o^+ \le \delta_o^+)$$

$$(\varepsilon_M/\nu)_o = K_o^2 {y_o^+}^2[1 - exp(-y_o^+/A_o^+)]^2 \mid \frac{\partial u_o^+}{\partial y_o^+} \mid \qquad \text{(Eq. 3.14)}$$
$$(0 \le y_o^+ \le y_{os}^+)$$

$$(\varepsilon_M/\nu)_i = K_i^2 {y_i^+}^2 \mid \partial u_i^+/\partial y_i^+ \mid \qquad \text{(Eq. 3.15)}$$
$$(Z_{ro}^+ \le y_i^+ \le \delta_i^+)$$

Table 4.1 Essential Dimensions

Main Annular Duct Assembly unit: mm

	O. D.	I. D.	material	$\alpha(R_i/R_o)$	De
outer tube	101.6	97.4($2R_o$)	copper	.	97.4
core tube	39.2($2R_i$)	32.2	steel	0.4	58.2

Table 5.1(a) Velocity vs. $y/(R_0 - R_i)$: Experimental

$\alpha = 0.4$, $Pc = 2$, $S/c = 19.4$

Re	17000	32300	46300	59600	Re	17000	32300	46300	59600
$y/(R_o - R_i)$	u/u_m				$y/(R_o - R_i)$	u/u_m			
0.118	0.773	0.746	0.752	0.750	0.515	1.000	0.996	0.996	0.987
0.138	0.802	0.772	0.774	0.781	0.535	0.999	0.998	0.998	0.992
0.159	0.822	0.802	0.804	0.804	0.555	0.997	1.000	0.999	0.992
0.178	0.844	0.823	0.824	0.820	0.575	0.995	1.000	1.000	0.999
0.198	0.862	0.841	0.842	0.838	0.595	0.994	0.999	0.999	0.999
0.218	0.878	0.859	0.861	0.855	0.615	0.990	0.998	0.998	1.000
0.238	0.890	0.870	0.872	0.866	0.634	0.985	0.996	0.996	1.000
0.258	0.908	0.891	0.887	0.877	0.654	0.979	0.992	0.991	0.999
0.277	0.918	0.903	0.901	0.892	0.674	0.973	0.990	0.986	0.997
0.297	0.930	0.916	0.913	0.913	0.694	0.961	0.987	0.982	0.995
0.317	0.943	0.929	0.924	0.924	0.714	0.957	0.981	0.976	0.990
0.337	0.950	0.939	0.934	0.929	0.734	0.948	0.976	0.967	0.983
0.357	0.963	0.948	0.940	0.939	0.754	0.940	0.970	0.959	0.973
0.376	0.970	0.959	0.956	0.944	0.773	0.931	0.961	0.950	0.964
0.396	0.975	0.968	0.963	0.953	0.793	0.917	0.953	0.939	0.954
0.416	0.980	0.975	0.969	0.964	0.813	0.904	0.942	0.931	0.939
0.436	0.990	0.981	0.977	0.969	0.833	0.895	0.931	0.921	0.924
0.456	0.993	0.986	0.980	0.973	0.853	0.880	0.919	0.909	0.913
0.476	0.997	0.990	0.988	0.978	0.873	0.872	0.908	0.894	0.903
0.496	0.999	0.993	0.993	0.983	0.892	0.849	0.897	0.879	0.887

Table 5.1(b) Velocity vs. $y/(R_0 - R_i)$: Experimental

$\alpha = 0.4$, $P/c = 4$, $S/c = 19.4$

Re	17200	29500	44300	52600	Re	17200	29500	44300	52600
$y/(R_o - R_i)$	u/u_m				$y/(R_o - R_i)$	u/u_m			
0.118	0.619	0.616	0.608	0.577	0.515	0.966	0.950	0.940	0.931
0.138	0.678	0.644	0.640	0.611	0.535	0.971	0.959	0.951	0.935
0.159	0.696	0.680	0.671	0.660	0.555	0.979	0.970	0.959	0.939
0.178	0.726	0.701	0.689	0.689	0.575	0.984	0.975	0.968	0.950
0.198	0.750	0.727	0.721	0.721	0.595	0.989	0.983	0.976	0.958
0.218	0.771	0.739	0.731	0.736	0.615	0.990	0.988	0.980	0.970
0.238	0.790	0.758	0.758	0.760	0.634	0.996	0.994	0.986	0.972
0.258	0.808	0.791	0.776	0.771	0.654	0.998	0.996	0.992	0.976
0.277	0.821	0.802	0.790	0.790	0.674	1.000	0.999	0.996	0.987
0.297	0.841	0.820	0.810	0.802	0.694	0.996	0.999	0.998	0.994
0.317	0.849	0.831	0.824	0.810	0.714	0.996	1.000	0.999	0.998
0.337	0.868	0.851	0.838	0.815	0.734	0.990	0.998	1.000	0.999
0.357	0.881	0.860	0.854	0.828	0.754	0.986	0.994	0.999	1.000
0.376	0.897	0.880	0.869	0.841	0.773	0.977	0.988	0.995	0.999
0.396	0.910	0.892	0.880	0.852	0.793	0.970	0.980	0.989	0.994
0.416	0.919	0.902	0.891	0.870	0.813	0.957	0.971	0.980	0.983
0.436	0.931	0.911	0.901	0.881	0.833	0.940	0.958	0.971	0.965
0.456	0.942	0.920	0.910	0.891	0.853	0.931	0.946	0.959	0.954
0.476	0.949	0.929	0.922	0.910	0.873	0.910	0.931	0.945	0.940
0.496	0.960	0.942	0.933	0.920	0.892	0.901	0.911	0.927	0.925

Table 5.1(c) Velocity vs. $y/(R_o - R_i)$: Experimental

$\alpha = 0.4$, $P/c = 8$, $S/c = 19.4$

Re	16500	22200	42000	49100	Re	16500	22200	42000	49100
$y/(R_o - R_i)$	u/u_m				$y/(R_o - R_i)$	u/u_m			
0.118	0.588	0.482	0.595	0.598	0.515	0.913	0.898	0.897	0.903
0.138	0.623	0.534	0.633	0.649	0.535	0.920	0.902	0.909	0.914
0.159	0.667	0.579	0.647	0.677	0.555	0.936	0.916	0.918	0.924
0.178	0.678	0.597	0.668	0.696	0.575	0.940	0.929	0.933	0.935
0.198	0.701	0.616	0.703	0.714	0.595	0.953	0.933	0.942	0.942
0.218	0.718	0.635	0.718	0.727	0.615	0.960	0.940	0.950	0.950
0.238	0.739	0.654	0.738	0.740	0.634	0.965	0.948	0.961	0.955
0.258	0.758	0.686	0.750	0.756	0.654	0.974	0.954	0.964	0.966
0.277	0.767	0.703	0.768	0.771	0.674	0.984	0.970	0.973	0.976
0.297	0.785	0.717	0.785	0.778	0.694	0.990	0.973	0.982	0.982
0.317	0.794	0.743	0.806	0.790	0.714	0.994	0.979	0.989	0.984
0.337	0.810	0.758	0.809	0.806	0.734	0.996	0.989	0.994	0.990
0.357	0.825	0.776	0.817	0.818	0.754	1.000	1.000	0.998	0.994
0.376	0.840	0.805	0.835	0.829	0.773	1.000	0.992	1.000	0.996
0.396	0.850	0.809	0.840	0.845	0.793	0.996	0.978	1.000	1.000
0.416	0.859	0.840	0.853	0.856	0.813	0.993	0.971	0.999	0.997
0.436	0.874	0.859	0.865	0.866	0.833	0.987	0.958	0.994	0.990
0.456	0.880	0.872	0.873	0.878	0.853	0.978	0.944	0.990	0.984
0.476	0.889	0.883	0.880	0.884	0.873	0.967	0.930	0.976	0.977
0.496	0.905	0.885	0.890	0.899	0.892	0.947	0.921	0.971	0.965

Table 5.2 (a) Velocity vs. $y/(R_0 - R_i)$: Theoretical

$\alpha = 0.4$, $P/c = 2$, $S/c = 19.4$

Re	17000		32300		46300		59600	
No	$y/(R_o - R_i)$	u/u_m	$y/(R_o - R_i)$	u/u_m	$y/(R_o - R_i)$	u/u_m	$y/(R_o - R_i)$	u/u_m
1	0.002	0.000	0.003	0.000	0.003	0.000	0.003	0.000
2	0.042	0.538	0.046	0.536	0.048	0.537	0.049	0.539
3	0.082	0.659	0.090	0.658	0.094	0.659	0.095	0.661
4	0.122	0.731	0.134	0.731	0.139	0.732	0.142	0.734
5	0.162	0.783	0.177	0.783	0.185	0.785	0.188	0.786
6	0.202	0.823	0.221	0.824	0.229	0.825	0.234	0.826
7	0.242	0.855	0.264	0.857	0.275	0.858	0.281	0.859
8	0.283	0.883	0.308	0.885	0.321	0.886	0.327	0.887
9	0.323	0.907	0.352	0.909	0.366	0.911	0.373	0.911
10	0.430	0.959	0.465	0.960	0.480	0.961	0.489	0.961
11	0.538	1.000	0.577	1.000	0.594	1.000	0.605	1.000
12	0.607	0.991	0.643	0.991	0.659	0.992	0.668	0.992
13	0.676	0.964	0.709	0.964	0.723	0.966	0.731	0.967
14	0.745	0.923	0.775	0.922	0.787	0.924	0.794	0.926
15	0.813	0.867	0.841	0.865	0.852	0.866	0.858	0.869
16	0.883	0.791	0.907	0.784	0.915	0.784	0.921	0.785
17	0.952	0.666	0.972	0.625	0.980	0.605	0.984	0.592
18	0.964	0.608	0.979	0.570	0.985	0.552	0.988	0.540
19	0.976	0.512	0.986	0.480	0.990	0.464	0.992	0.454
20	0.988	0.320	0.993	0.299	0.995	0.289	0.996	0.283
21	1.000	0.000	1.000	0.000	1.000	0.000	1.000	0.000

Table 5.2 (b) Velocity vs. $y/(R_0 - R_i)$: Theoretical

$\alpha = 0.4,\ P/c = 4, S/c \doteq 19.4$

Re	17000		29500		44300		52600	
No	$y/(R_o - R_i)$	u/u_m	$y/(R_o - R_i)$	u/u_m	$y/(R_o - R_i)$	u/u_m	$y/(R_o - R_i)$	u/u_m
1	0.006	0.000	0.007	0.000	0.008	0.000	0.008	0.000
2	0.053	0.471	0.057	0.466	0.061	0.462	0.062	0.461
3	0.099	0.608	0.107	0.604	0.113	0.602	0.116	0.601
4	0.145	0.691	0.158	0.689	0.165	0.687	0.169	0.687
5	0.192	0.751	0.208	0.749	0.218	0.749	0.223	0.749
6	0.238	0.797	0.259	0.797	0.271	0.797	0.277	0.797
7	0.285	0.836	0.309	0.837	0.323	0.870	0.330	0.837
8	0.332	0.868	0.358	0.870	0.376	0.899	0.384	0.871
9	0.378	0.897	0.409	0.899	0.429	0.955	0.437	0.900
10	0.495	0.955	0.529	0.955	0.550	0.961	0.559	0.956
11	0.611	1.000	0.648	1.000	0.672	1.000	0.681	1.000
12	0.725	0.991	0.702	0.991	0.723	0.992	0.731	0.992
13	0.782	0.965	0.756	0.965	0.775	0.965	0.782	0.966
14	0.839	0.925	0.809	0.923	0.826	0.924	0.832	0.925
15	0.896	0.871	0.863	0.867	0.877	0.867	0.882	0.868
16	0.954	0.796	0.917	0.788	0.928	0.785	0.933	0.785
17	0.965	0.679	0.971	0.645	0.980	0.622	0.983	0.612
18	0.977	0.620	0.979	0.588	0.985	0.567	0.987	0.558
19	0.988	0.523	0.986	0.495	0.990	0.477	0.991	0.470
20	0.988	0.327	0.993	0.309	0.995	0.298	0.996	0.293
21	1.000	0.000	1.000	0.000	1.000	0.000	0.000	0.000

Table 5.2 (c) Velocity vs. $y/(R_o - R_i)$: Theoretical

$\alpha = 0.4,\ P/e = 8,\ S/e = 19.4$

Re	16500		22000		33000		49000	
No	$y/(R_o - R_i)$	u/u_m	$y/(R_o - R_i)$	u/u_m	$y/(R_o - R_i)$	u/u_m	$y/(R_o - R_i)$	u/u_m
1	0.017	0.00	0.019	0.000	0.026	0.000	0.027	0.000
2	0.071	0.394	0.076	0.389	0.086	0.377	0.089	0.375
3	0.125	0.544	0 132	0.539	0.147	0.530	0.151	0.528
4	0.178	0.639	0.188	0.635	0.207	0.629	0.212	0.628
5	0.232	0.709	0.244	0.707	0.268	0.702	0.274	0.701
6	0.285	0.764	0.299	0.763	0.329	0.761	0.336	0.760
7	0.339	0.810	0.355	0.809	0.390	0.809	0.398	0.809
8	0.392	0.849	0.411	0.849	0.450	0.851	0.459	0.851
9	0.446	0.883	0.467	0.884	0.511	0.887	0.521	0.887
10	0.568	0.948	0.591	0.948	0.635	0.949	0.645	0.949
11	0.691	1.000	0.714	1.000	0.759	1.000	0.769	1.000
12	0.735	0.992	0.756	0.991	0.796	0.991	0.805	0.991
13	0.779	0.967	0.798	0.966	0.833	0.966	0.841	0.966
14	0.823	0.928	0.840	0.927	0.870	0.925	0.876	0.925
15	0.867	0.876	0.882	0.873	0.907	0.869	0.912	0.869
16	0.911	0.807	0.923	0.799	0.944	0.790	0.948	0.789
17	0.955	0.702	0.966	0.683	0.981	0.646	0.983	0.638
18	0.966	0.642	0.974	0.624	0.986	0.589	0.987	0.582
19	0.978	0.542	0.983	0.526	0.990	0.496	0.992	0.489
20	0.989	0.339	0.991	0.329	0.995	0.310	0.996	0.306
21	1.000	0.000	1.000	0.000	1.000	0.000	1.000	0.000

Table 5.3(a) H/F vs. Re and P/e : Theoretical

$\alpha = 0.4$, $S/e = 9.7$, $Pr = 0.72$

P/e	Re	f_r	f_s	F f_r/f_s	Nu_r	Nu_s	H Nu_r/Nu_s	H/F
2	10000	0.0113	0.0094	1.20	44.48	35.89	1.24	1.03
2	50000	0.0094	0.0058	1.62	229.47	107.78	2.13	1.31
2	100000	0.0086	0.0050	1.72	445.60	184.29	2.42	1.41
4	10000	0.0140	0.0094	1.48	62.29	35.89	1.74	1.17
4	50000	0.0129	0.0058	2.22	362.92	107.78	3.37	1.52
4	100000	0.0127	0.0050	2.54	764.95	184.29	4.15	1.63
8	10000	0.0193	0.0094	2.05	98.22	35.89	2.74	1.34
8	50000	0.0217	0.0058	3.74	705.14	107.78	6.54	1.75
8	100000	0.0247	0.0050	4.94	1735.11	184.29	9.42	1.91

Table 5.3(b) H/F vs. Re and P/e : Theoretical

$\alpha = 0.4$, $S/e = 19.4$, $Pr = 0.72$

P/e	Re	f_r	f_s	$\frac{F}{f_r/f_s}$	Nu_r	Nu_s	$\frac{H}{Nu_r/Nu_s}$	H/F
2	10000	0.0108	0.0094	1.15	40.77	35.89	1.14	0.99
2	50000	0.0087	0.0058	1.50	204.75	107.78	1.90	1.27
2	100000	0.0079	0.0050	1.58	389.91	184.29	2.12	1.34
4	10000	0.0131	0.0094	1.39	55.73	35.89	1.55	1.12
4	50000	0.0115	0.0058	1.98	310.84	107.78	2.88	1.46
4	100000	0.0110	0.0050	2.20	636.34	184.29	3.45	1.57
8	10000	0.0173	0.0094	1.84	84.12	35.89	2.34	1.27
8	50000	0.0179	0.0058	3.09	557.46	107.78	5.17	1.67
8	100000	0.0192	0.0050	3.84	1289.53	184.29	6.99	1.82

Table 5.3(c) H/F vs. Re and P/e : Theoretical

$a = 0.4$, $S/e = 25$, $Pr = 0.72$

P/e	Re	f_r	f_s	F f_r/f_s	Nu_r	Nu_s	H Nu_r/Nu_s	H/F
2	10000	0.0106	0.0094	1.13	39.56	35.89	1.10	0.97
2	50000	0.0085	0.0058	1.47	196.84	107.78	1.83	1.24
2	100000	0.0077	0.0050	1.54	372.53	184.29	2.02	1.31
4	10000	0.0127	0.0094	1.35	53.62	35.89	1.49	1.10
4	50000	0.0111	0.0058	1.91	294.84	107.78	2.74	1.43
4	100000	0.0106	0.0050	2.12	598.06	184.29	3.25	1.53
8	10000	0.0166	0.0094	1.77	79.81	35.89	2.22	1.25
8	50000	0.0169	0.0058	2.91	515.98	107.78	4.79	1.65
8	100000	0.0178	0.0050	3.56	1172.21	184.29	6.36	1.79

Table 5.4(a) H/F vs. Re and α : Theoretical

$P/e = 2$, $S/e = 19.4$, $Pr = 0.72$

α	Re	f_r	f_s	F f_r/f_s	Nu_r	Nu_s	H Nu_r/Nu_s	H/F
0.2	10000	0.0118	0.0093	1.27	62.71	43.79	1.43	1.13
0.2	50000	0.0091	0.0058	1.57	320.14	131.01	2.44	1.55
0.2	100000	0.0083	0.0050	1.66	618.69	224.04	2.76	1.66
0.5	10000	0.0103	0.0094	1.09	36.11	34.13	1.06	0.97
0.5	50000	0.0084	0.0058	1.45	180.76	102.54	1.76	1.21
0.5	100000	0.0077	0.0049	1.57	342.44	175.23	1.95	1.24
0.8	10000	0.0091	0.0093	0.98	26.70	31.45	0.85	0.87
0.8	50000	0.0077	0.0057	1.35	139.83	94.43	1.48	1.10
0.8	100000	0.0069	0.0049	1.41	261.90	161.04	1.63	1.16
0.99	10000	0.0082	0.0093	0.88	24.00	30.68	0.78	0.89
0.99	50000	0.0070	0.0057	1.23	125.08	92.12	1.36	1.11
0.99	100000	0.0064	0.0049	1.36	233.58	156.90	1.49	1.14

Table 5.4(b) H/F vs. Re and α : Theoretical

$P/\epsilon = 4$, $S/\epsilon = 19.4$, $Pr = 0.72$

α	Re	f_r	f_s	F f_r/f_s	Nu_r	Nu_s	H Nu_r/Nu_s	H/F
0.2	10000	0.0139	0.0093	1.49	87.16	43.79	1.99	1.33
0.2	50000	0.0117	0.0058	2.02	488.41	131.01	3.73	1.85
0.2	100000	0.0110	0.0050	2.20	1005.78	224.04	4.49	2.04
0.5	10000	0.0126	0.0094	1.34	49.16	34.13	1.44	1.07
0.5	50000	0.0113	0.0058	1.95	273.28	102.54	2.67	1.37
0.5	100000	0.0108	0.0049	2.20	558.28	175.23	3.19	1.45
0.8	10000	0.0112	0.0093	1.20	37.90	31.45	1.21	1.01
0.8	50000	0.0105	0.0057	1.84	210.63	94.43	2.23	1.21
0.8	100000	0.0101	0.0049	2.06	427.24	161.04	2.65	1.29
0.99	10000	0.0103	0.0093	1.11	33.62	30.68	1.10	0.99
0.99	50000	0.0098	0.0057	1.72	192.43	92.12	2.09	1.22
0.99	100000	0.0095	0.0049	1.94	391.19	156.9	2.49	1.28

Table 5.4(c) H/F vs. Re and α : Theoretical

$P/c = 8$, $S/c = 19.4$, $Pr = 0.72$

α	Re	f_r	f_s	F f_r/f_s	Nu_r	Nu_s	H Nu_r/Nu_s	H/F
0.2	10000	0.0176	0.0093	1.89	131.91	43.79	3.01	1.59
0.2	50000	0.0166	0.0058	2.86	854.21	131.01	6.52	2.28
0.2	100000	0.0170	0.0050	3.40	1956.00	224.04	8.73	2.57
0.5	10000	0.0168	0.0094	1.79	73.93	34.13	2.17	1.21
0.5	50000	0.0179	0.0058	3.09	491.61	102.54	4.79	1.55
0.5	100000	0.0193	0.0049	3.94	1138.92	175.23	6.49	1.64
0.8	10000	0.0153	0.0093	1.65	56.93	31.45	1.81	1.10
0.8	50000	0.0172	0.0057	3.02	381.50	94.43	4.04	1.34
0.8	100000	0.0189	0.0049	3.86	887.19	161.04	5.51	1.43
0.99	10000	0.0143	0.0093	1.54	51.99	30.68	1.69	1.10
0.99	50000	0.0165	0.0057	2.89	362.81	92.12	3.94	1.36
0.99	100000	0.0182	0.0049	3.71	857.99	156.90	5.47	1.47

Table 5.5(a) H/F vs. Pr and P/e : Theoretical

$\alpha = 0.4$, $S/e = 9.7$, $Re = 10000$

P/e	Pr	f_r	f_s	F f_r/f_s	Nu_r	Nu_s	H Nu_r/Nu_s	H/F
2	0.10	0.0113	0.0094	1.20	11.66	13.54	0.86	0.72
2	0.72	0.0113	0.0094	1.20	44.48	35.89	1.24	1.03
2	1.0	0.0113	0.0094	1.20	57.58	42.63	1.35	1.13
2	10.0	0.0113	0.0094	1.20	440.69	123.03	3.58	2.98
2	30.0	0.0113	0.0094	1.20	1277.98	184.16	6.94	5.78
4	0.10	0.0140	0.0094	1.49	14.12	13.54	1.04	0.70
4	0.72	0.0140	0.0094	1.49	62.29	35.89	1.74	1.17
4	1.0	0.0140	0.0094	1.49	83.93	42.63	1.95	1.31
4	10.0	0.0140	0.0094	1.49	757.01	123.03	5.99	4.02
4	30.0	0.0140	0.0094	1.49	2187.26	184.16	11.88	7.97
8	0.10	0.0193	0.0094	2.05	19.07	13.54	1.41	0.69
8	0.72	0.0193	0.0094	2.05	98.24	35.89	2.74	1.34
8	1.0	0.0193	0.0094	2.05	133.47	42.63	3.13	1.53
8	10.0	0.0193	0.0094	2.05	1263.07	123.03	10.27	5.01
8	30.0	0.0193	0.0094	2.05	3772.45	184.16	20.48	9.99

Table 5.5(b) H/F vs.Pr and P/ϵ : Theoretical

$\alpha = 0.4$, $S/\epsilon = 9.7$, $Re = 50000$

P/ϵ	Pr	f_r	f_s	F f_r/f_s	Nu_r	Nu_s	H Nu_r/Nu_s	H/F
2	0.10	0.0094	0.0058	1.62	40.90	29.26	1.40	0.86
2	0.72	0.0094	0.0058	1.62	229.50	107.78	2.13	1.31
2	1.0	0.0094	0.0058	1.62	313.19	132.08	2.37	1.46
2	10.0	0.0094	0.0058	1.62	2990.07	435.20	6.87	4.24
2	30.0	0.0094	0.0058	1.62	8936.26	670.11	13.33	8.23
4	0.10	0.0129	0.0058	2.22	58.02	29.26	1.98	0.89
4	0.72	0.0129	0.0058	2.22	362.99	107.78	3.37	1.52
4	1.0	0.0129	0.0058	2.22	500.33	132.08	3.79	1.71
4	10.0	0.0129	0.0058	2.22	4912.75	435.20	11.29	5.09
4	30.0	0.0129	0.0058	2.22	14717.82	670.11	21.96	9.89
8	0.10	0.0217	0.0058	3.74	106.69	29.26	3.65	0.98
8	0.72	0.0217	0.0058	3.74	705.35	107.78	6.54	1.75
8	1.0	0.0217	0.0058	3.74	975.08	132.08	7.38	1.97
8	10.0	0.0217	0.0058	3.74	9642.19	435.20	22.16	5.93
8	30.0	0.0217	0.0058	3.74	28901.91	670.11	43.13	11.53

Table 5.5(c) H/F vs. Pr and P/ϵ : Theoretical

$\alpha = 0.4$, $S/\epsilon = 9.7$, $Re = 100000$

P/ϵ	Pr	f_r	f_s	F f_r/f_s	Nu_r	Nu_s	H Nu_r/Nu_s	H/F
2	0.10	0.0086	0.0050	1.72	72.64	45.89	1.58	0.92
2	0.72	0.0086	0.0050	1.72	445.67	184.29	2.42	1.41
2	1.0	0.0086	0.0050	1.72	612.90	227.91	2.69	1.56
2	10.0	0.0086	0.0050	1.72	5981.00	784.78	7.62	4.43
2	30.0	0.0086	0.0050	1.72	17908.73	1221.29	14.66	8.52
4	0.10	0.0127	0.0050	2.54	114.54	45.89	2.50	0.98
4	0.72	0.0127	0.0050	2.54	765.12	184.29	4.15	1.63
4	1.0	0.0127	0.0050	2.54	1058.70	227.91	4.65	1.83
4	10.0	0.0127	0.0050	2.54	10494.14	784.78	13.37	5.26
4	30.0	0.0127	0.0050	2.54	31461.61	1221.29	25.76	10.14
8	0.10	0.0247	0.0050	4.94	253.80	45.89	5.53	1.12
8	0.72	0.0247	0.0050	4.94	1735.76	184.29	9.42	1.91
8	1.0	0.0247	0.0050	4.94	2404.23	227.91	10.55	2.14
8	10.0	0.0247	0.0050	4.94	23887.49	784.78	30.44	6.16
8	30.0	0.0247	0.0050	4.94	71627.00	1221.29	58.65	11.87

Table 5.6(a) H/F vs. Pr and P/e : Theoretical

$\alpha = 0.4$, $S/e = 19.4$, $Re = 10000$

P/e	Pr	f_r	f_s	$\frac{F}{f_r/f_s}$	Nu_r	Nu_s	$\frac{H}{Nu_r/Nu_s}$	H/F
2	0.10	0.0108	0.0094	1.15	11.13	13.54	0.82	0.71
2	0.72	0.0108	0.0094	1.15	40.78	35.89	1.14	0.99
2	1.0	0.0108	0.0094	1.15	52.29	42.63	1.23	1.07
2	10.0	0.0108	0.0094	1.15	374.37	123.03	3.04	1.15
2	30.0	0.0108	0.0094	1.15	1069.93	184.16	5.81	5.05
4	0.10	0.0131	0.0094	1.39	13.23	13.54	0.98	0.71
4	0.72	0.0131	0.0094	1.39	55.74	35.89	1.55	1.12
4	1.0	0.0131	0.0094	1.39	73.68	42.63	1.73	1.24
4	10.0	0.0131	0.0094	1.39	632.19	123.03	5.14	3.70
4	30.0	0.0131	0.0094	1.39	1868.29	184.16	10.14	7.29
8	0.10	0.0173	0.0094	1.84	17.11	13.54	1.26	0.68
8	0.72	0.0173	0.0094	1.84	84.14	35.89	2.34	1.27
8	1.0	0.0173	0.0094	1.84	113.81	42.63	2.67	1.45
8	10.0	0.0173	0.0094	1.84	1062.84	123.03	8.64	4.70
8	30.0	0.0173	0.0094	1.84	3170.81	184.16	17.22	9.36

Table 5.6(b) H/F vs. Pr and P/e : Theoretical

$\alpha = 0.4$, $S/e = 19.4$, $Re = 50000$

P/e	Pr	f_r	f_s	F f_r/f_s	Nu_r	Nu_s	H Nu_r/Nu_s	H/F
2	0.10	0.0087	0.0058	1.50	37.89	29.26	1.29	0.86
2	0.72	0.0087	0.0058	1.50	204.77	107.78	1.90	1.27
2	1.0	0.0087	0.0058	1.50	277.97	132.08	2.10	1.40
2	10.0	0.0087	0.0058	1.50	2610.47	435.20	5.99	3.99
2	30.0	0.0087	0.0058	1.50	7789.19	670.11	11.62	7.75
4	0.10	0.0115	0.0058	1.98	51.14	29.26	1.75	0.88
4	0.72	0.0115	0.0058	1.98	310.89	107.78	2.28	1.45
4	1.0	0.0115	0.0058	1.98	427.61	132.08	3.24	1.64
4	10.0	0.0115	0.0058	1.98	4176.17	435.20	9.60	4.85
4	30.0	0.0115	0.0058	1.98	12505.74	670.11	18.66	9.42
8	0.10	0.0179	0.0058	3.09	85.21	29.26	2.91	0.94
8	0.72	0.0179	0.0058	3.09	557.60	107.78	5.17	1.67
8	1.0	0.0179	0.0058	3.09	770.54	132.08	5.83	1.89
8	10.0	0.0179	0.0058	3.09	7613.38	435.20	17.49	5.66
8	30.0	0.0179	0.0058	3.09	22819.36	670.11	34.05	11.02

Table 5.6(c) H/F vs. Pr and P/e : Theoretical

$\alpha = 0.4$, $S/e = 19.4$, $Re = 100000$

P/e	Pr	f_r	f_s	$\frac{F}{f_r/f_s}$	Nu_r	Nu_s	$\frac{H}{Nu_r/Nu_s}$	H/F
2	0.10	0.0079	0.0050	1.58	65.91	45.89	1.44	0.92
2	0.72	0.0079	0.0050	1.58	389.97	184.29	2.12	1.34
2	1.0	0.0079	0.0050	1.58	534.30	227.91	2.34	1.48
2	10.0	0.0079	0.0050	1.58	5159.39	784.78	6.57	4.16
2	30.0	0.0079	0.0050	1.58	15434.54	1221.29	12.64	8.00
4	0.10	0.0110	0.0050	2.20	97.12	45.89	2.12	0.96
4	0.72	0.0110	0.0050	2.20	636.47	184.29	3.45	1.57
4	1.0	0.0110	0.0050	2.20	879.69	227.91	3.86	1.75
4	10.0	0.0110	0.0050	2.20	8696.22	784.78	11.08	5.04
4	30.0	0.0110	0.0050	2.20	26066.06	1221.29	21.34	9.70
8	0.10	0.0192	0.0050	3.84	188.87	45.89	4.12	1.07
8	0.72	0.0192	0.0050	3.84	1289.93	184.29	7.00	1.82
8	1.0	0.0192	0.0050	3.84	1786.77	227.91	7.84	2.04
8	10.0	0.0192	0.0050	3.84	17755.05	784.78	22.62	5.89
8	30.0	0.0192	0.0050	3.84	53239.82	1221.29	43.59	11.35

Table 5.7(a) H/F vs. Pr and P/e : Theoretical

$\alpha = 0.4$, $S/e = 25.0$, $Re = 10000$

P/e	Pr	f_r	f_s	F f_r/f_s	Nu_r	Nu_s	H Nu_r/Nu_s	H/F
2	0.10	0.0106	0.0094	1.13	10.95	13.54	0.82	0.71
2	0.72	0.0106	0.0094	1.13	39.55	35.89	1.14	0.99
2	1.0	0.0106	0.0094	1.13	50.54	42.63	1.23	1.07
2	10.0	0.0106	0.0094	1.13	352.21	123.03	3.04	1.15
2	30.0	0.0106	0.0094	1.13	999.79	184.16	5.81	5.05
4	0.10	0.0127	0.0094	1.35	12.93	13.54	0.95	0.70
4	0.72	0.0127	0.0094	1.35	53.62	35.89	1.49	1.10
4	1.0	0.0127	0.0094	1.35	70.66	42.63	1.66	1.23
4	10.0	0.0127	0.0094	1.35	597.42	123.03	4.86	3.60
4	30.0	0.0127	0.0094	1.35	1762.05	184.16	9.57	7.09
8	0.10	0.0166	0.0094	1.77	16.51	13.54	1.22	0.69
8	0.72	0.0166	0.0094	1.77	79.81	35.89	2.22	1.25
8	1.0	0.0166	0.0094	1.77	107.73	42.63	2.53	1.44
8	10.0	0.0166	0.0094	1.77	1000.27	123.03	8.13	4.59
8	30.0	0.0166	0.0094	1.77	2982.47	184.16	16.19	9.15

Table 5.7(b) H/F vs.Pr and P/e : Theoretical

$a = 0.4$, $S/e = 25.0$, $Re = 50000$

P/e	Pr	f_r	f_s	F f_r/f_s	Nu_r	Nu_s	H Nu_r/Nu_s	H/F
2	0.10	0.0085	0.0058	1.47	36.94	29.26	1.26	0.86
2	0.72	0.0085	0.0058	1.47	196.84	107.78	1.83	1.24
2	1.0	0.0085	0.0058	1.47	266.63	132.08	2.02	1.37
2	10.0	0.0085	0.0058	1.47	2485.19	435.20	5.71	3.88
2	30.0	0.0085	0.0058	1.47	7409.61	670.11	11.06	7.52
4	0.10	0.0111	0.0058	1.91	49.07	29.26	1.68	0.88
4	0.72	0.0111	0.0058	1.91	294.84	107.78	2.74	1.43
4	1.0	0.0111	0.0058	1.91	405.13	132.08	3.07	1.61
4	10.0	0.0111	0.0058	1.91	3946.59	435.20	9.07	4.75
4	30.0	0.0111	0.0058	1.91	11815.74	670.11	17.63	9.23
8	0 10	0.0168	0.0058	2.90	79.26	79.26	2.71	0.93
8	0.72	0.0168	0.0058	2.90	515.98	515.98	4.79	1.65
8	1.0	0.0168	0.0058	2.90	713.26	713.26	5.40	1.86
8	10.0	0.0168	0.0058	2.90	7043.66	435.20	16.18	5.58
8	30.0	0.0168	0.0058	2.90	21110.86	670.11	31.50	10.86

Table 5.7(c) H/F vs. Pr and P/c : Theoretical

$\alpha = 0.4$, $S/c = 25.0$, $Re = 100000$

P/c	Pr	f_r	f_s	F f_r/f_s	Nu_r	Nu_s	H Nu_r/Nu_s	H/F
2	0.10	0.0077	0.0050	1.54	63.84	45.89	1.39	0.90
2	0.72	0.0077	0.0050	1.54	372.42	184.29	2.02	1.31
2	1.0	0.0077	0.0050	1.54	509.42	227.91	2.24	1.45
2	10.0	0.0077	0.0050	1.54	4894.72	784.78	6.24	4.05
2	30.0	0.0077	0.0050	1.54	14636.17	1221.29	11.98	7.78
4	0.10	0.0105	0.0050	2.10	92.06	45.89	2.01	0.96
4	0.72	0.0105	0.0050	2.10	598.06	184.29	3.25	1.55
4	1.0	0.0105	0.0050	2.10	826.16	227.91	3.62	1.72
4	10.0	0.0105	0.0050	2.10	8156.22	784.78	10.39	4.95
4	30.0	0.0105	0.0050	2.10	24444.93	1221.29	20.02	9.53
8	0.10	0.0177	0.0050	3.54	171.92	45.89	3.75	1.06
8	0.72	0.0177	0.0050	3.54	1172.21	184.29	6.36	1.80
8	1.0	0.0177	0.0050	3.54	1623.62	227.91	7.12	2.01
8	10.0	0.0177	0.0050	3.54	16131.90	784.78	20.56	5.81
8	30.0	0.0177	0.0050	3.54	48372.29	1221.29	39.61	11.19

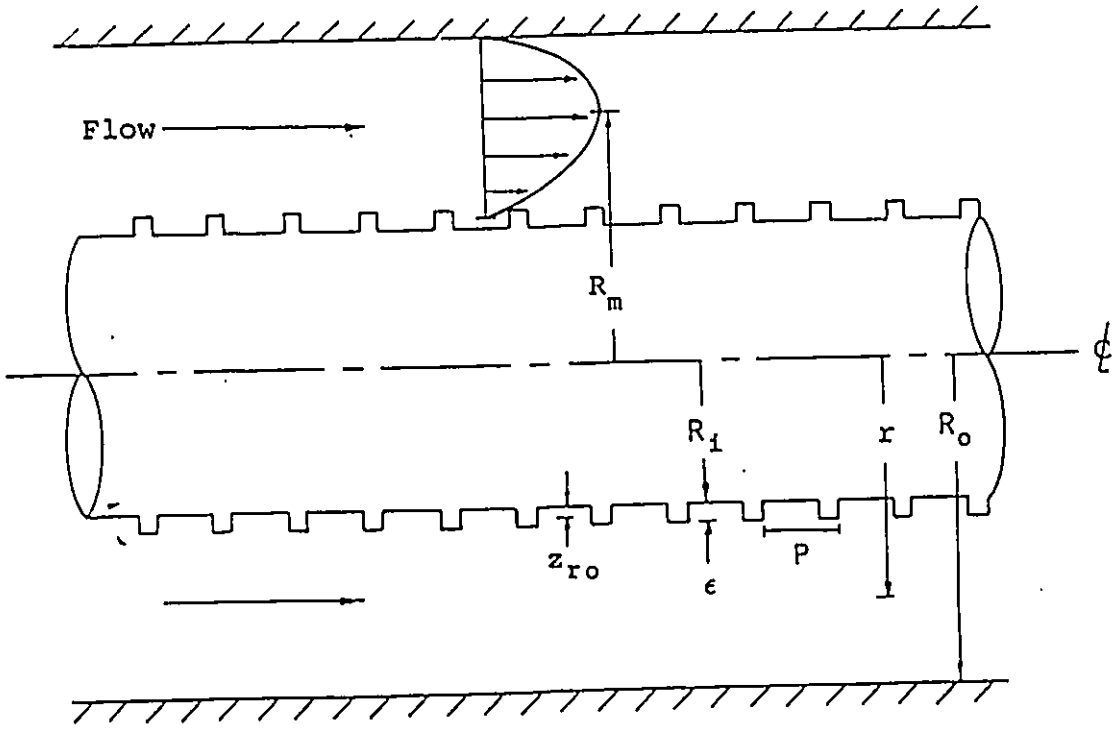

Fig. 3.1 Idealized Model

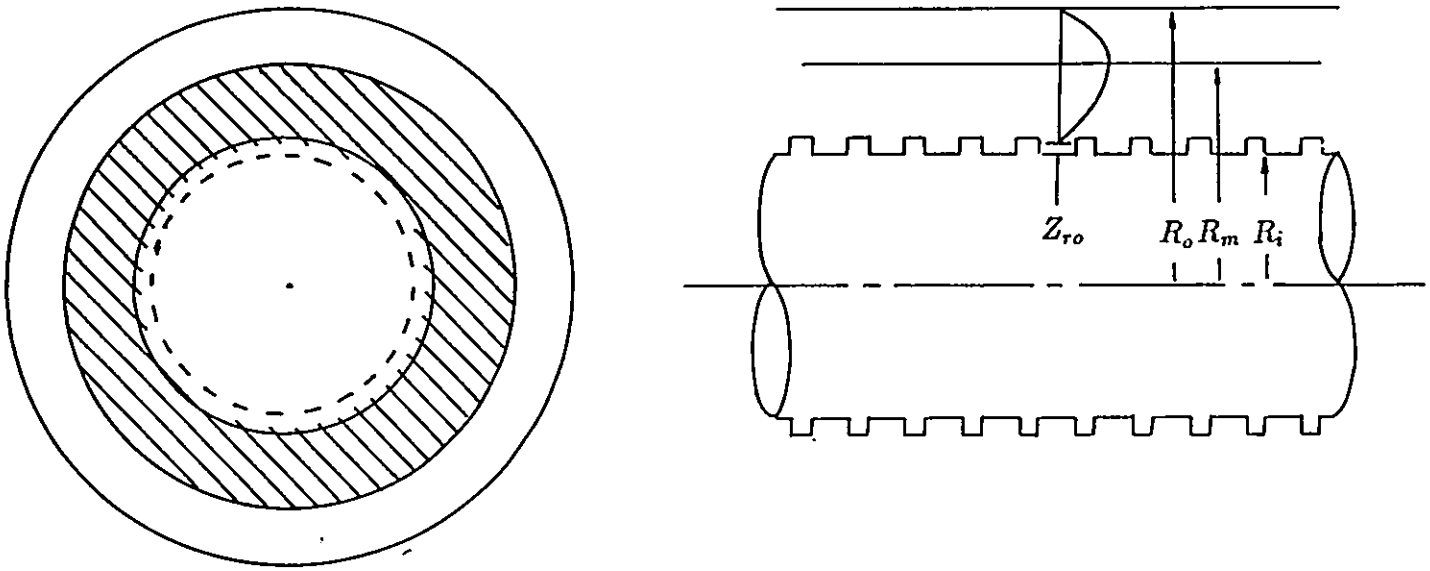

Fig. 3.2 A Force Balance Made on the Element

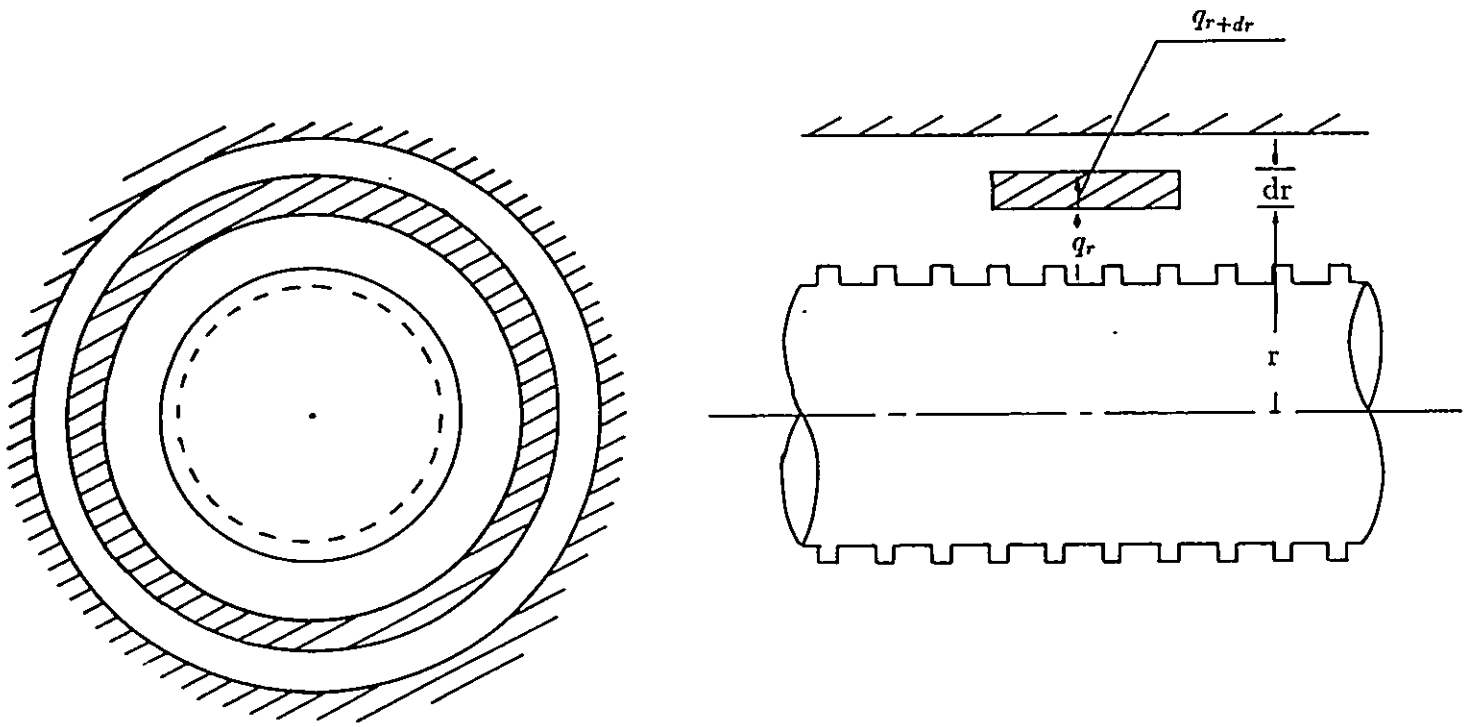

Fig. 3.3 An Energy Balance Made on the Element

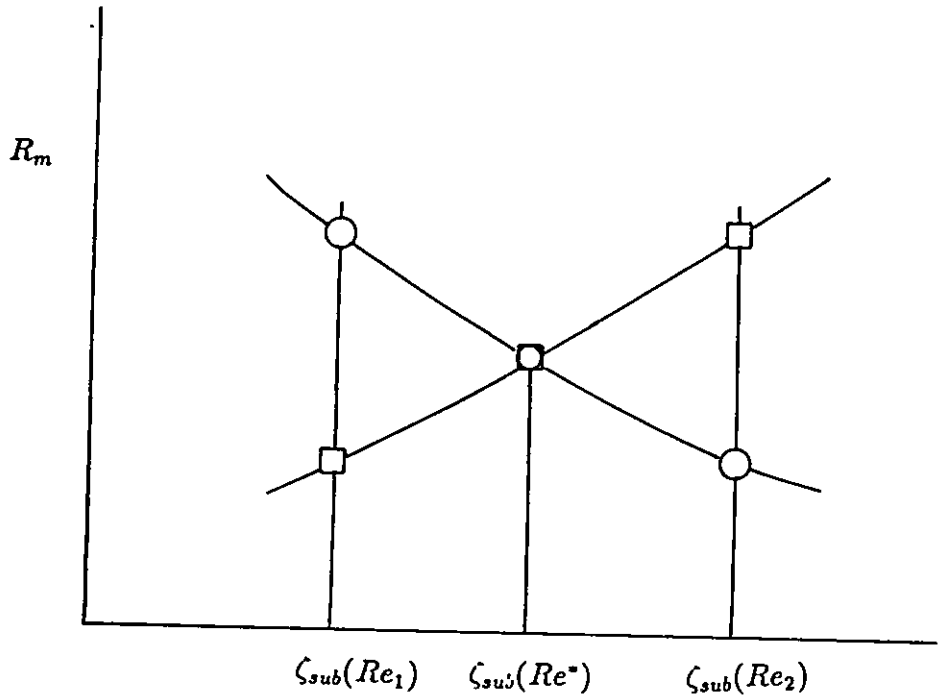

Fig. 3.4 Diagram of Two Variable Iteration Method

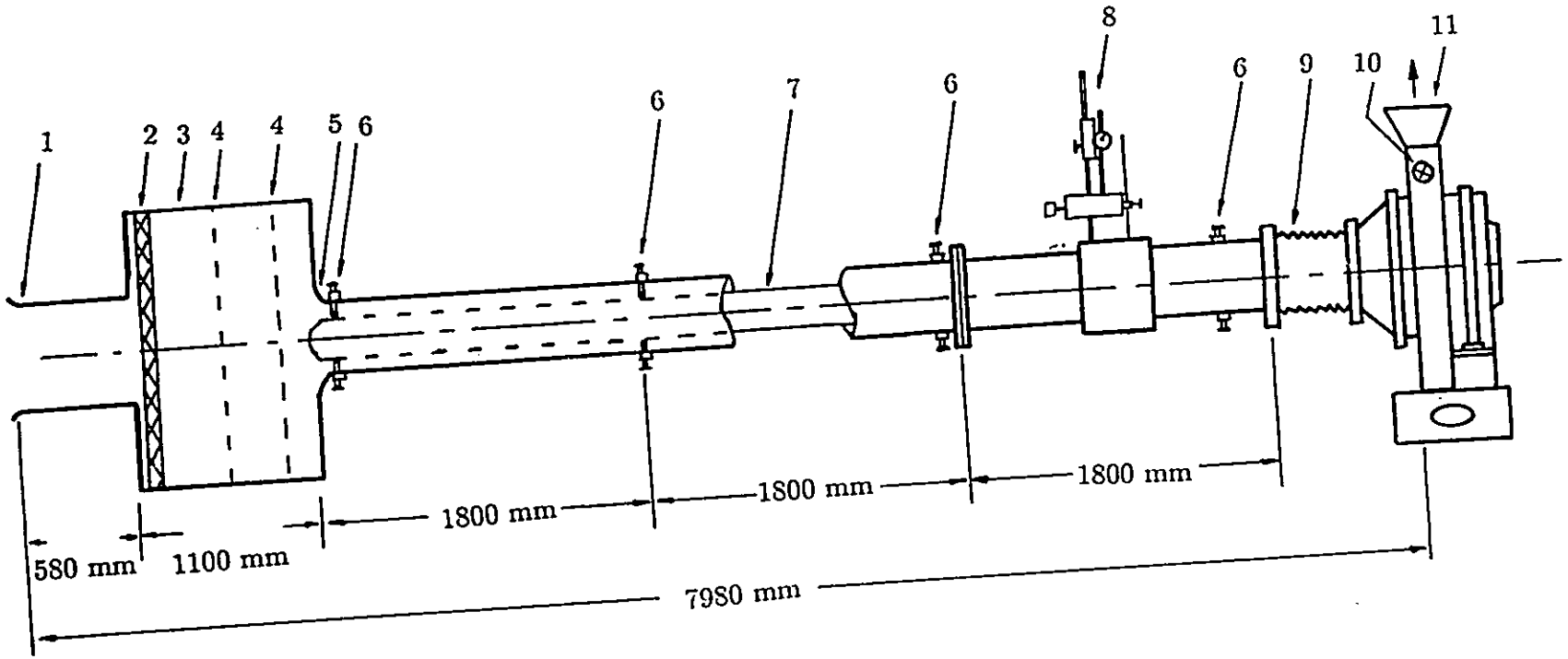

1. B. S. orifice
2. Air filter
3. Settling chamber
4. Settling screen
5. Bell mouth inlet and trip wire
6. Core tube support
7. Core tube
8. Pitot tube and traversing mechanism
9. Flexible tube
10. Flow control valve
11. Blower

Fig. 4.1 Schematic Diagram of Experimental Setup

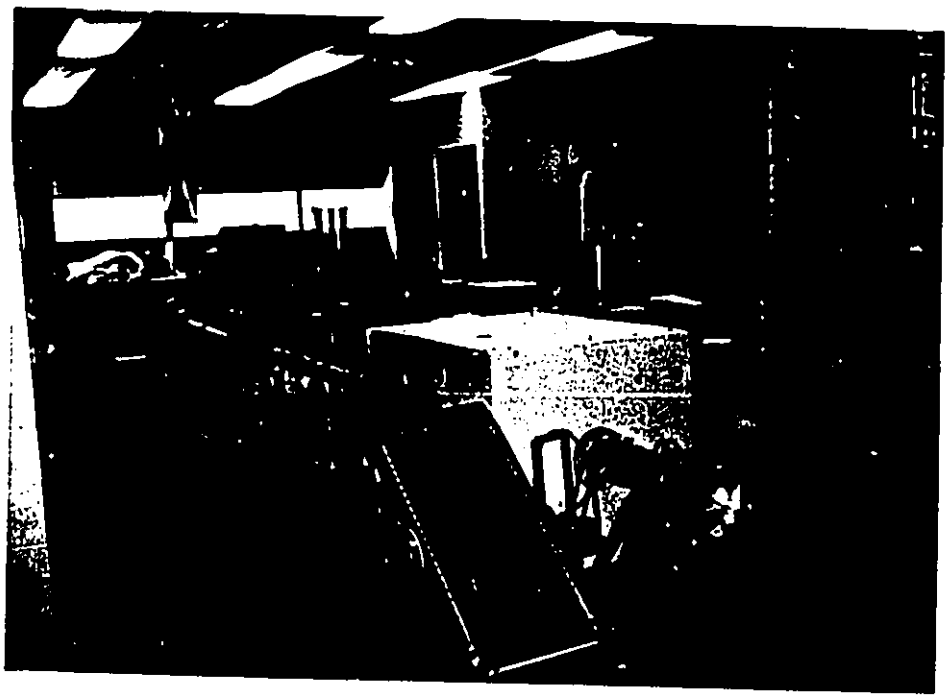

Fig.4.2 The Channel Assembly

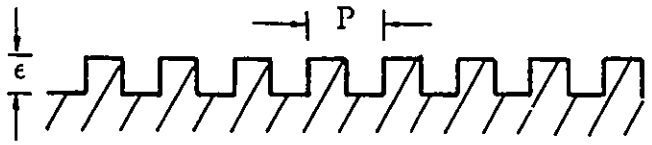

$P/\epsilon = 2$

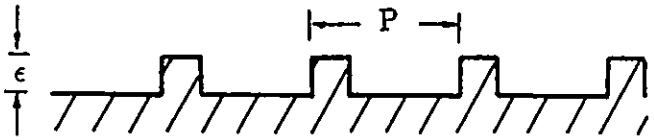

$P/\epsilon = 4$

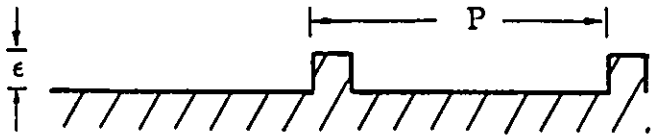

$P/\epsilon = 8$

Fig. 4.3 Pitch to Height Ratio used in the Experiment

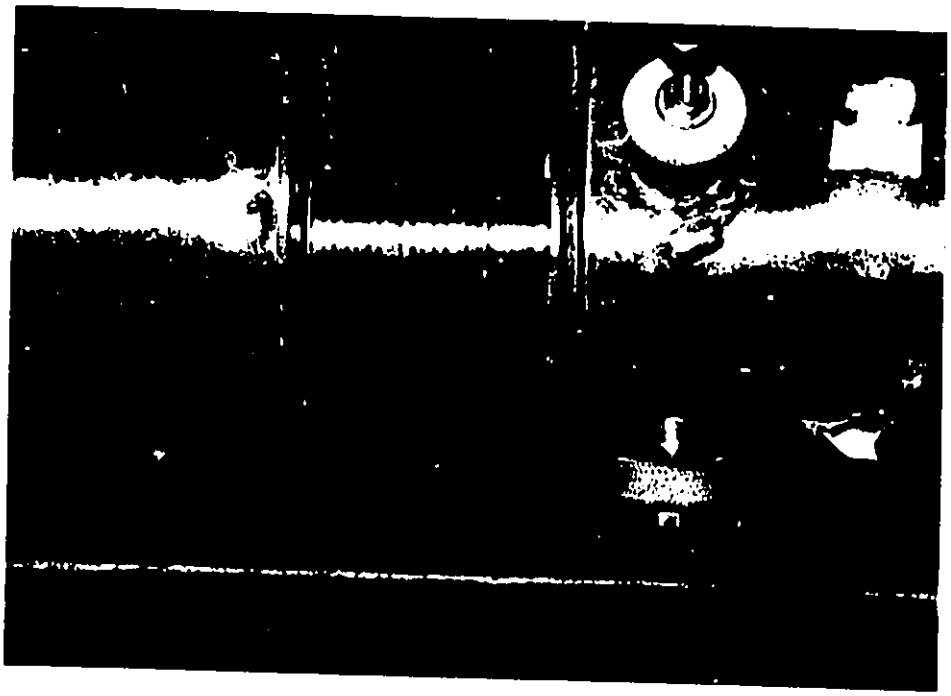

Fig. 4.4 The Core Tube

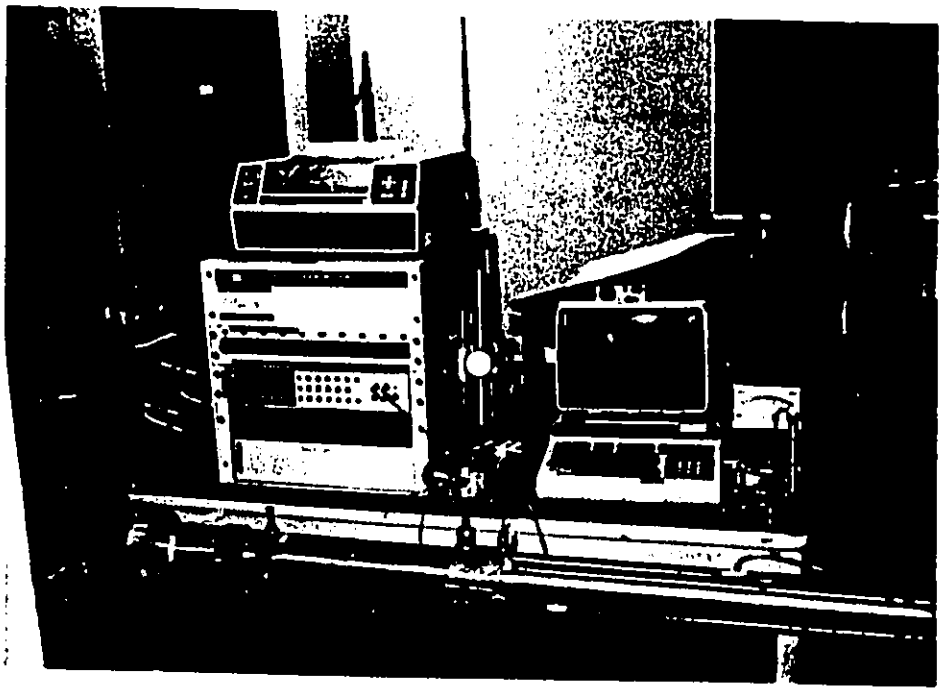

Fig. 4.5 Data Recording System

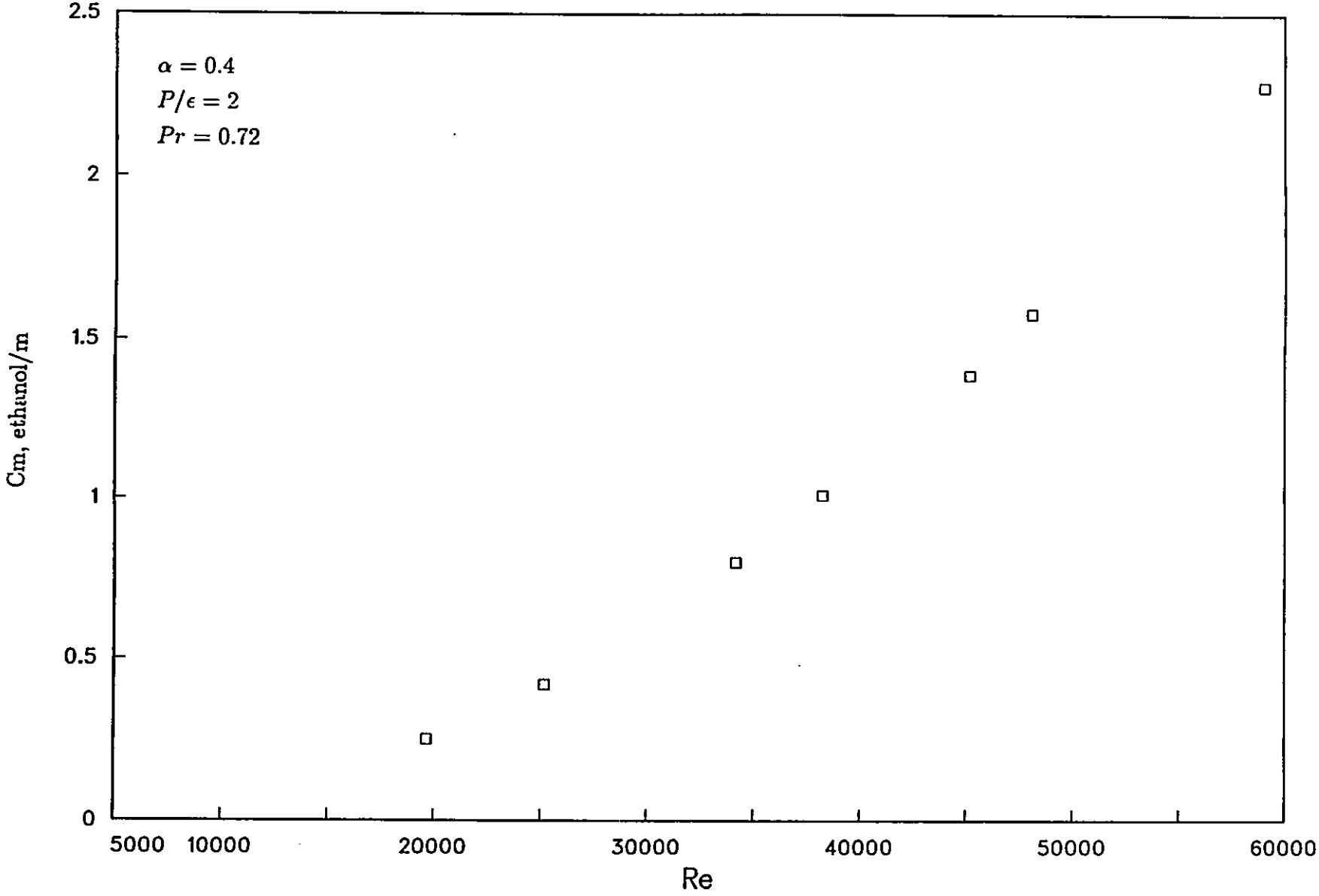

Fig. 4.6 Calibration of the Orifice

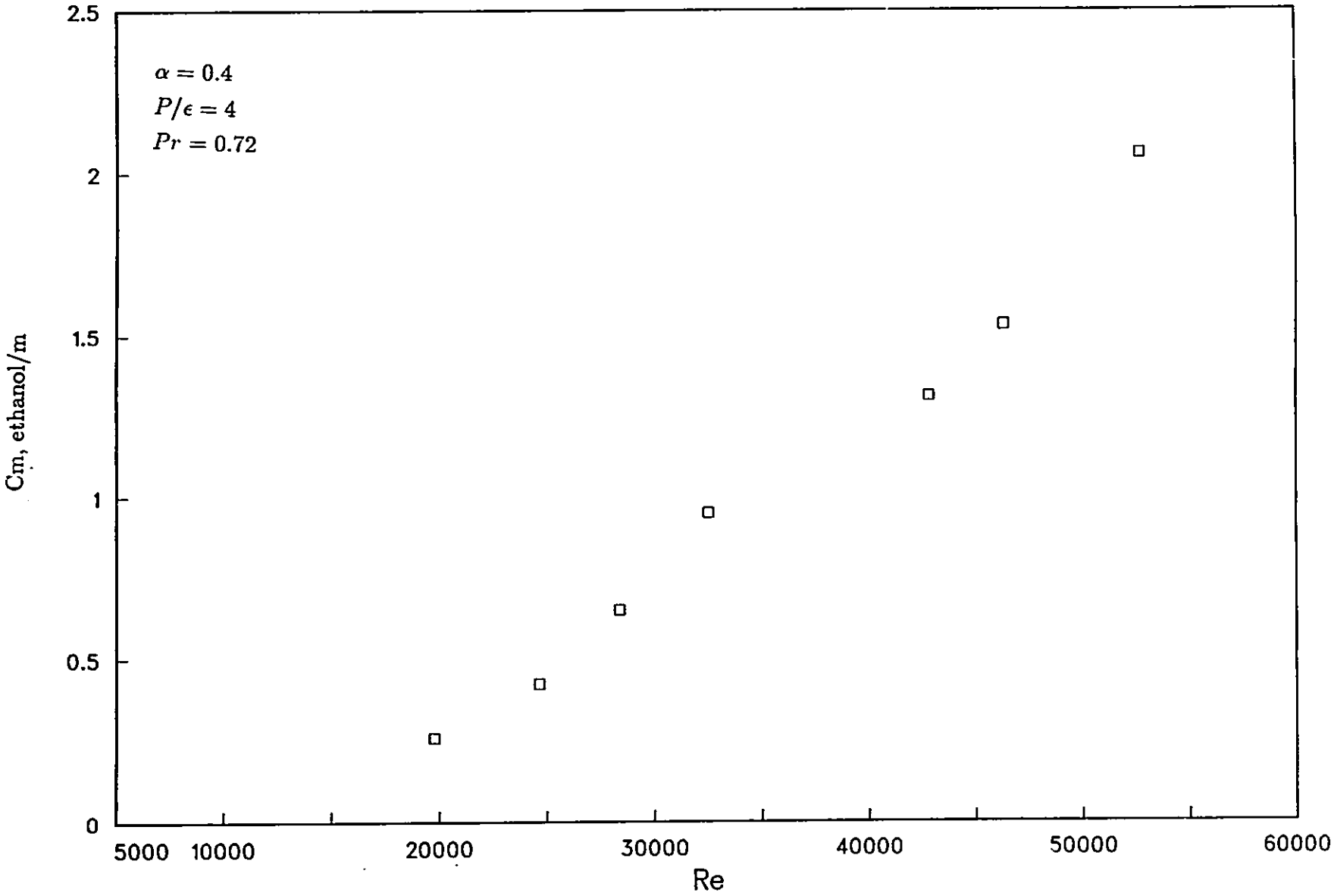

Fig. 4.7 Calibration of the Orifice

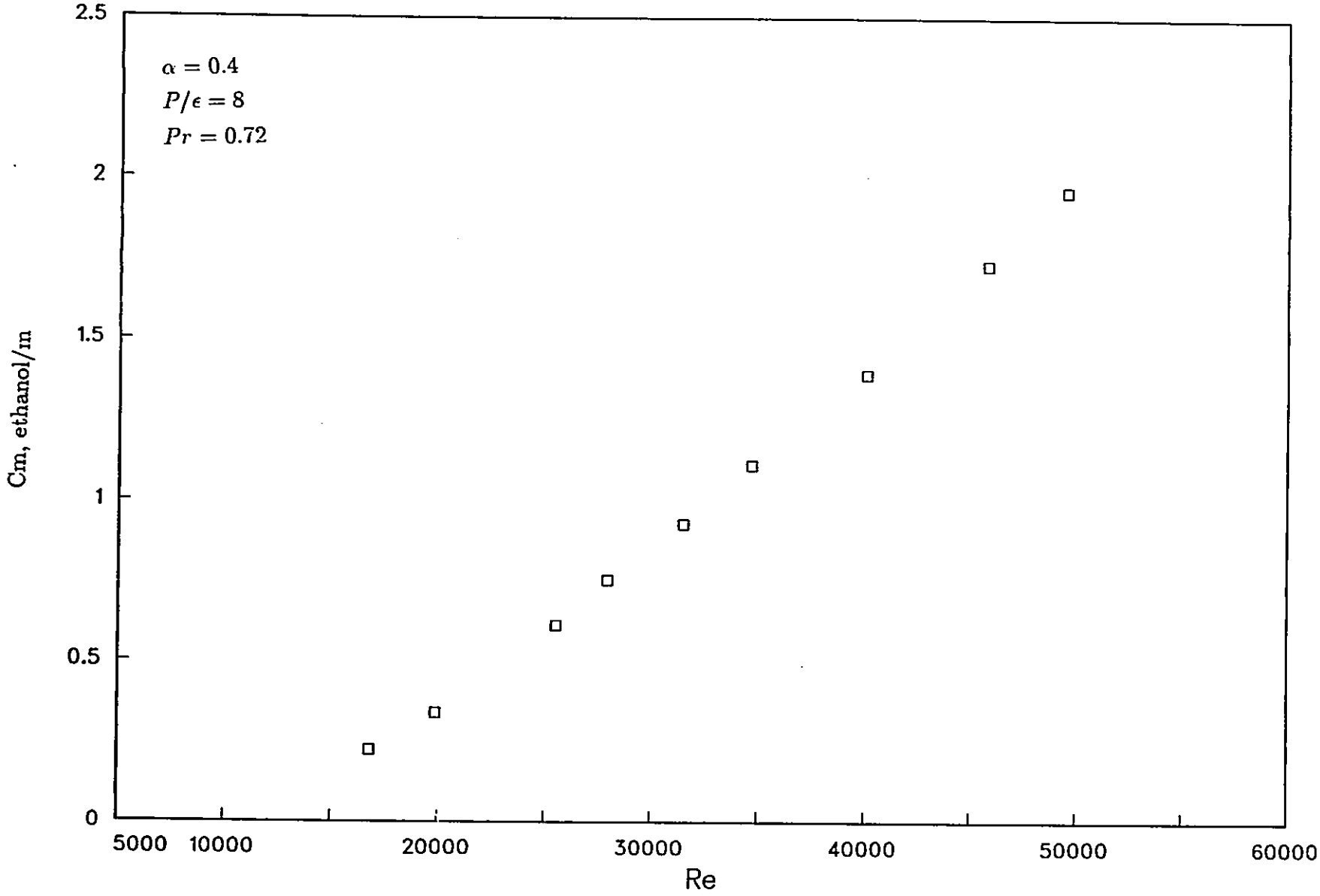

Fig. 4.8 Calibration of the Orifice

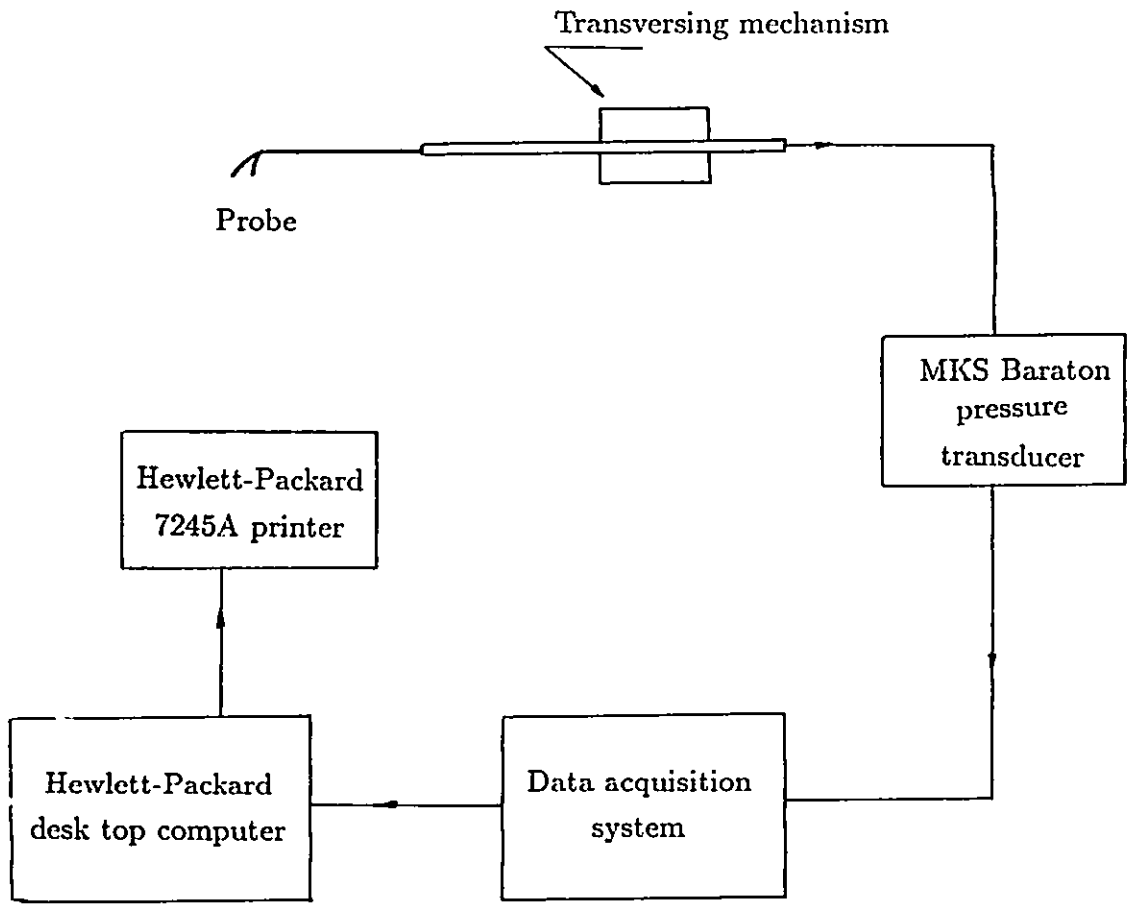

Fig. 4.9 Flowchart of Measurements

unit: mm

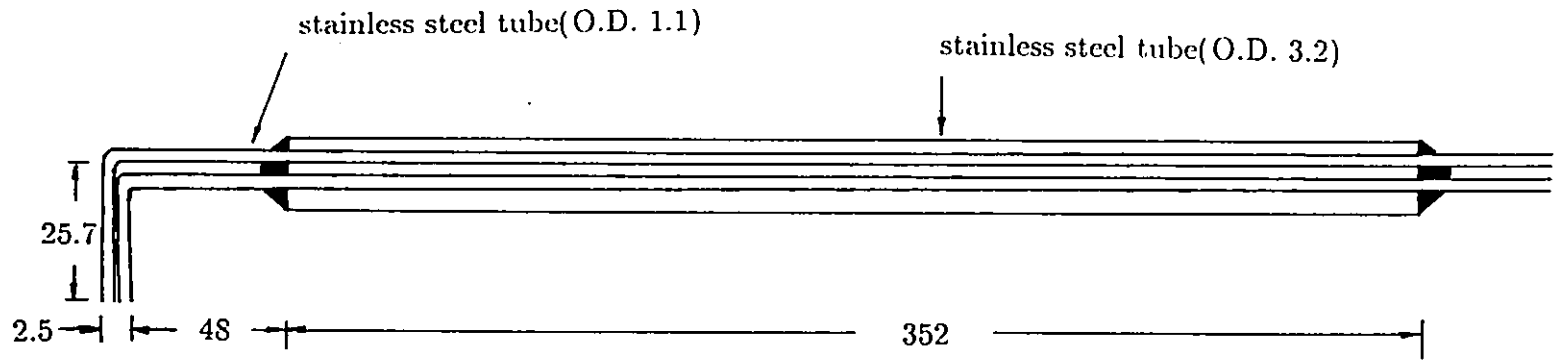

Fig. 4.9 (a) Double Pitot Tube

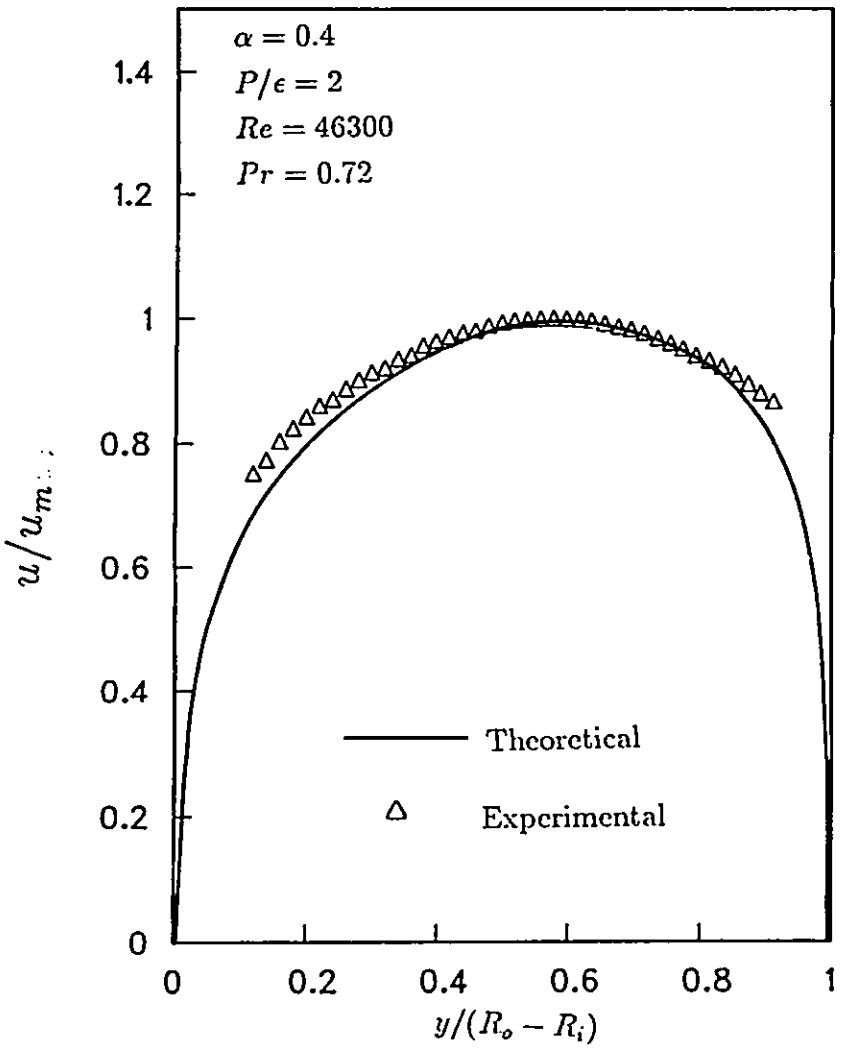

Fig. 4.10 Velocity Distribution

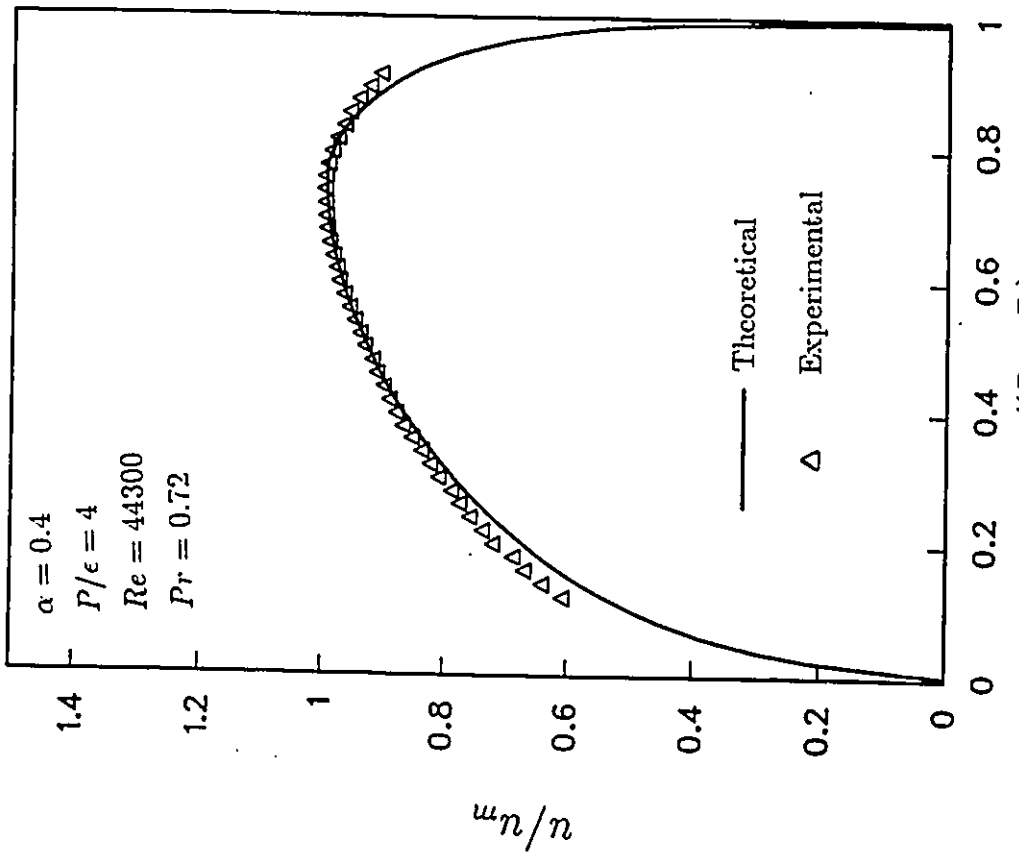

Fig. 4.11 Velocity Distribution

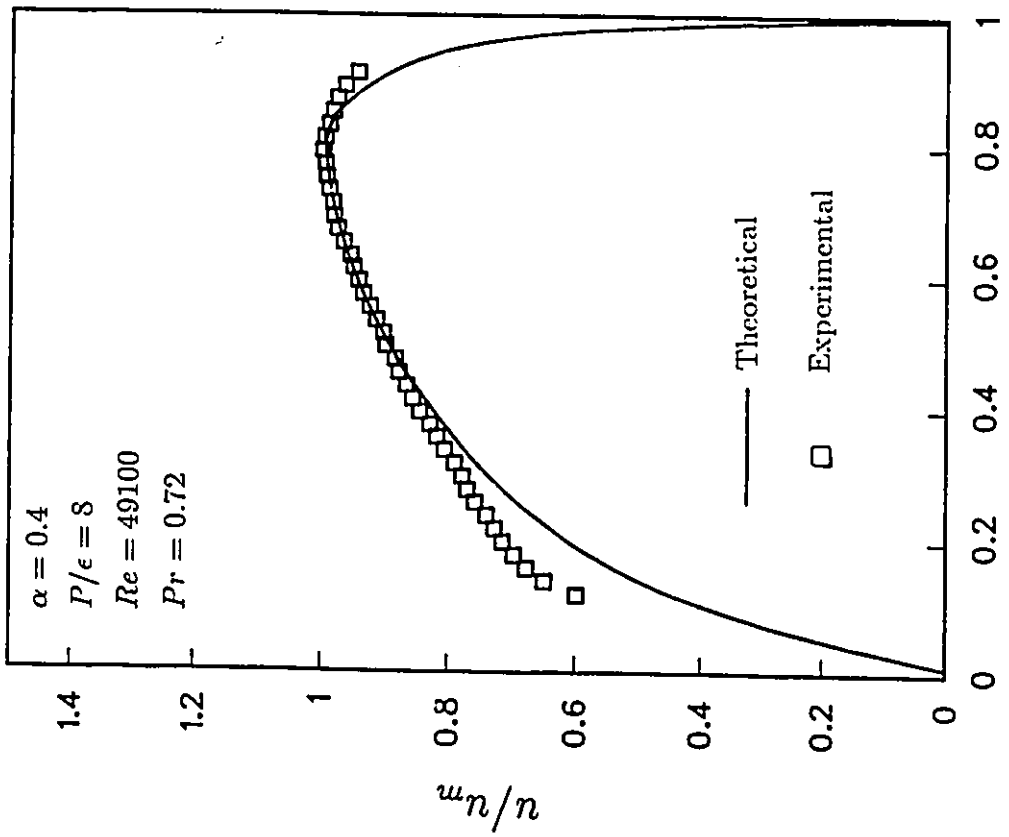

Fig. 4.12 Velocity Distribution

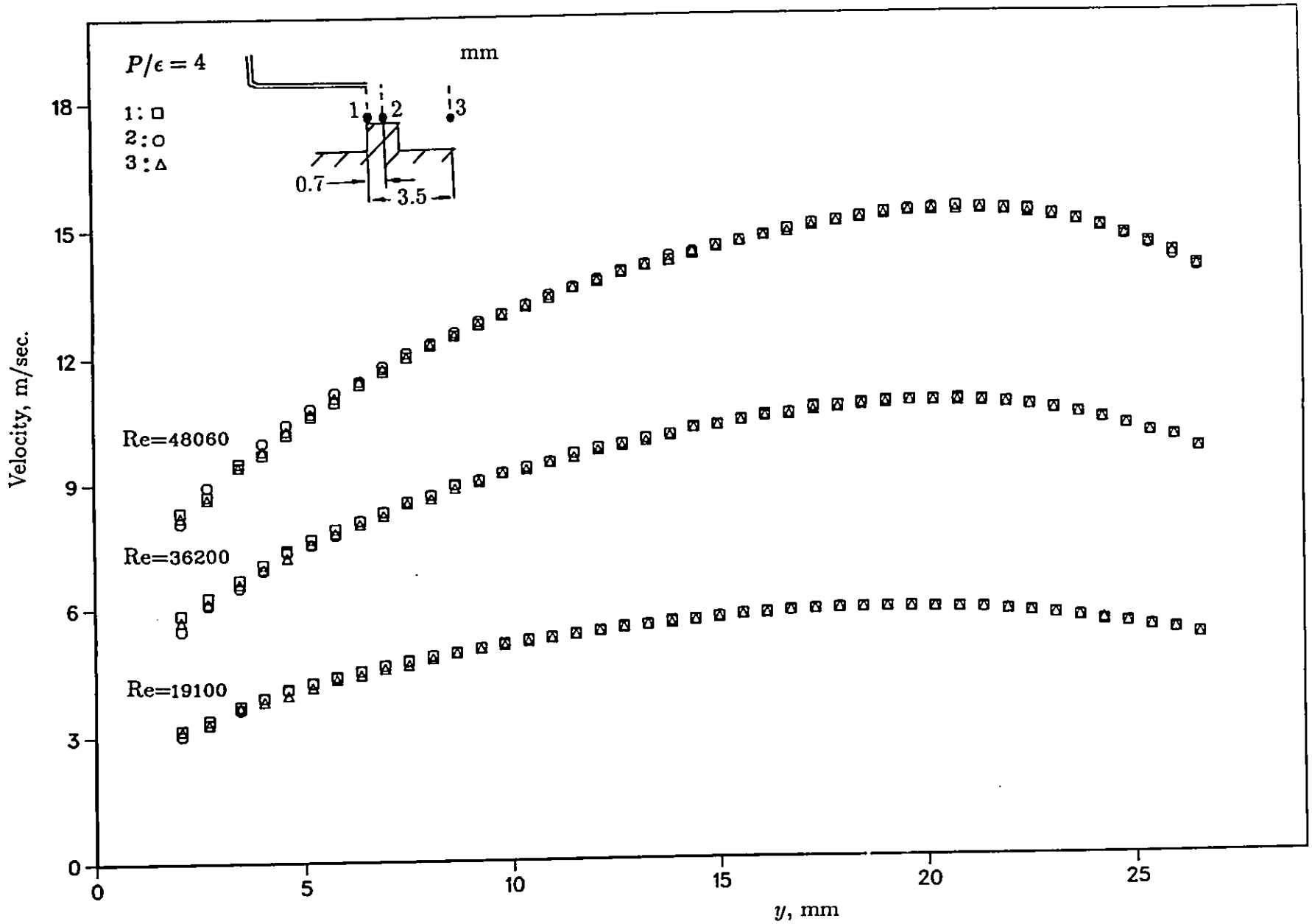

Fig. 4.13 Velocity Profiles at Different Location

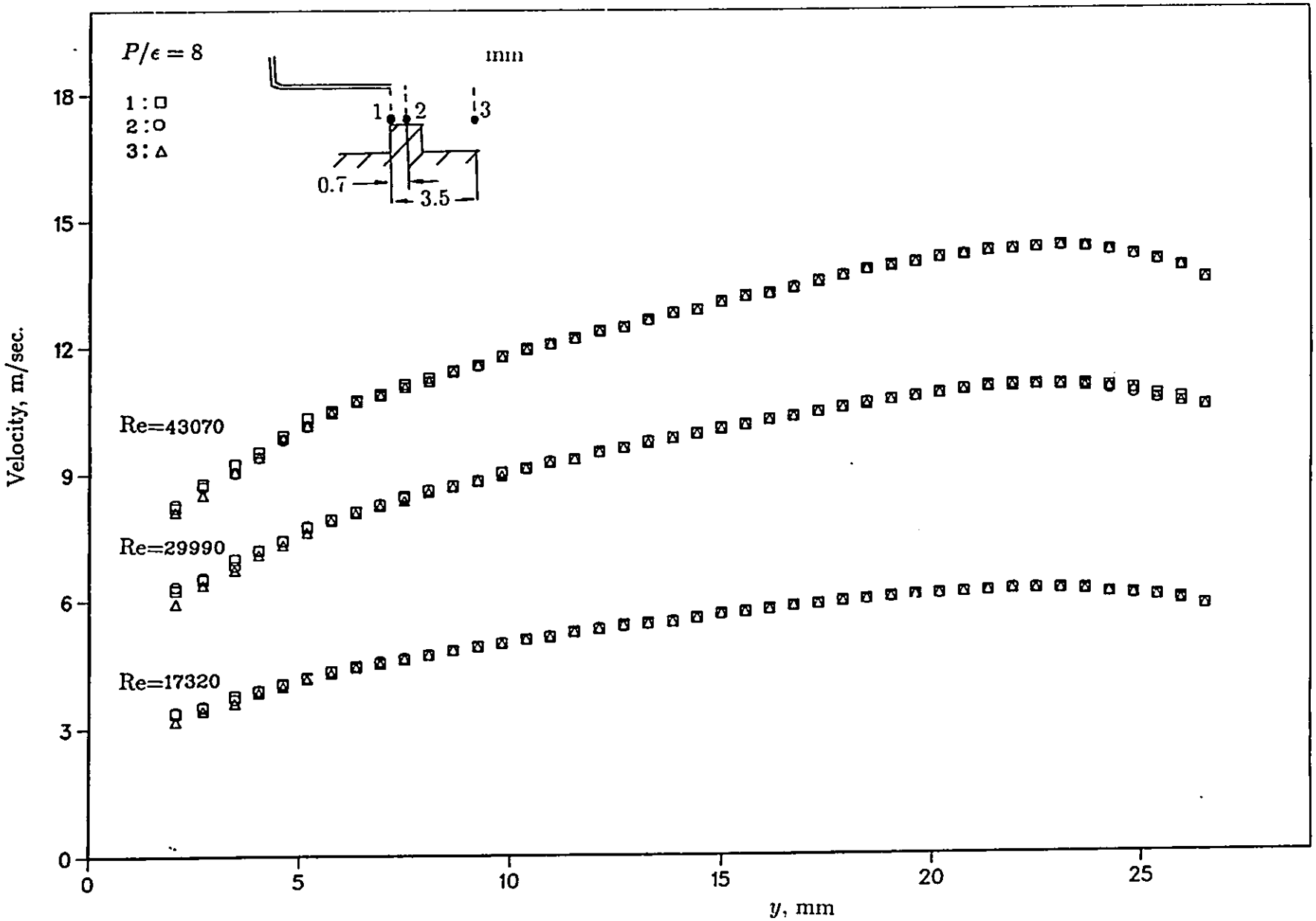

Fig. 4.14 Velocity Profiles at Different Location

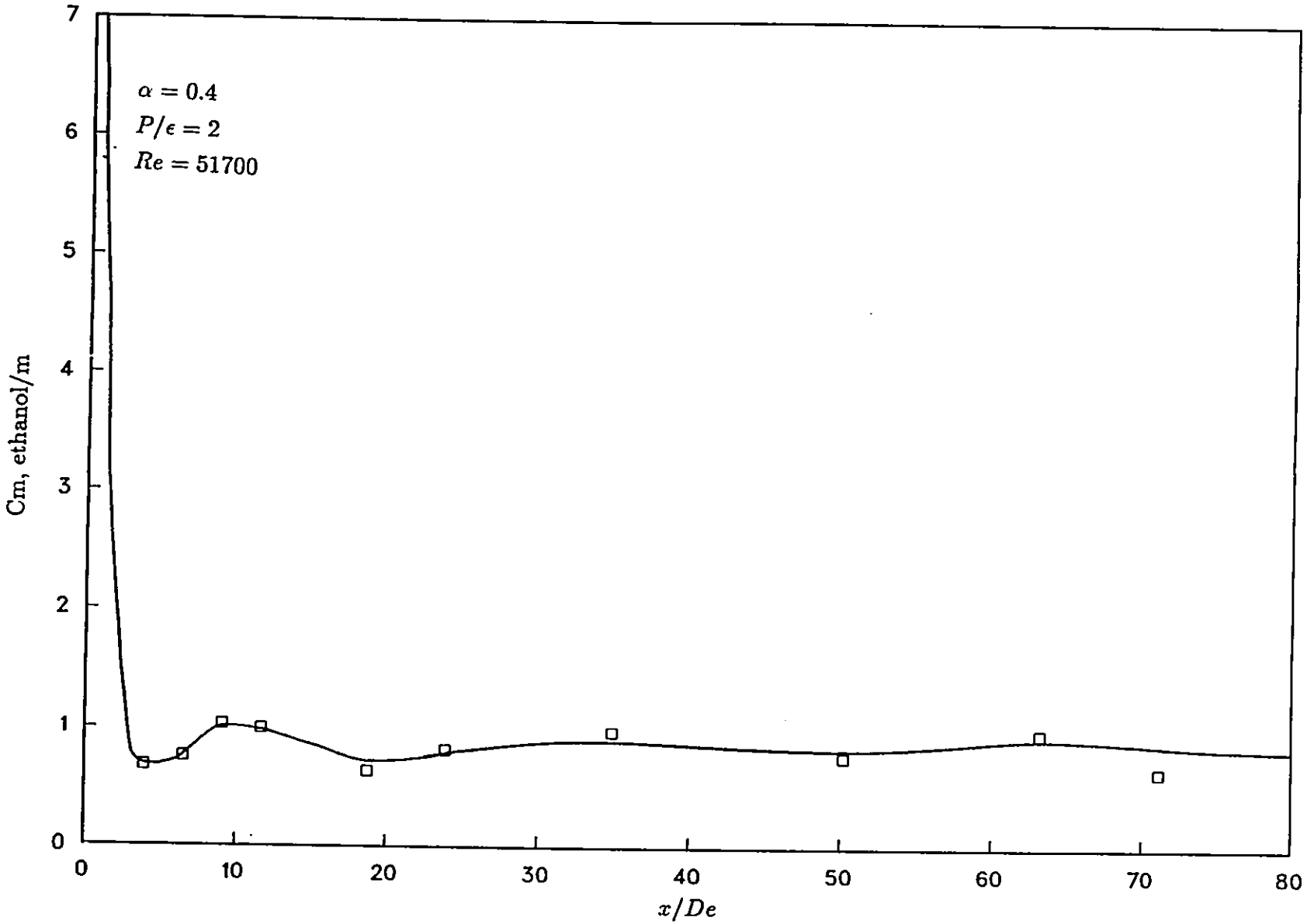

Fig. 4.15 Static Pressure Difference along the Test Section

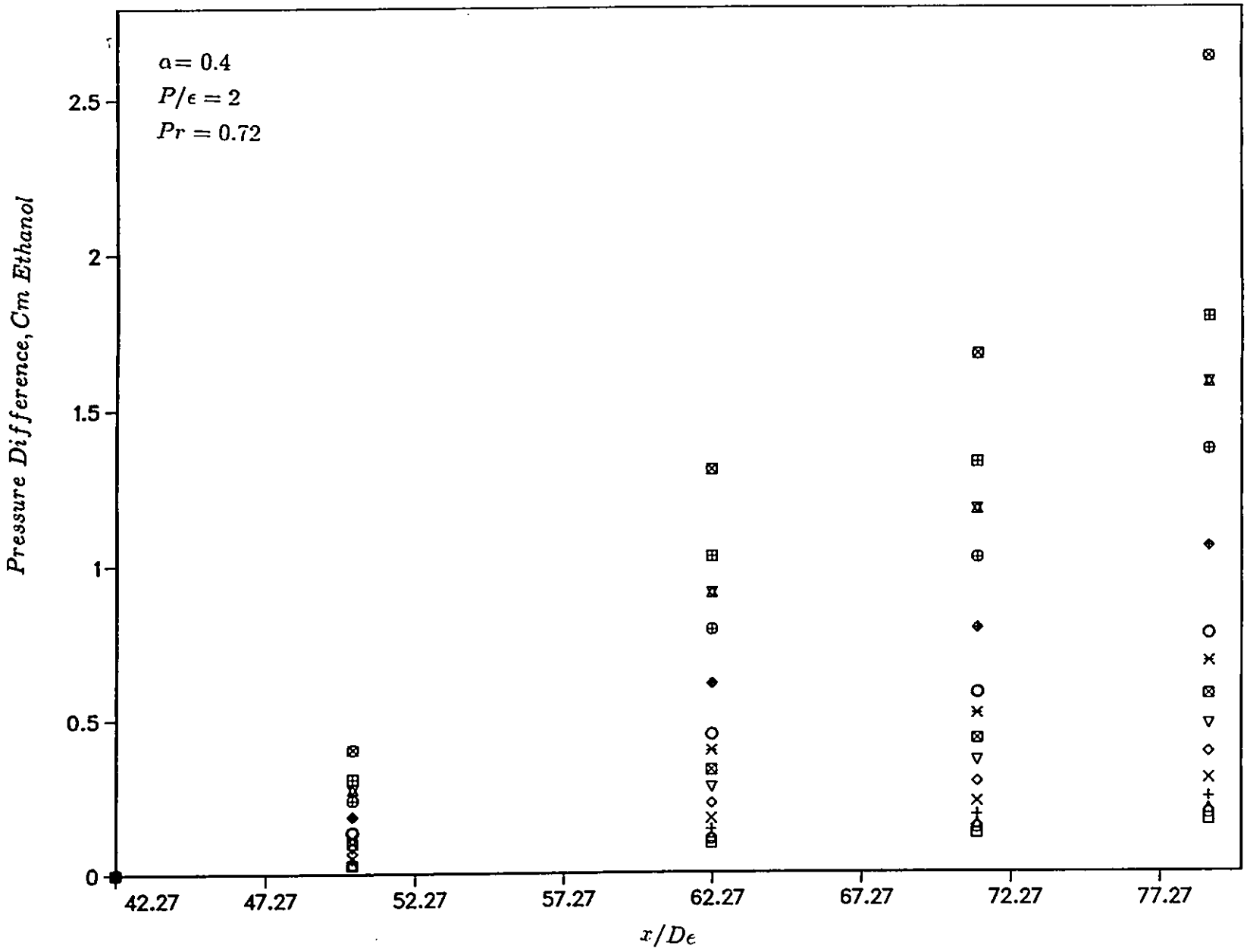

Fig. 4.16 Static Pressure Difference along the Test Section at Developed Region (Static Pressure Difference vs. x/De)

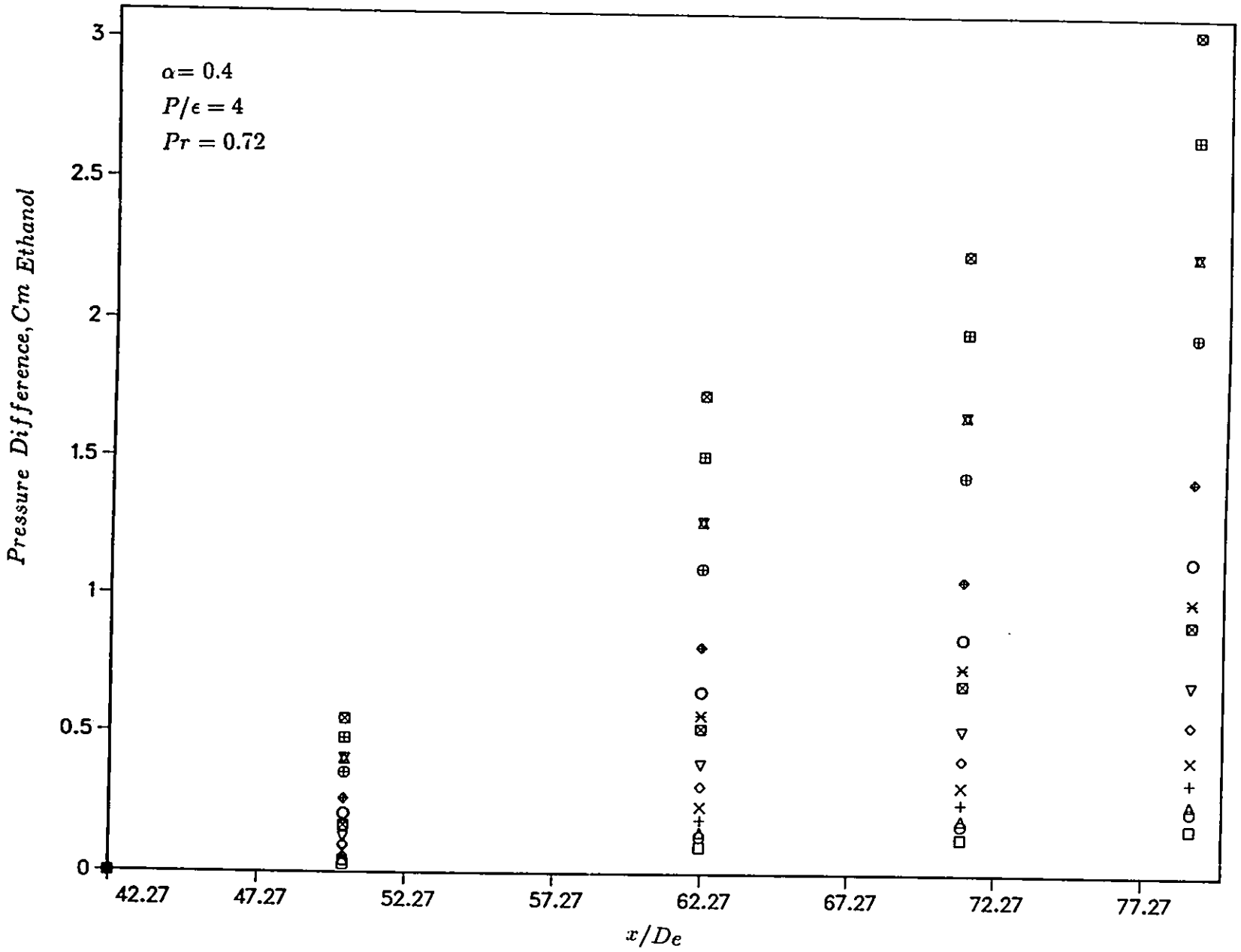

Fig. 4.17 Static Pressure Difference along the Test Section at Developed Region (Static Pressure Difference vs. x/De)

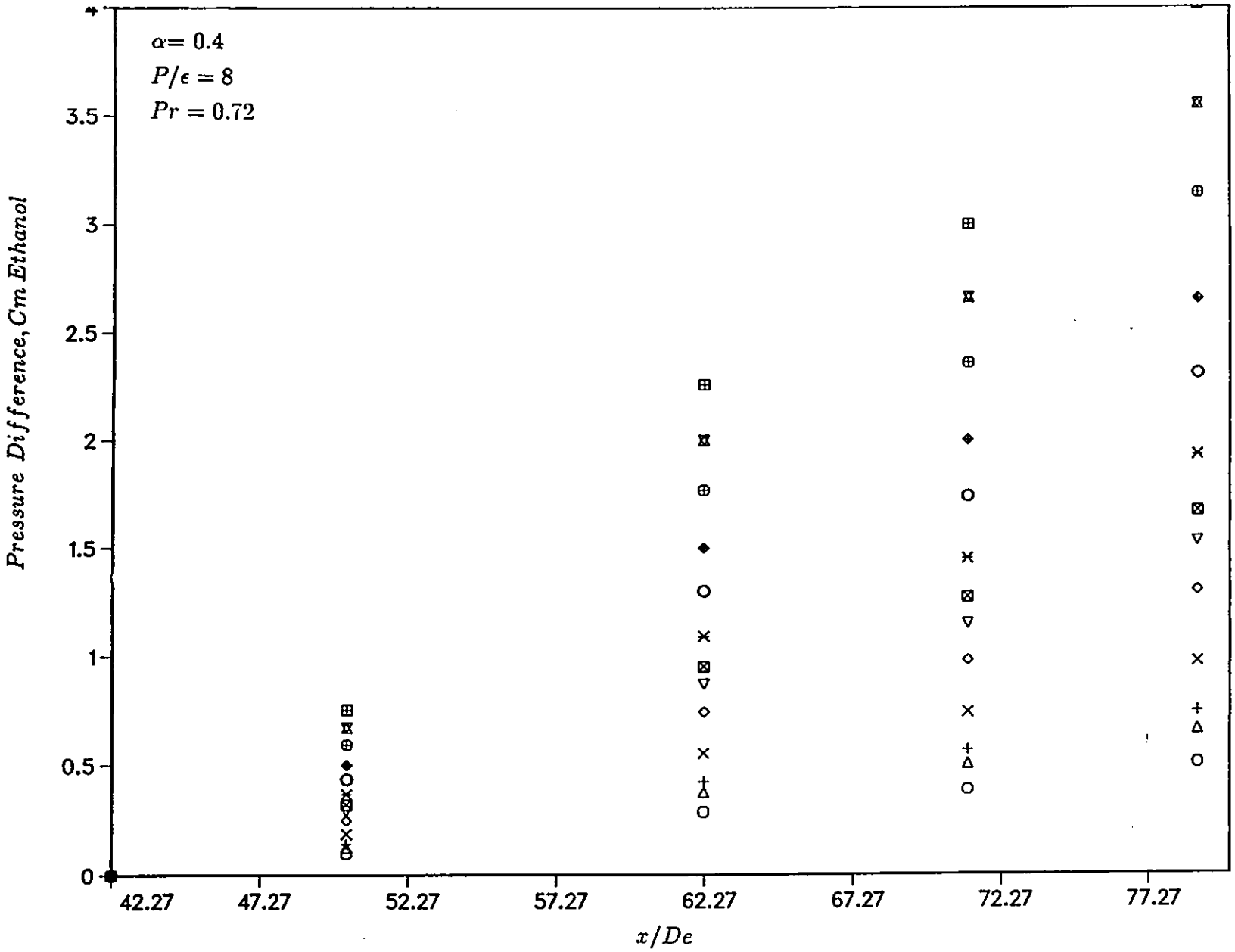

Fig. 4.18 Static Pressure Difference along the Test Section at Developed Region (Static Pressure Difference vs. x/De)

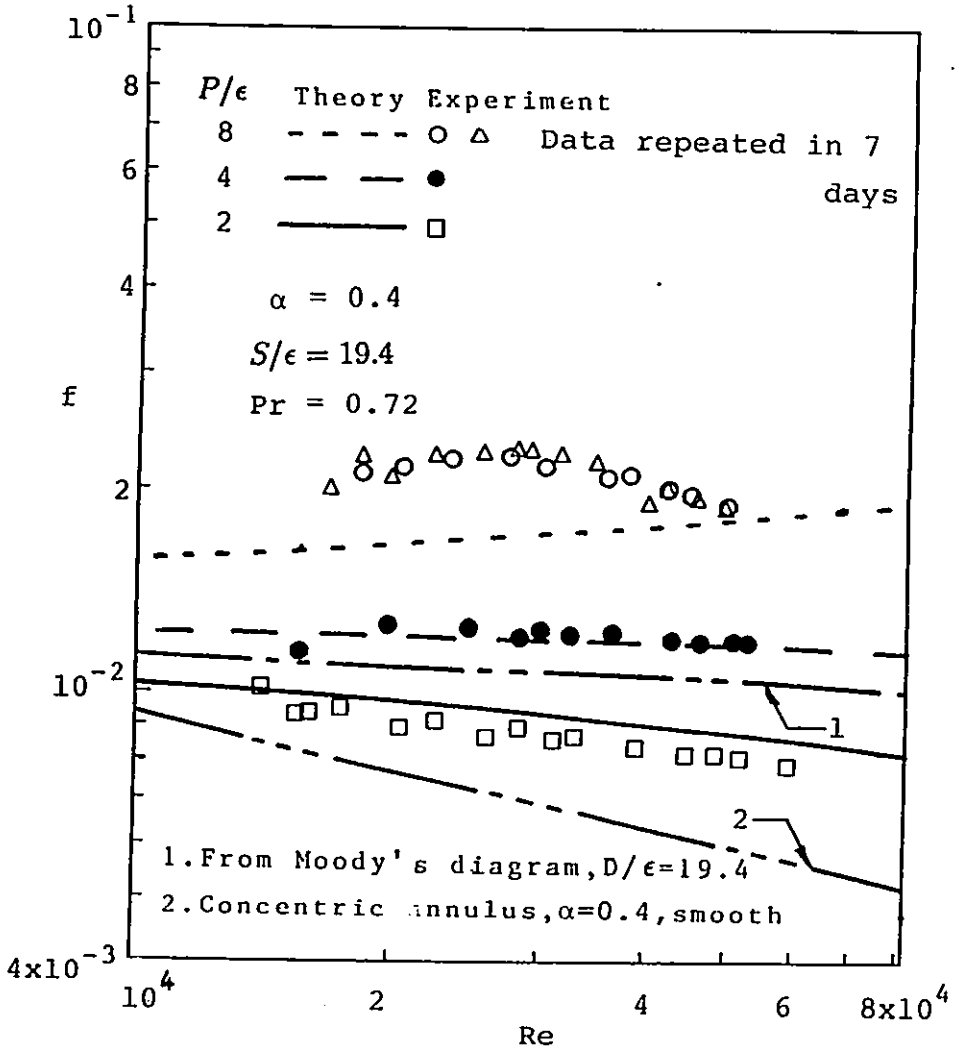

Fig. 4.19 Friction Factor

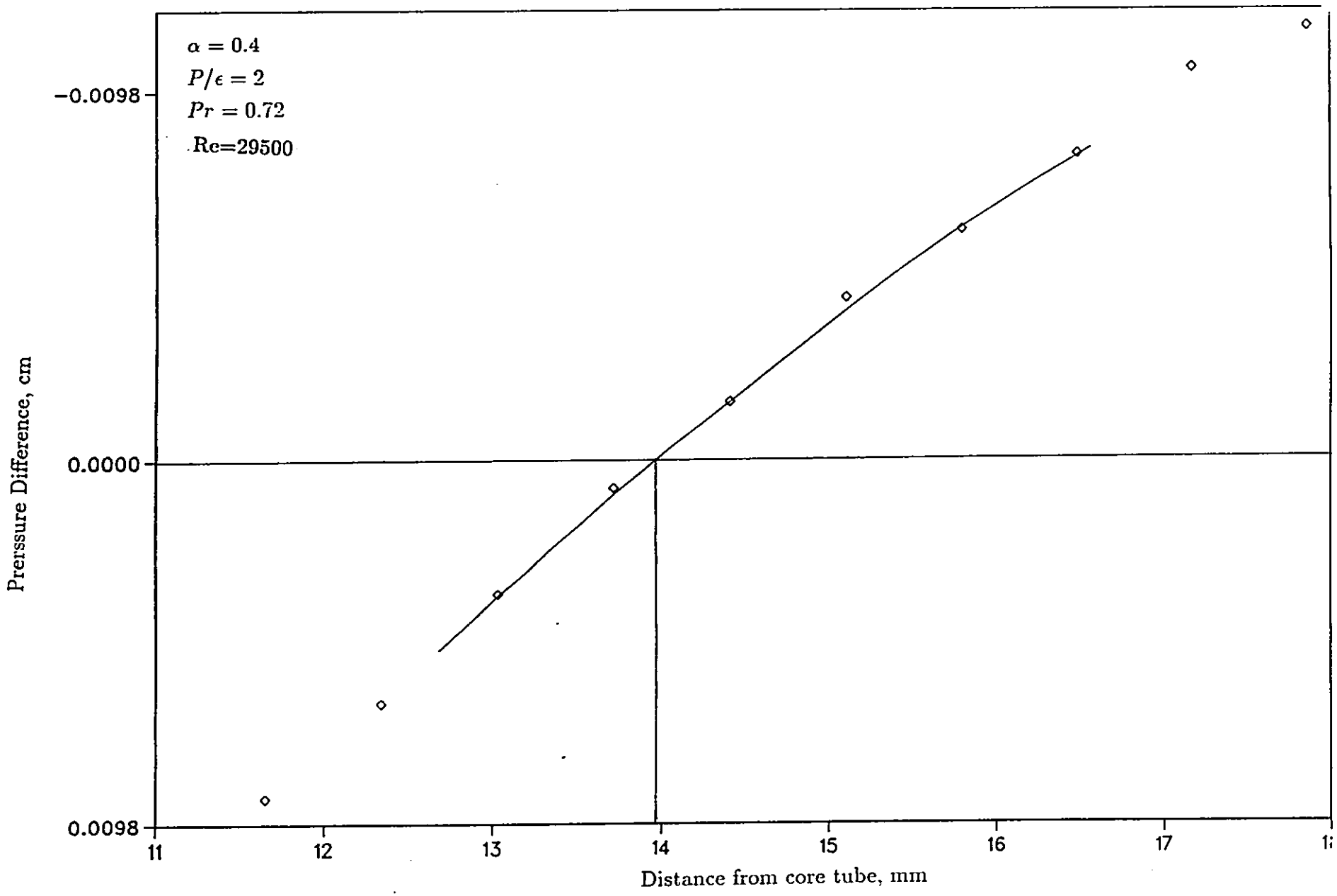

Fig. 4.20 Maximum Velocity Position

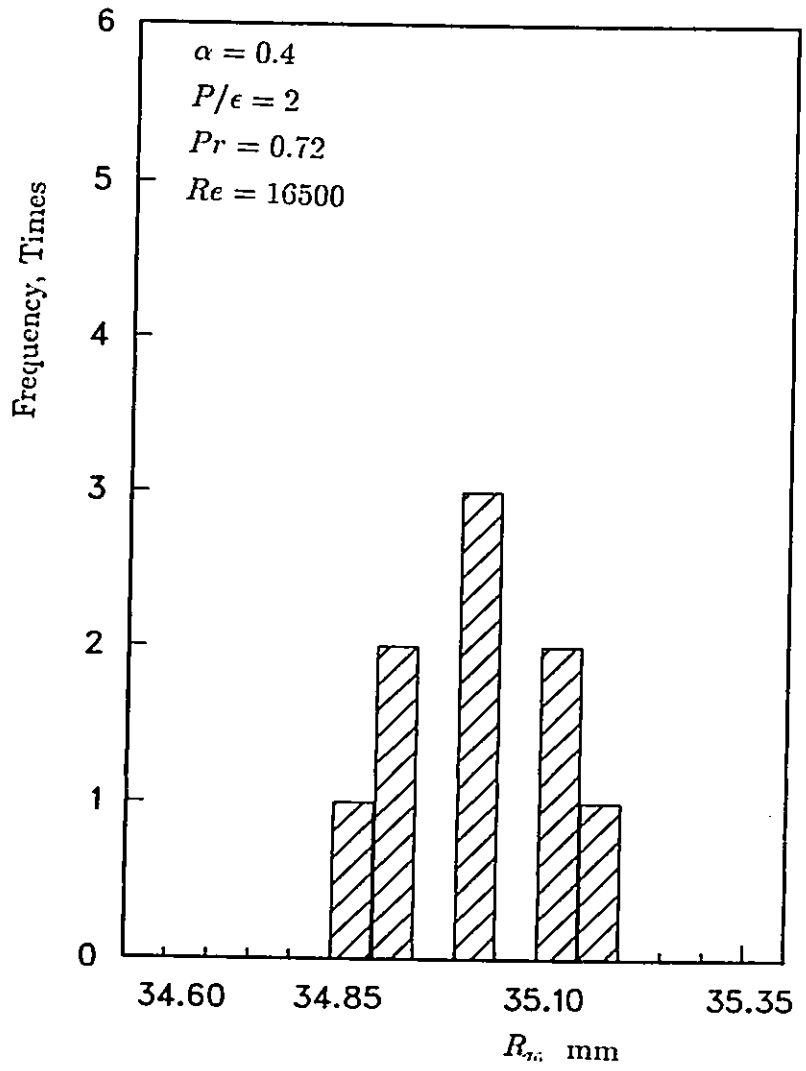

Fig. 4.21 Maximum Velocity Positions

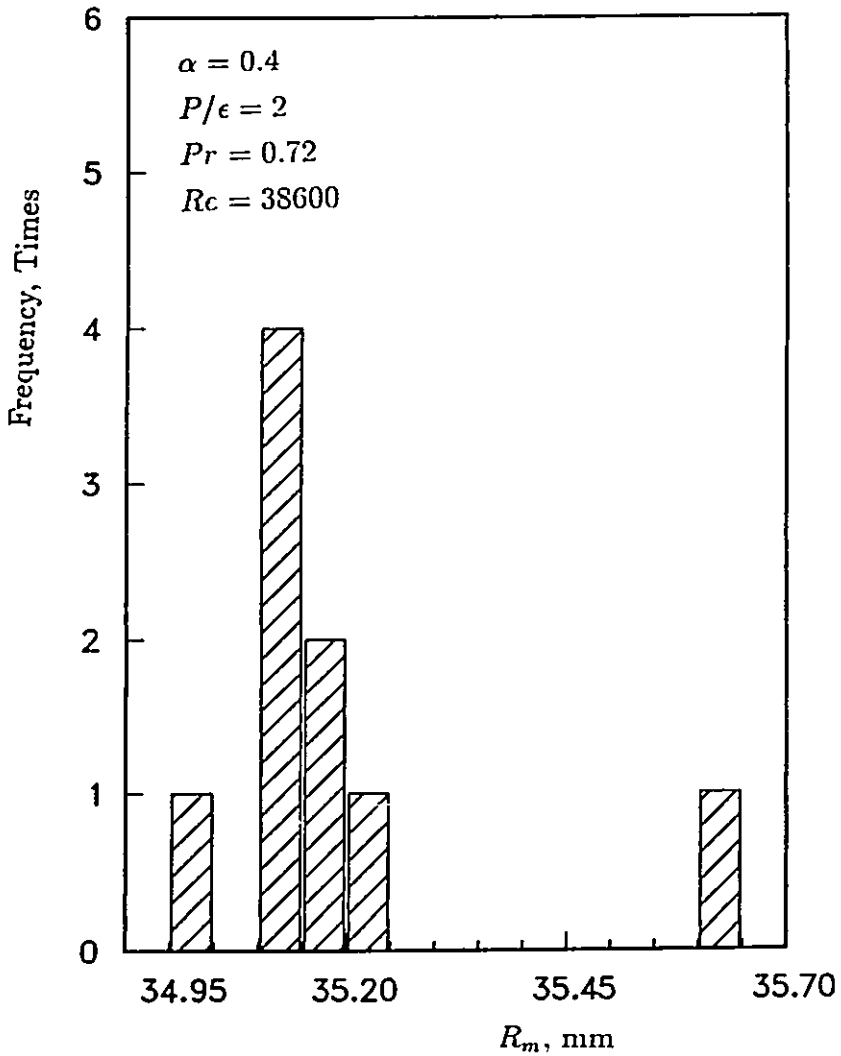

Fig. 4.22 Maximum Velocity Positions

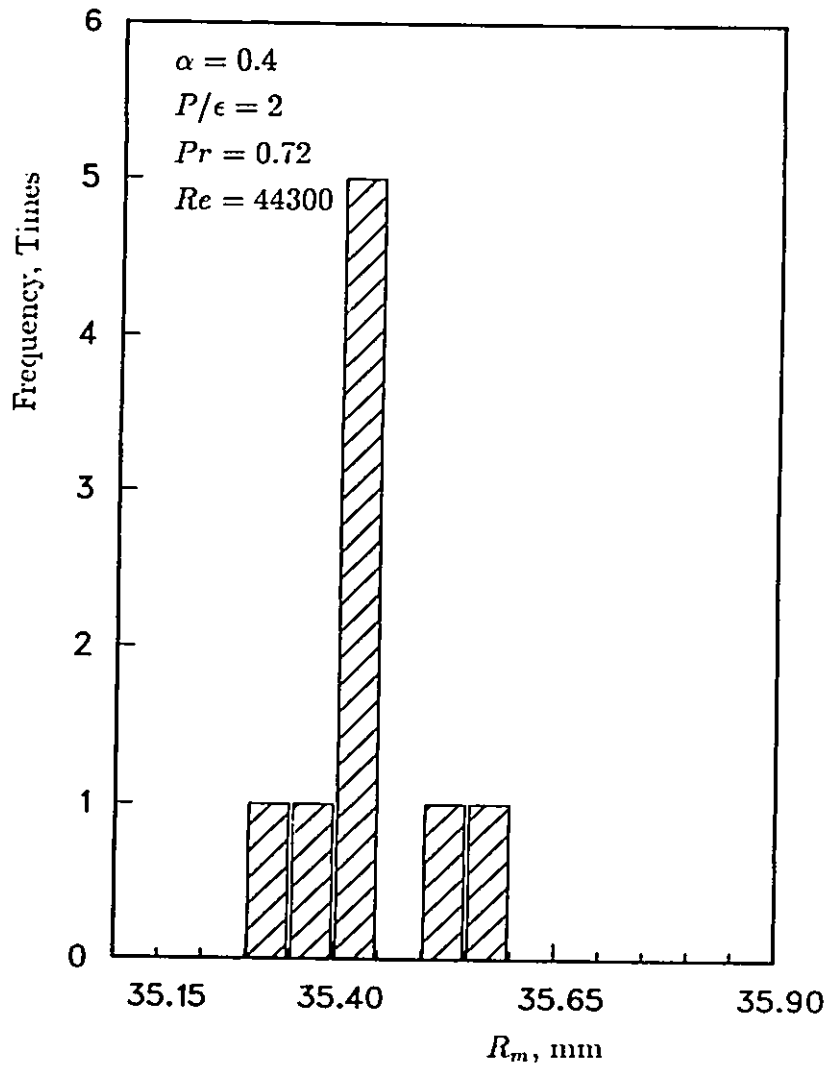

Fig. 4.23 Maximum Velocity Positions

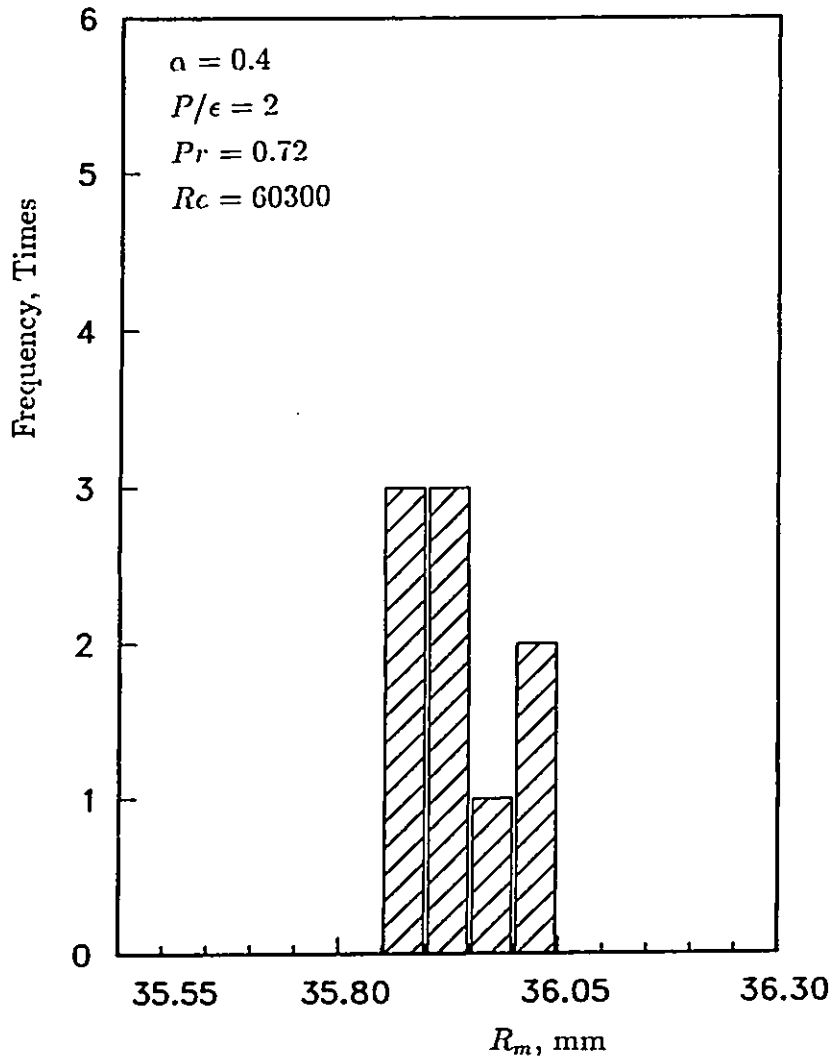

Fig. 4.24 Maximum Velocity Positions

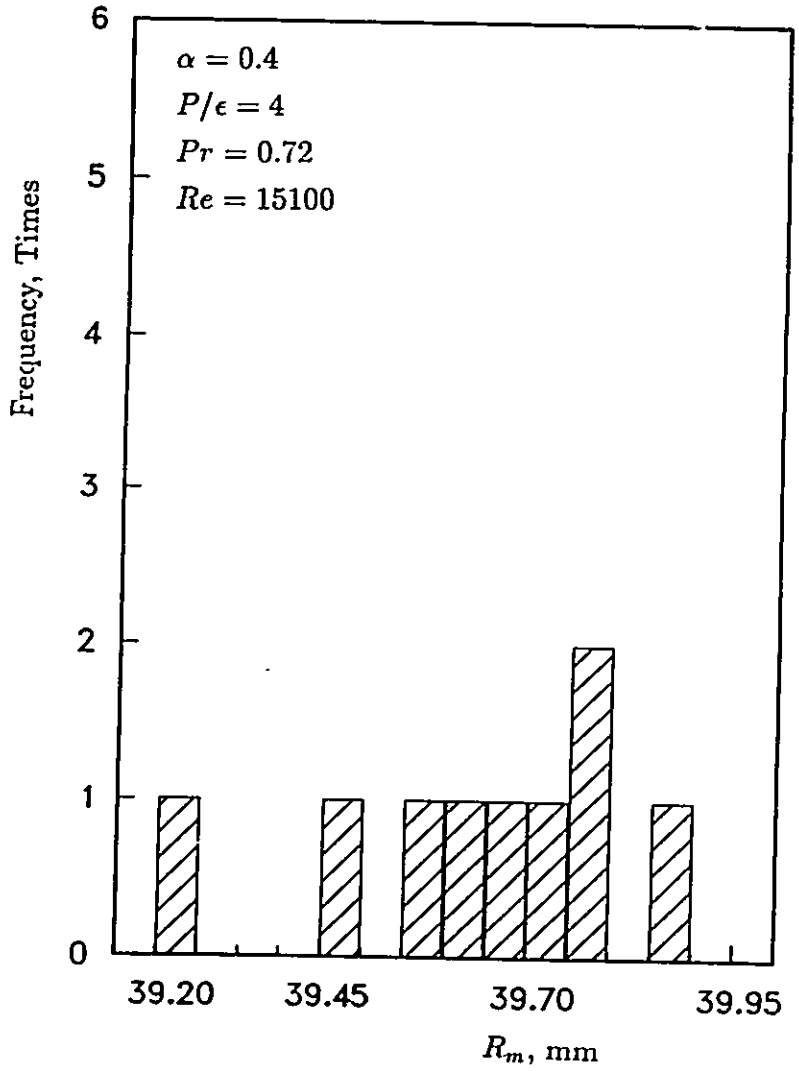

Fig. 4.25 Maximum Velocity Positions

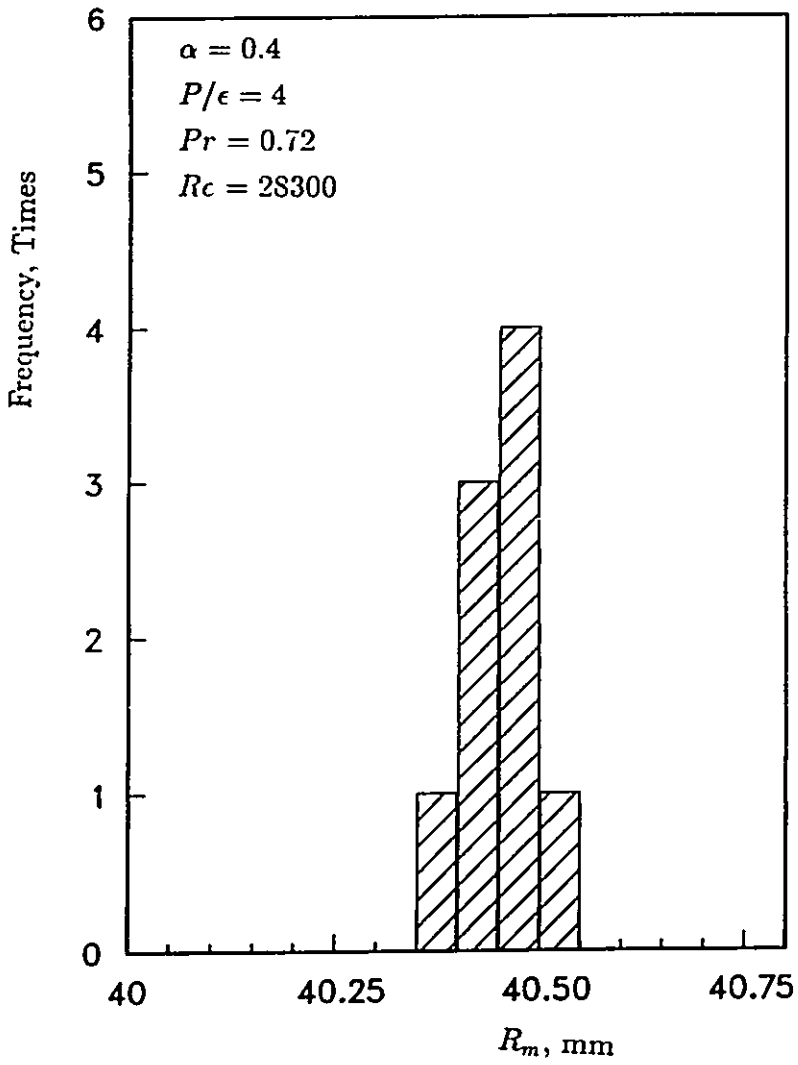

Fig. 4.26 Maximum Velocity Positions

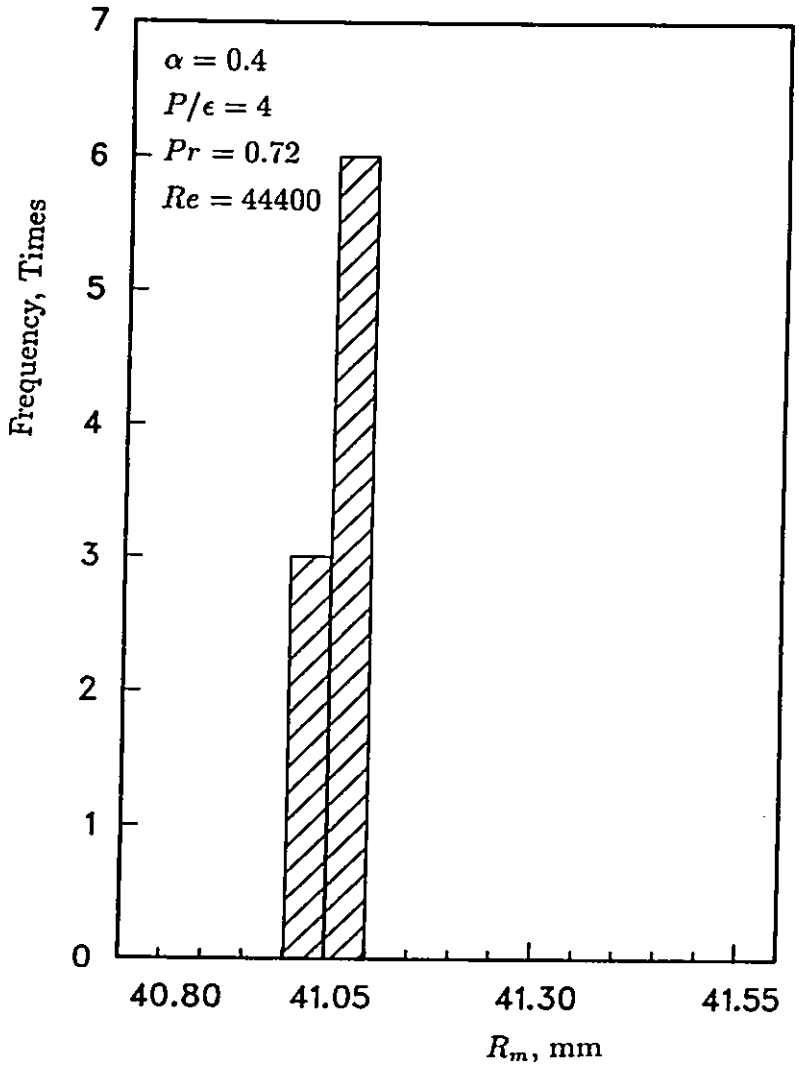

Fig. 4.27 Maximum Velocity Positions

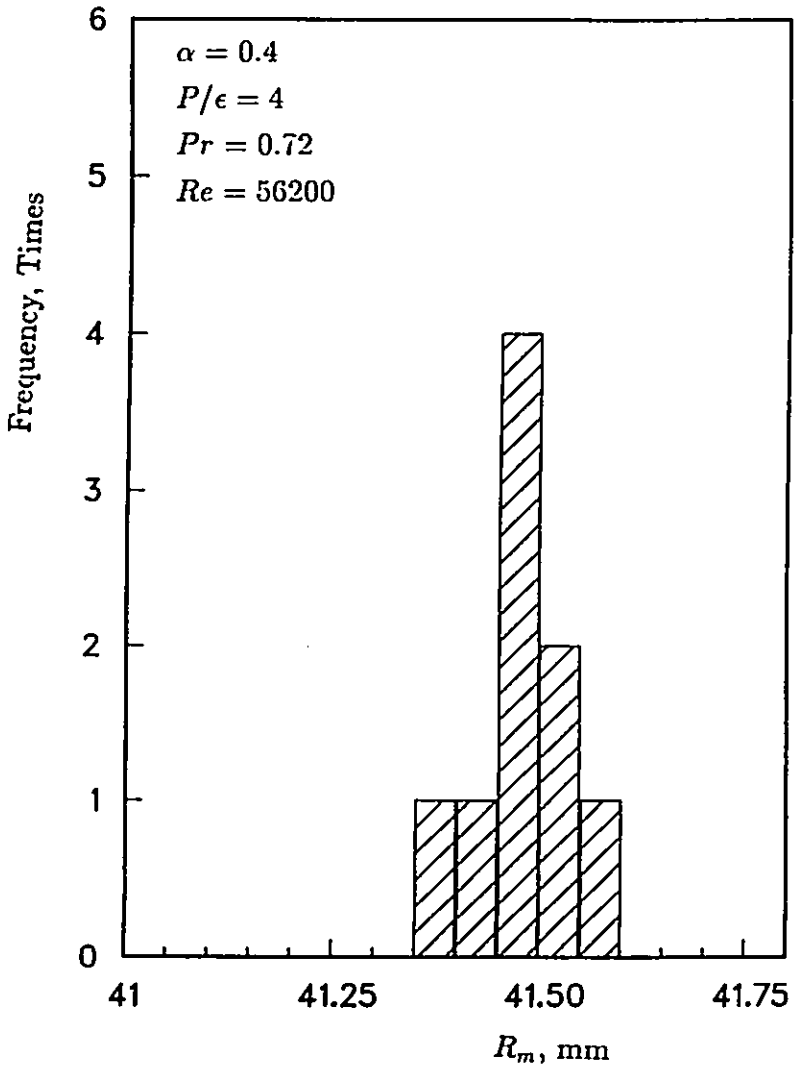

Fig. 4.28 Maximum Velocity Positions

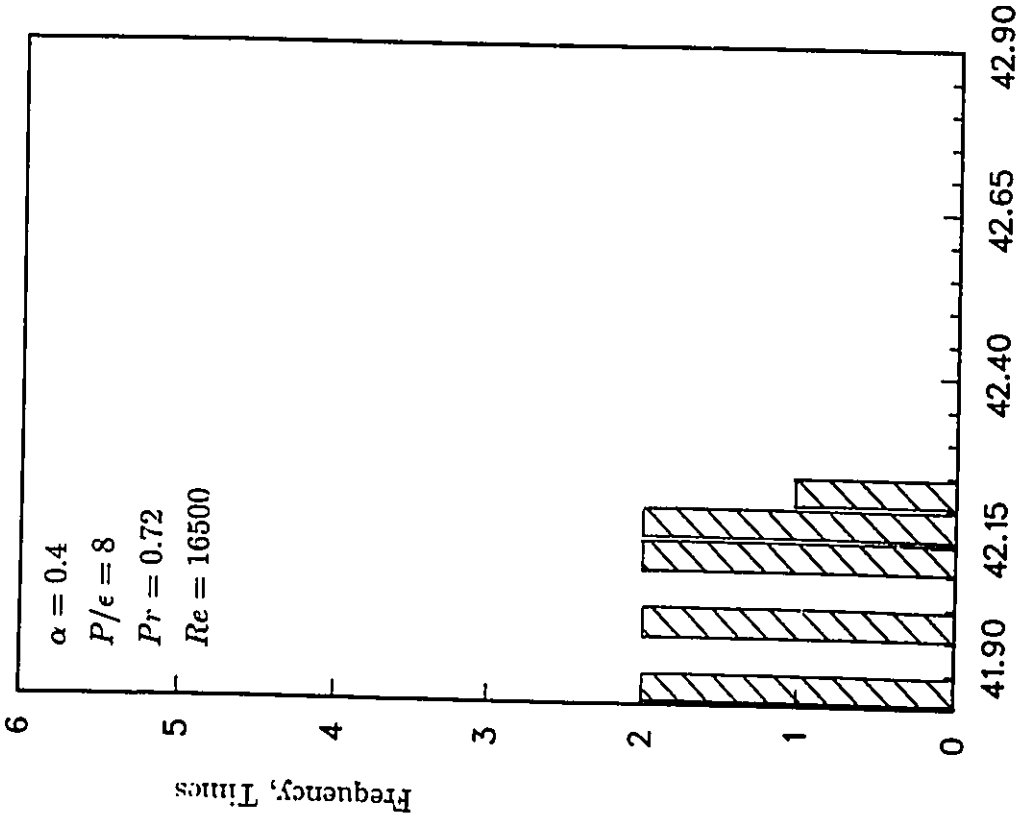

Fig. 4.29 Maximum Velocity Positions

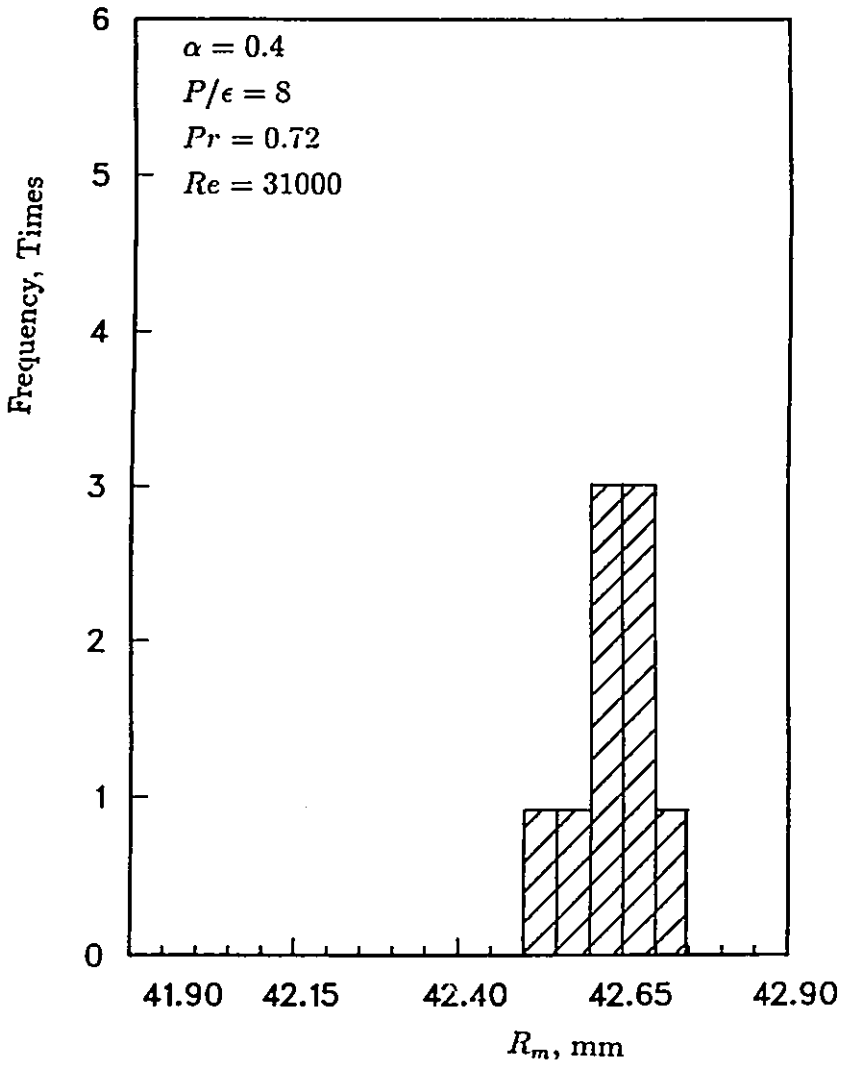

Fig. 4.30 Maximum Velocity Positions

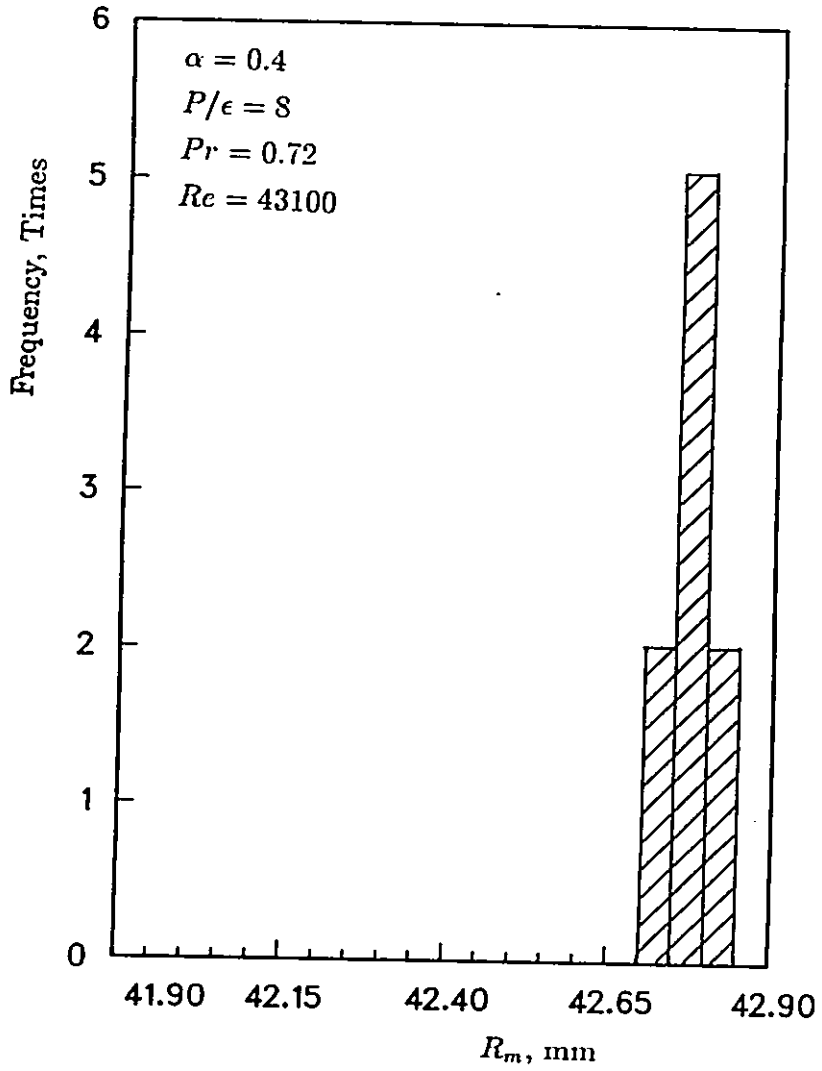

Fig. 4.31 Maximum Velocity Positions

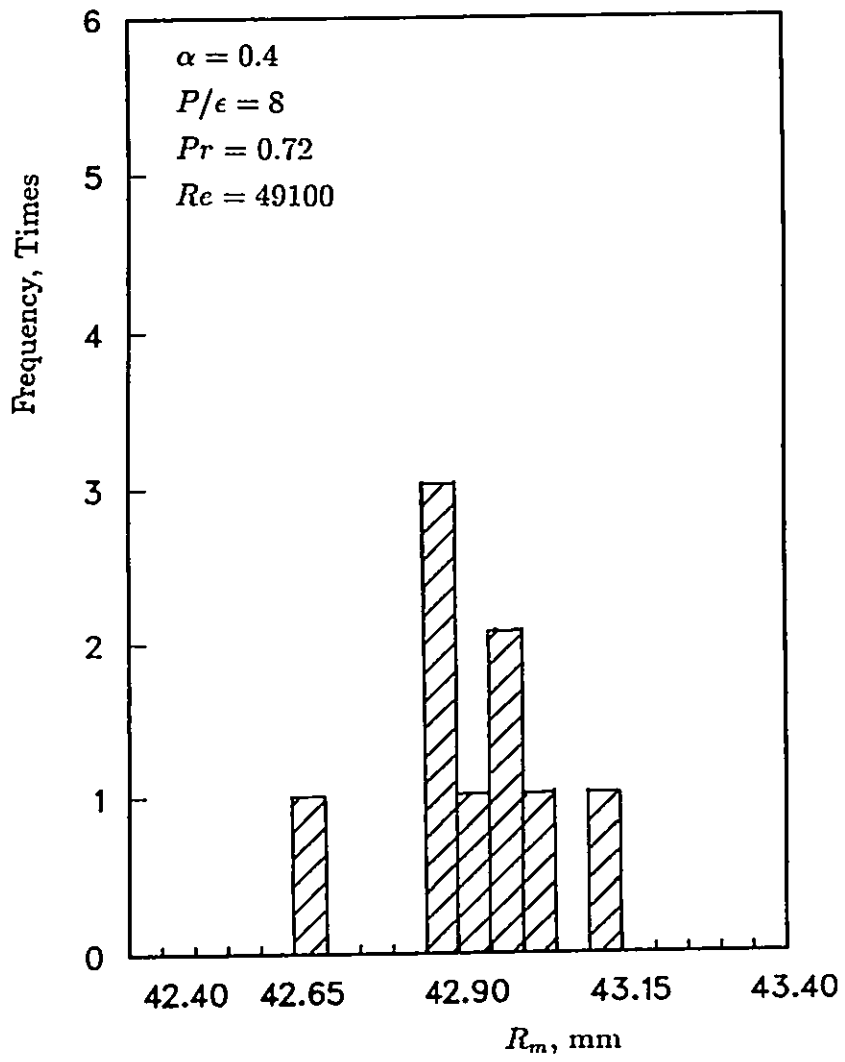

Fig. 4.32 Maximum Velocity Positions

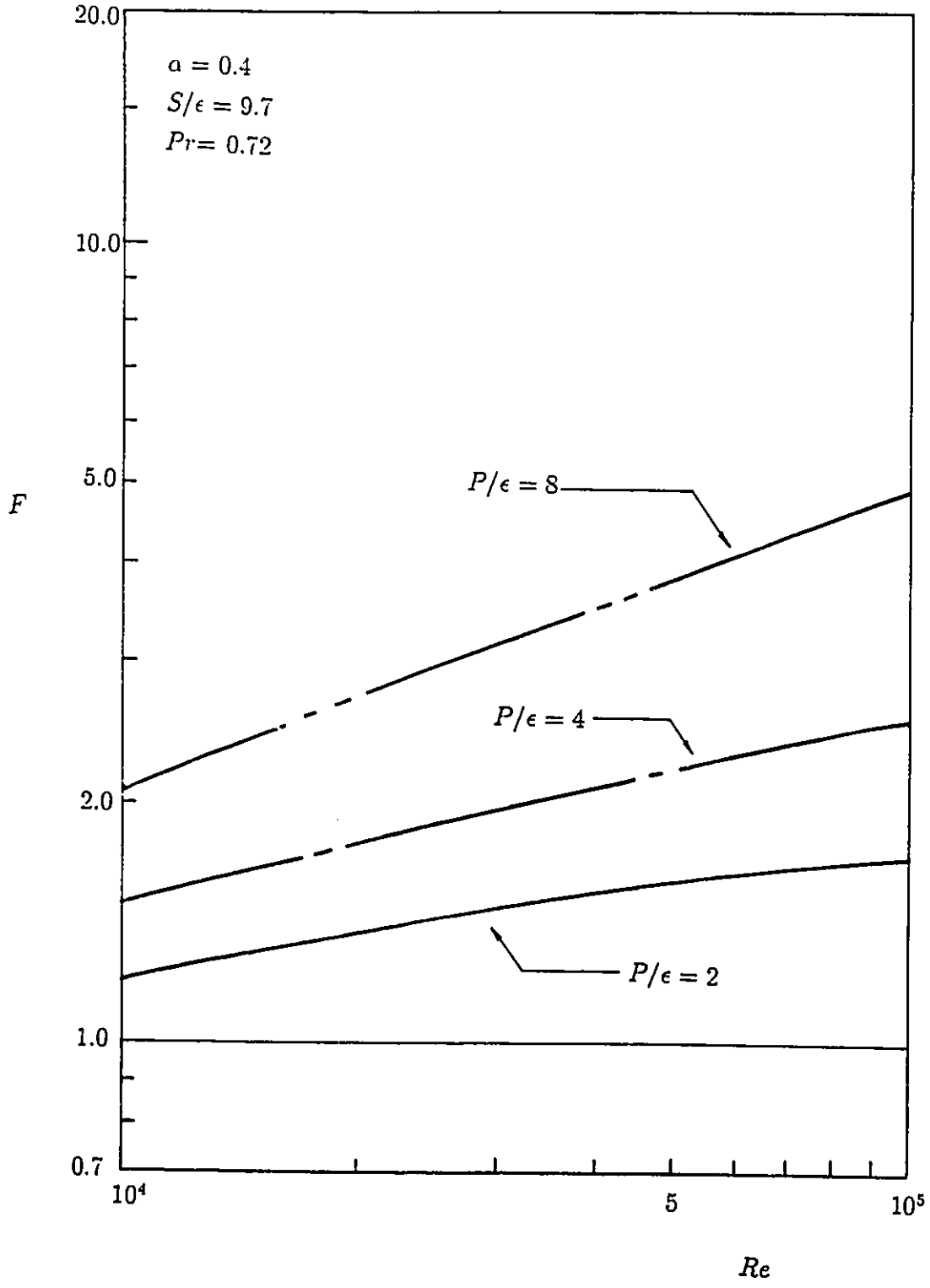

Fig. 5.1 Normalized Friction Factor versus Reynolds number

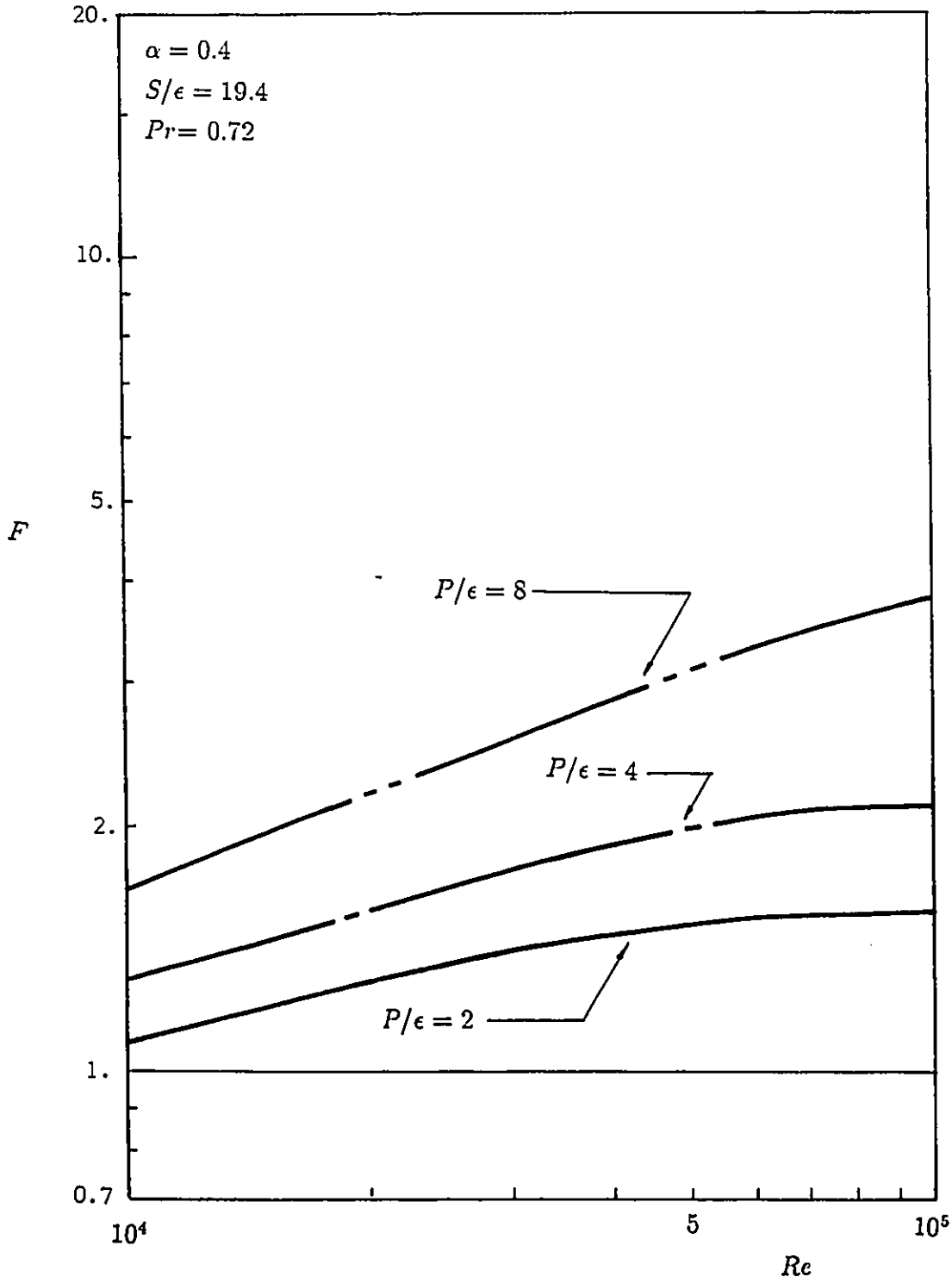

Fig. 5.2 Normalized Friction Factor versus Reynolds number

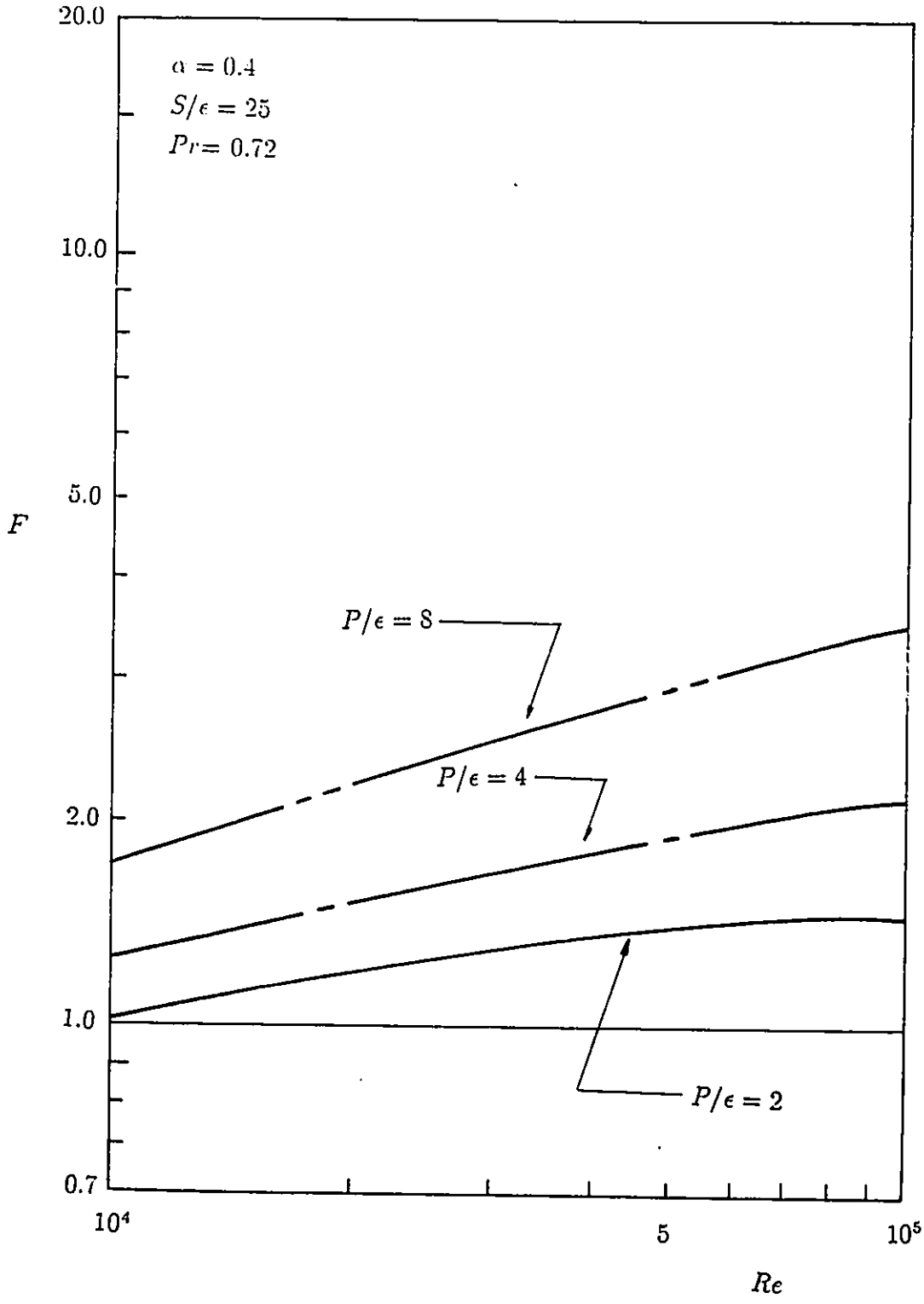

Fig. 5.3 Normalized Friction Factor versus Reynolds number

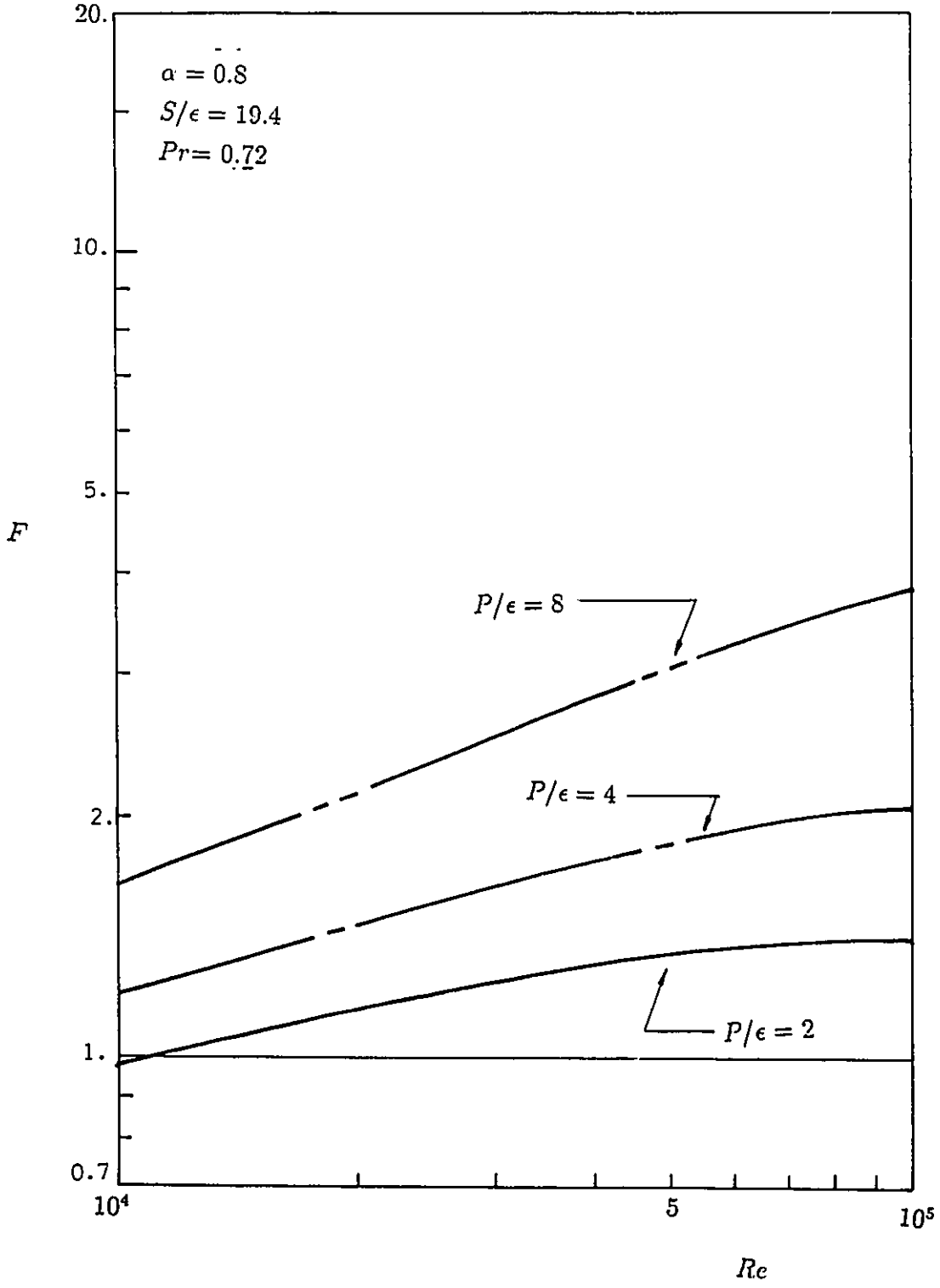

Fig. 5.4 Normalized Friction Factor versus Reynolds number

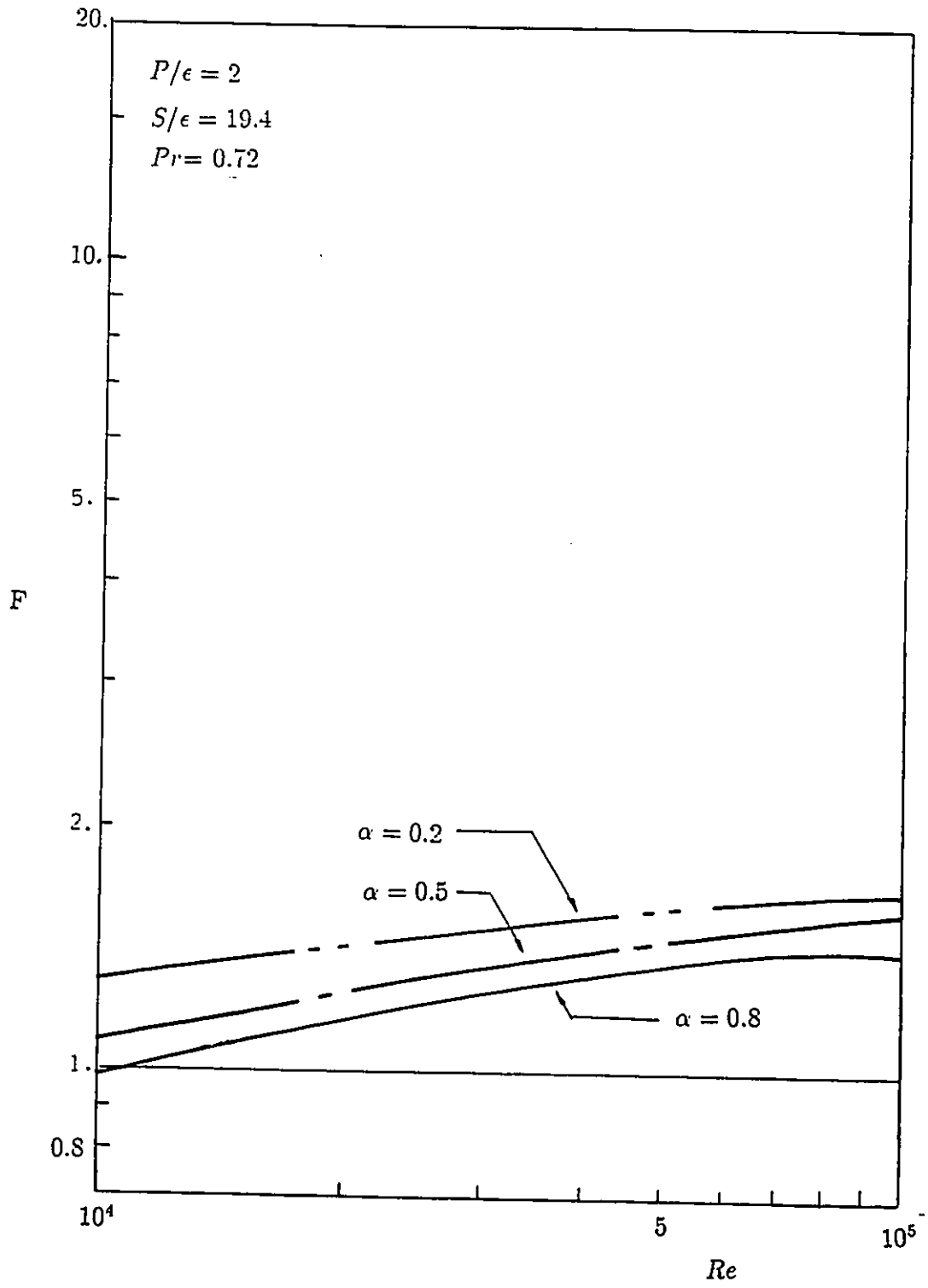

Fig. 5.5 Normalized Friction Factor versus Reynolds number

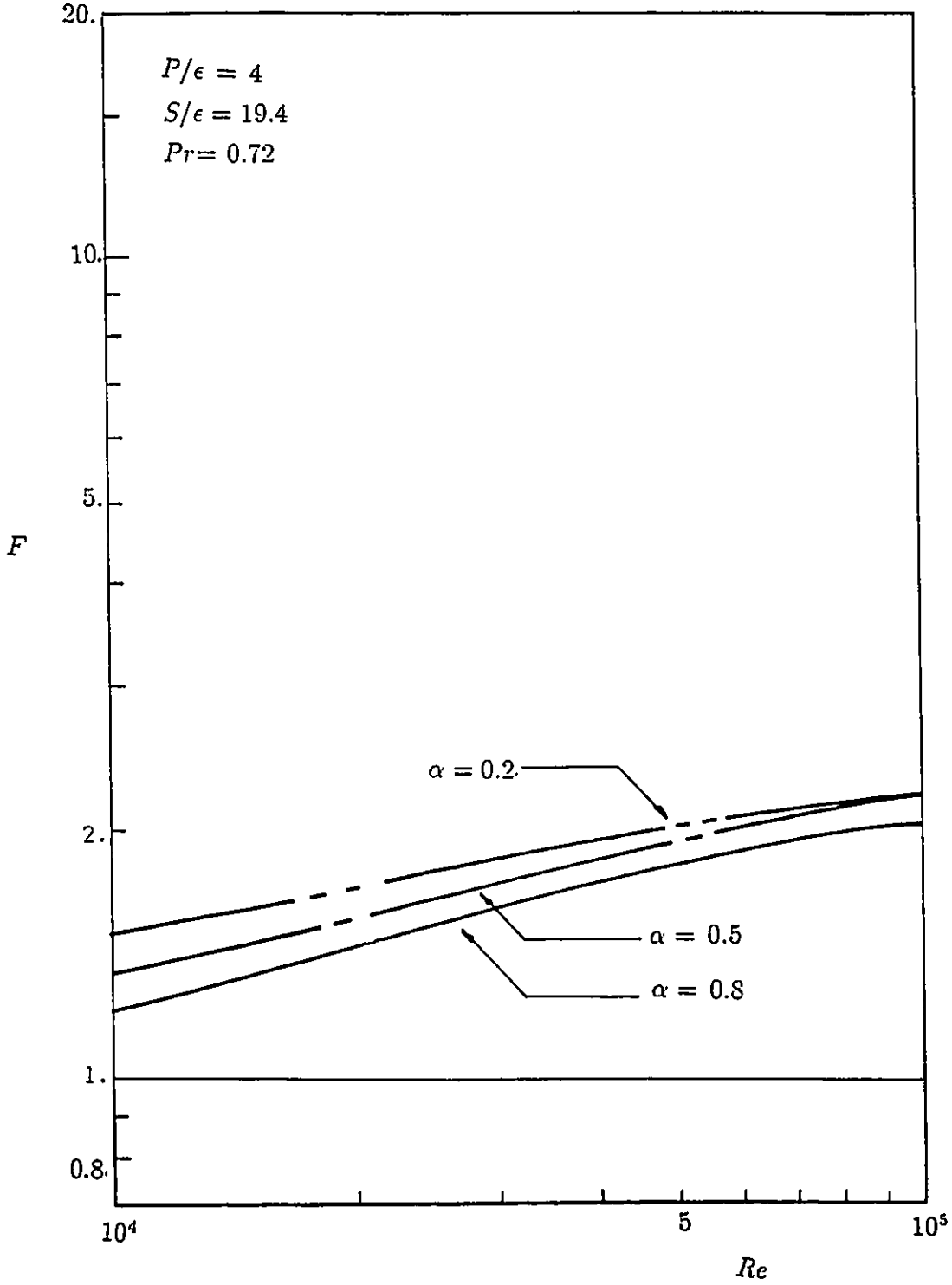

Fig. 5.6 Normalized Friction Factor versus Reynolds number

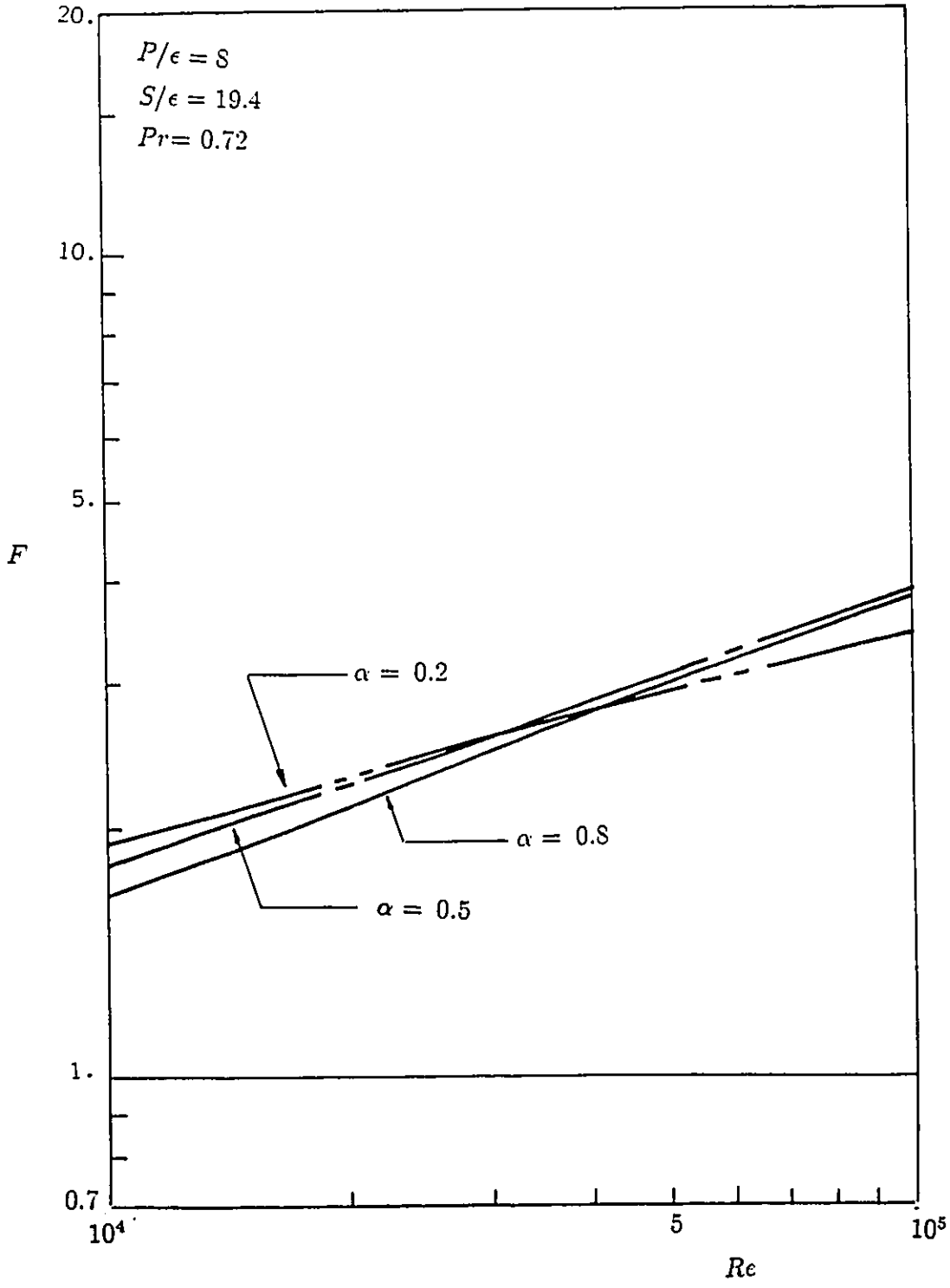

Fig. 5.7 Normalized Friction Factor versus Reynolds number

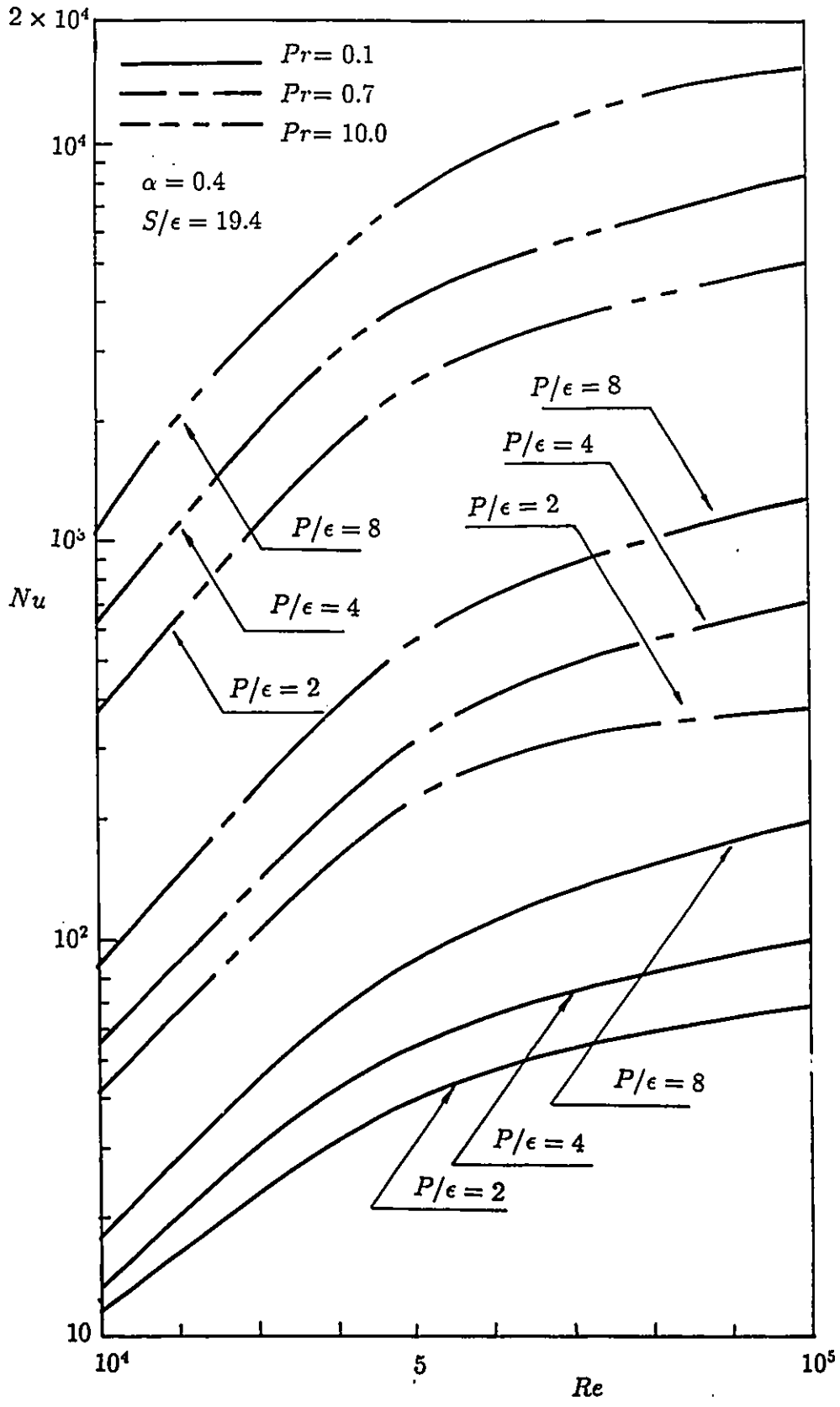

Fig. 5.8 Nusselt number versus Reynolds number

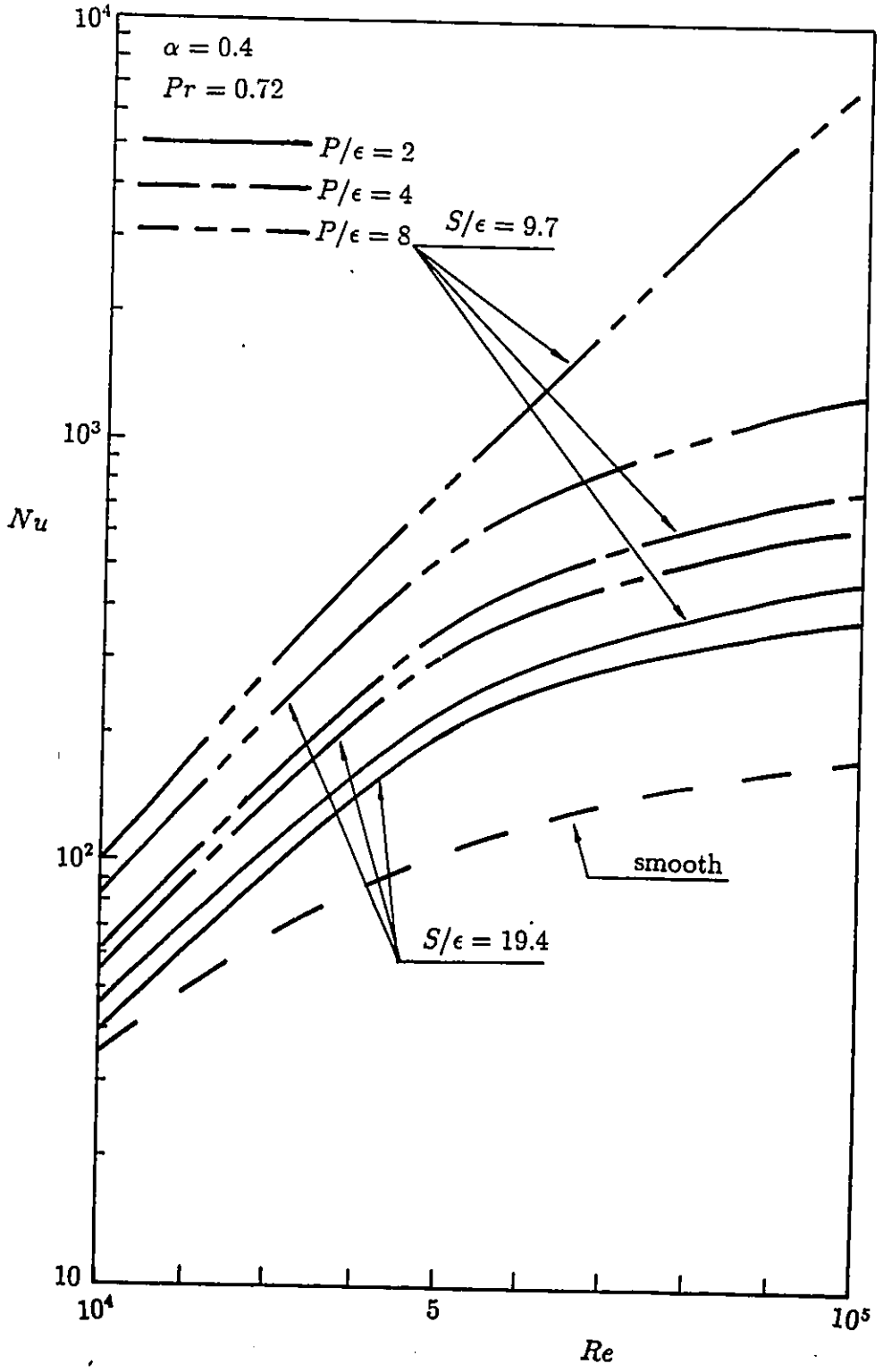

Fig. 5.9 Nusselt number versus Reynolds number

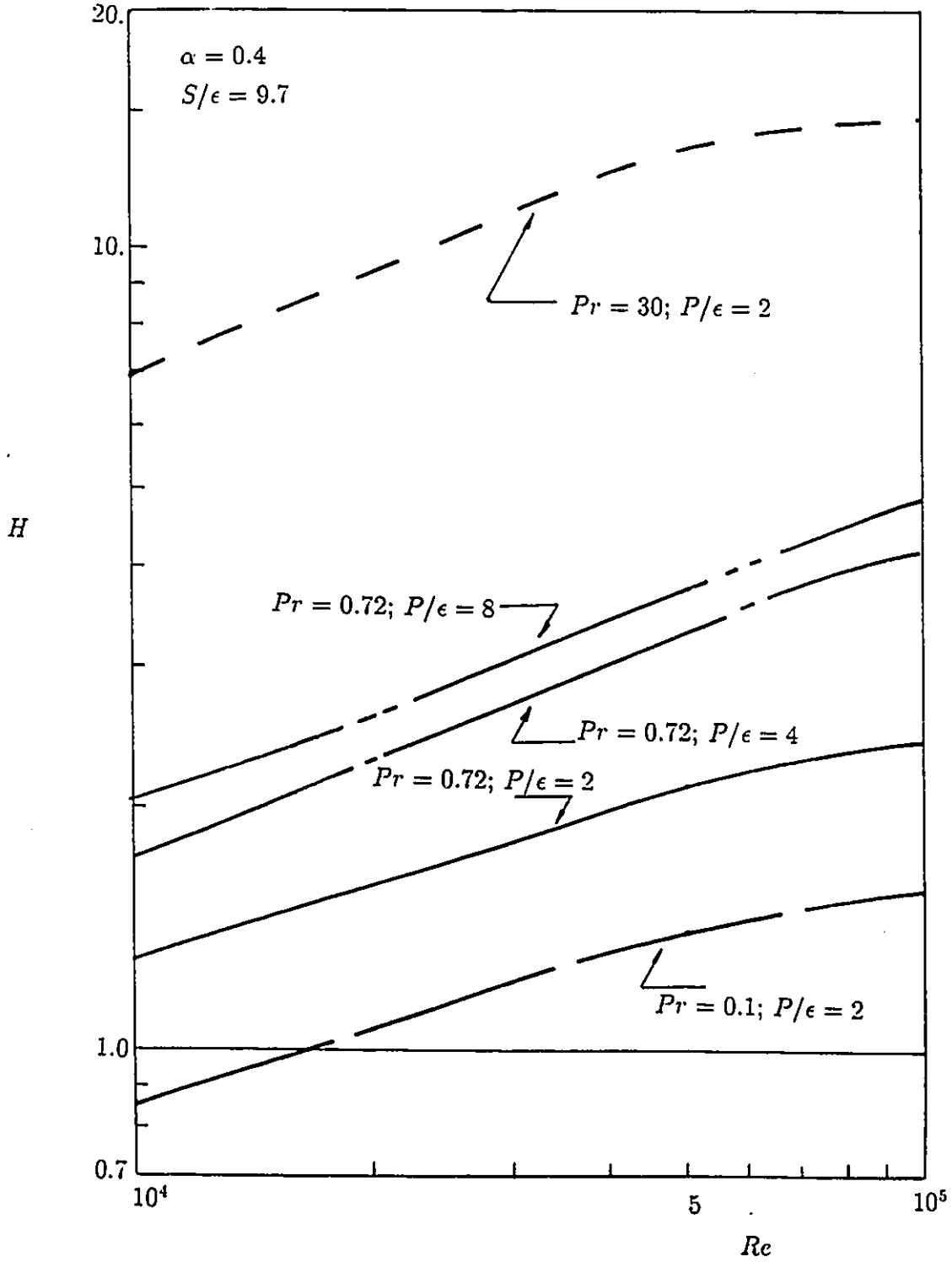

Fig. 5.10 Normalized Nusselt number versus Reynolds number

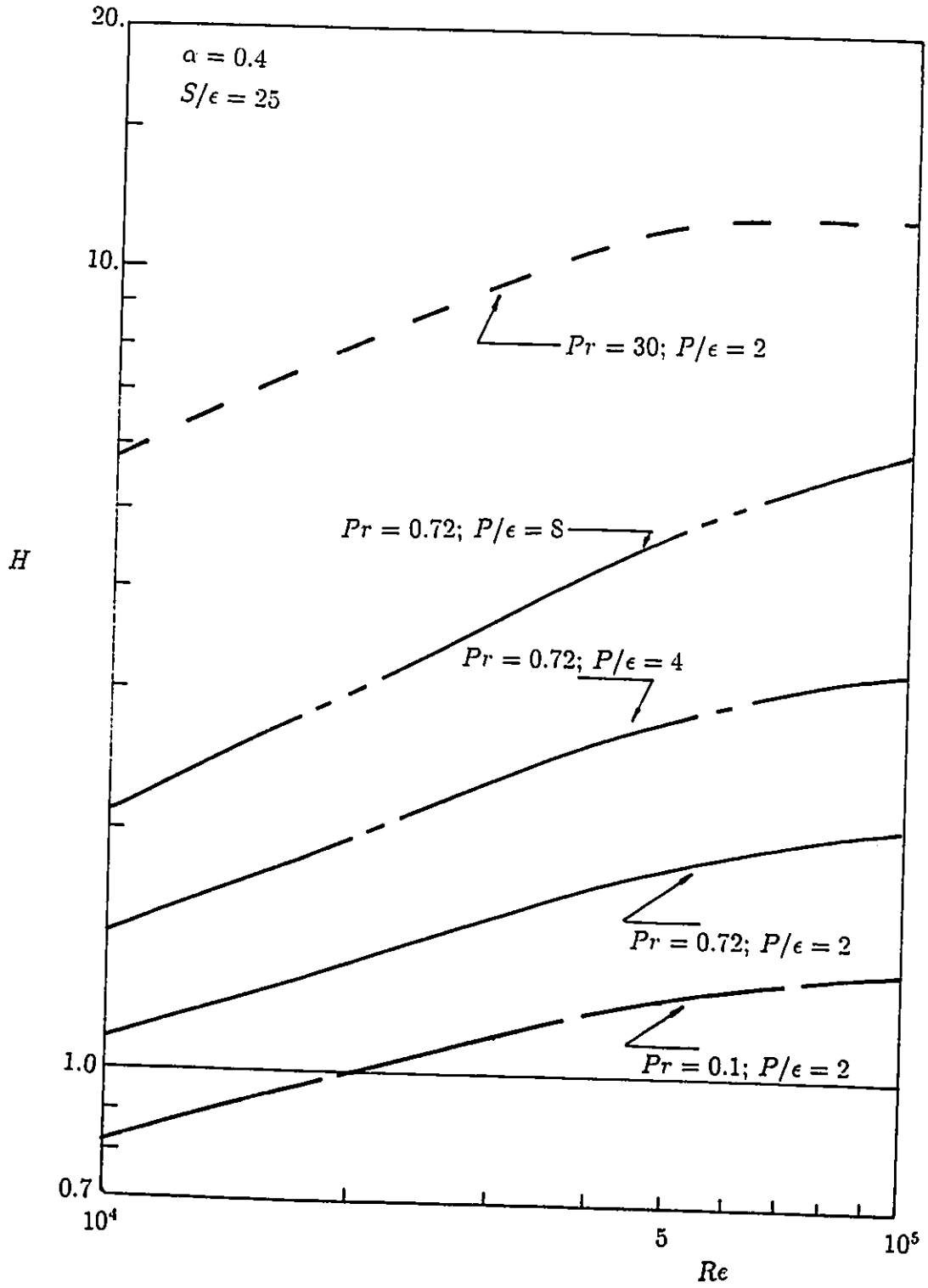

Fig. 5.11 Normalized Nusselt number versus Reynolds number

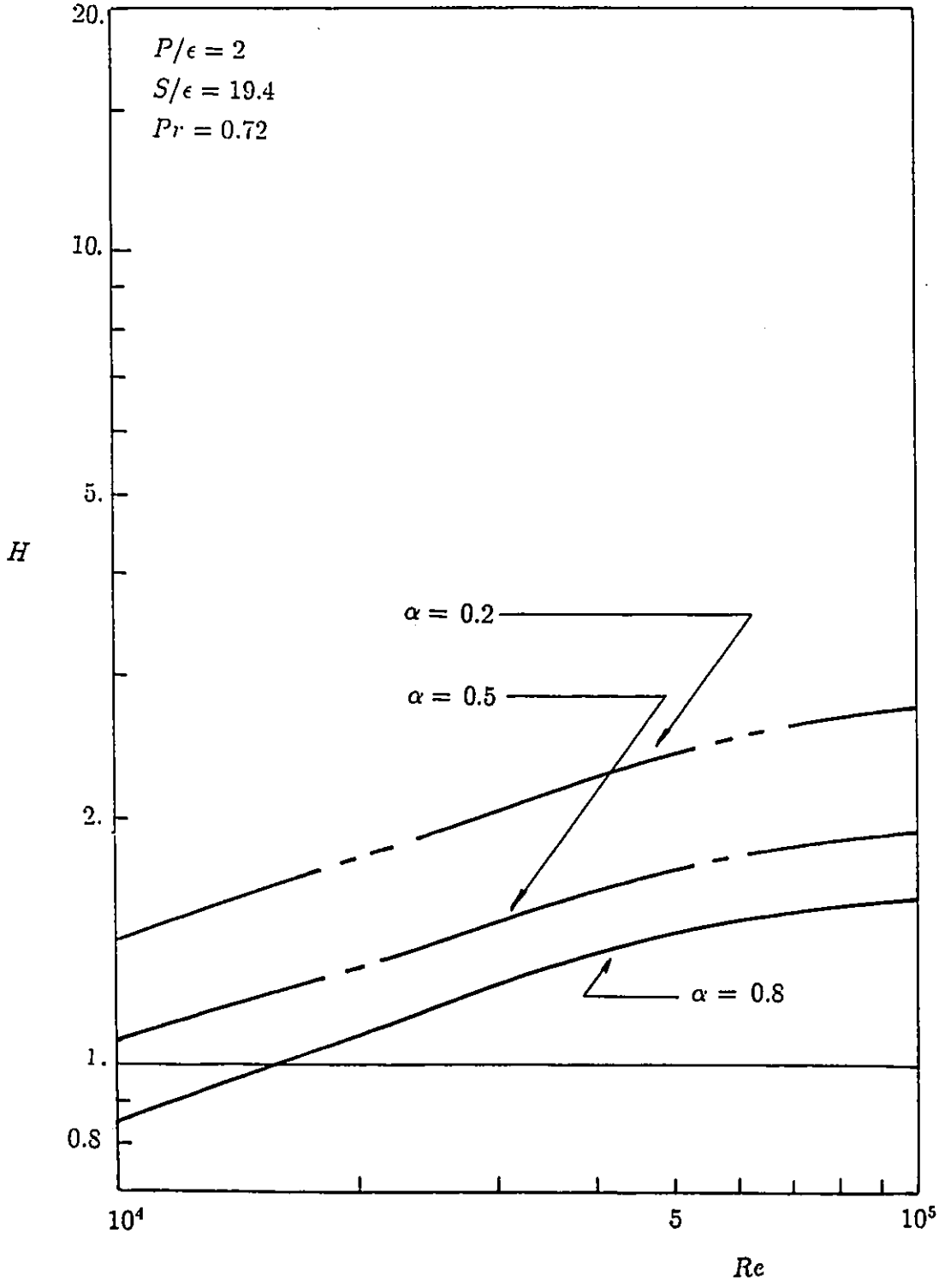

Fig. 5.12 Normalized Nusselt number versus Reynolds number

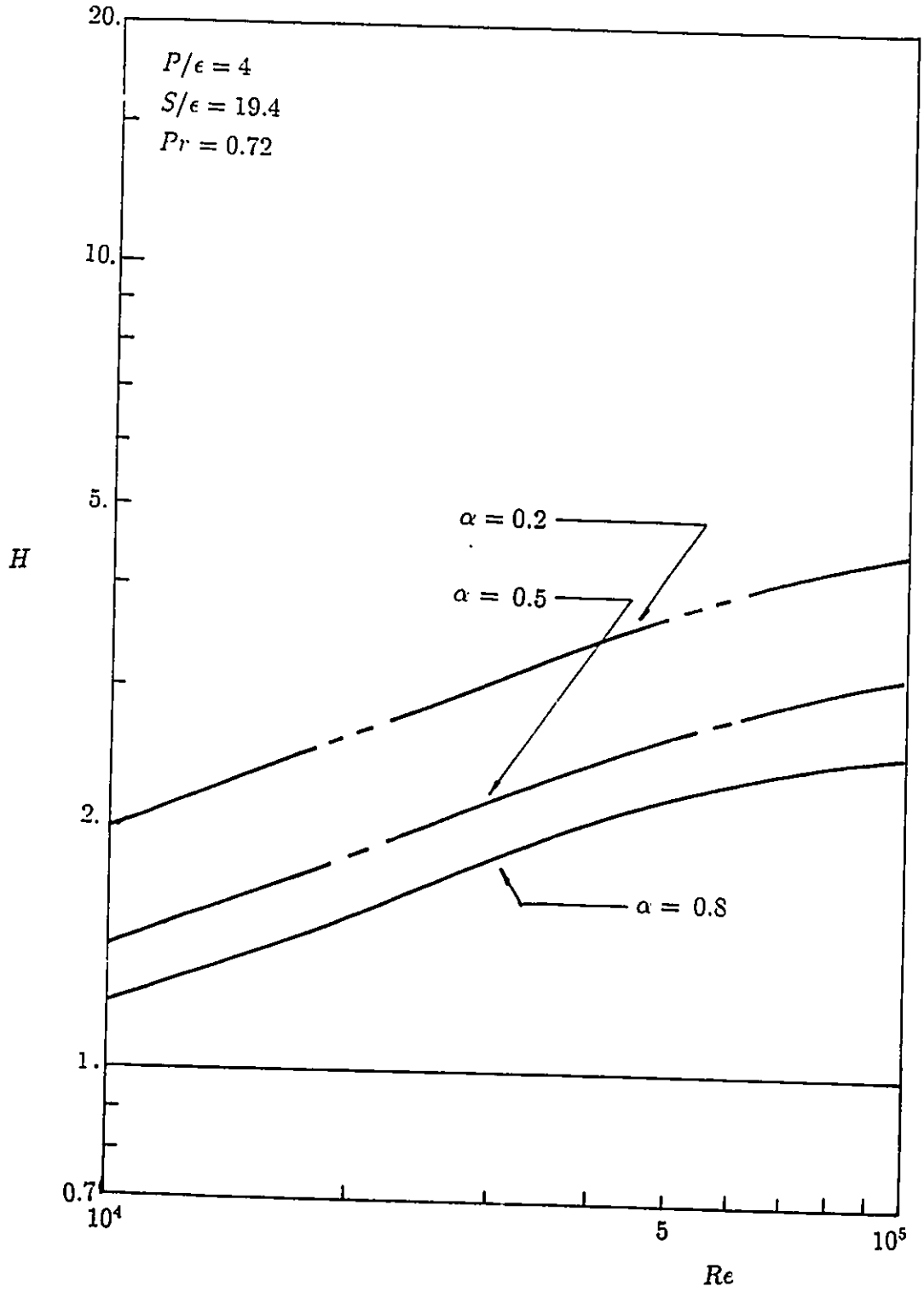

Fig. 5.13 Normalized Nusselt number versus Reynolds number

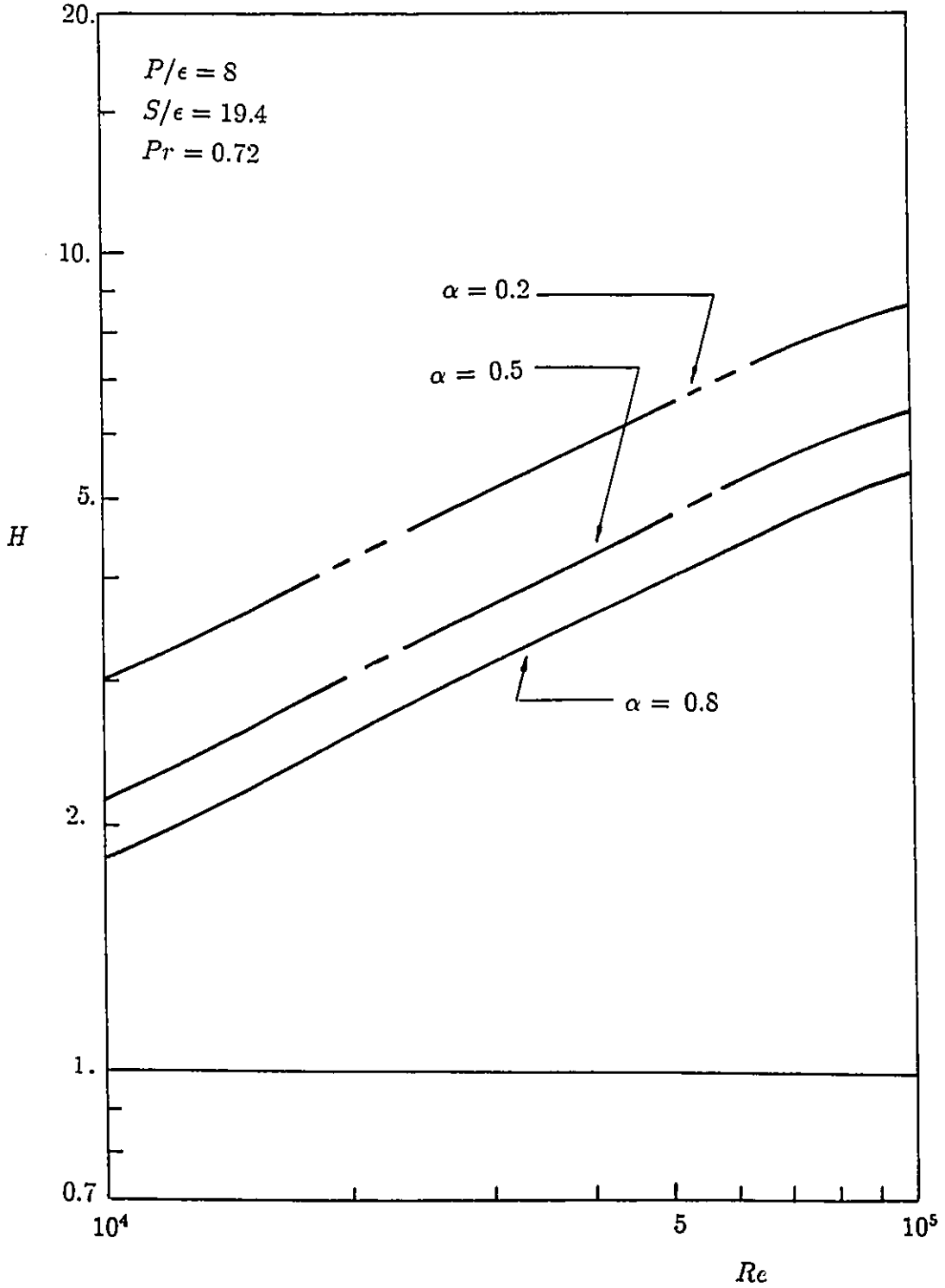

Fig. 5.14 Normalized Nusselt number versus Reynolds number

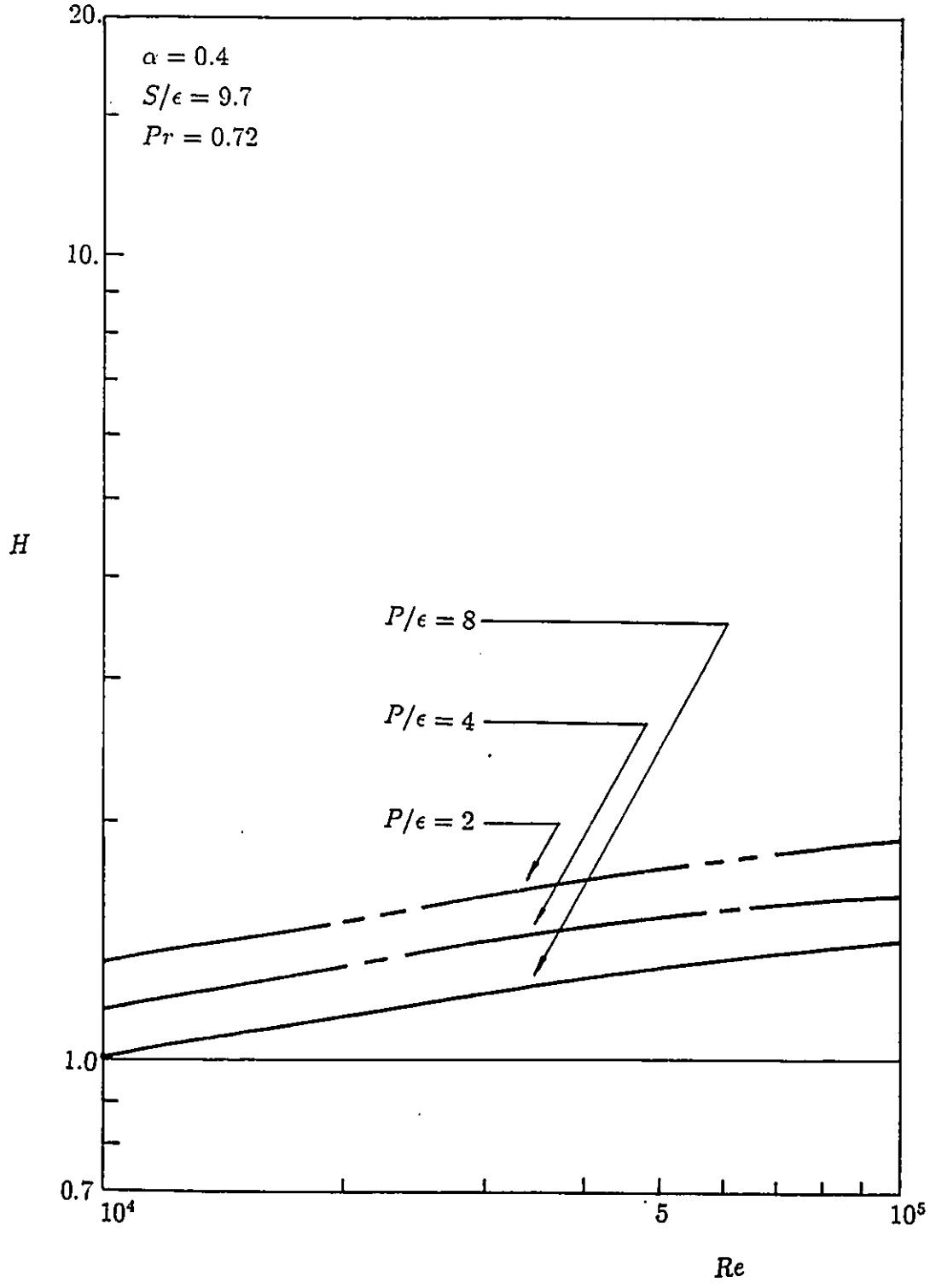

Fig. 5.15 H/F versus Reynolds number

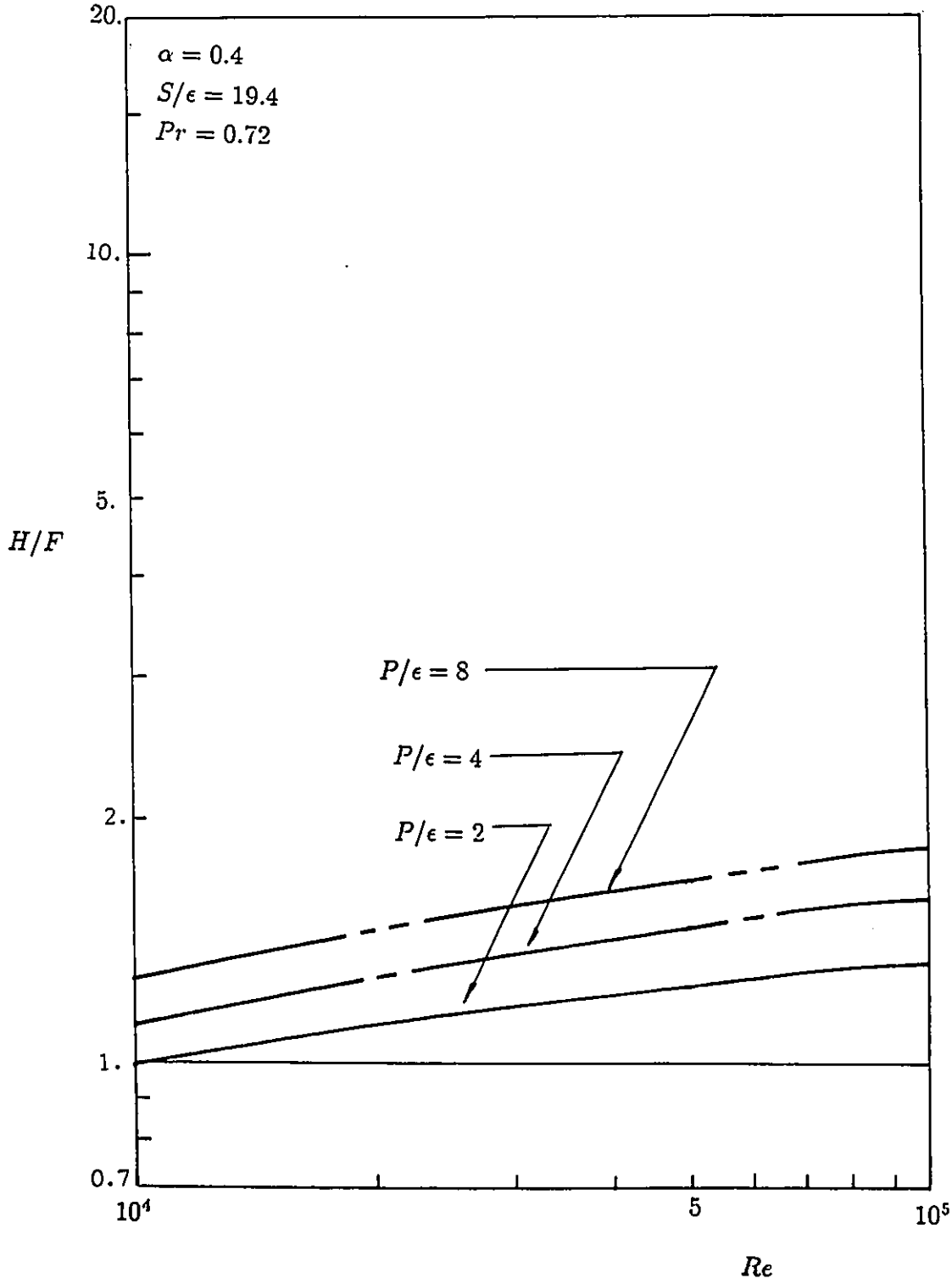

Fig. 5.16 H/F versus Reynolds number

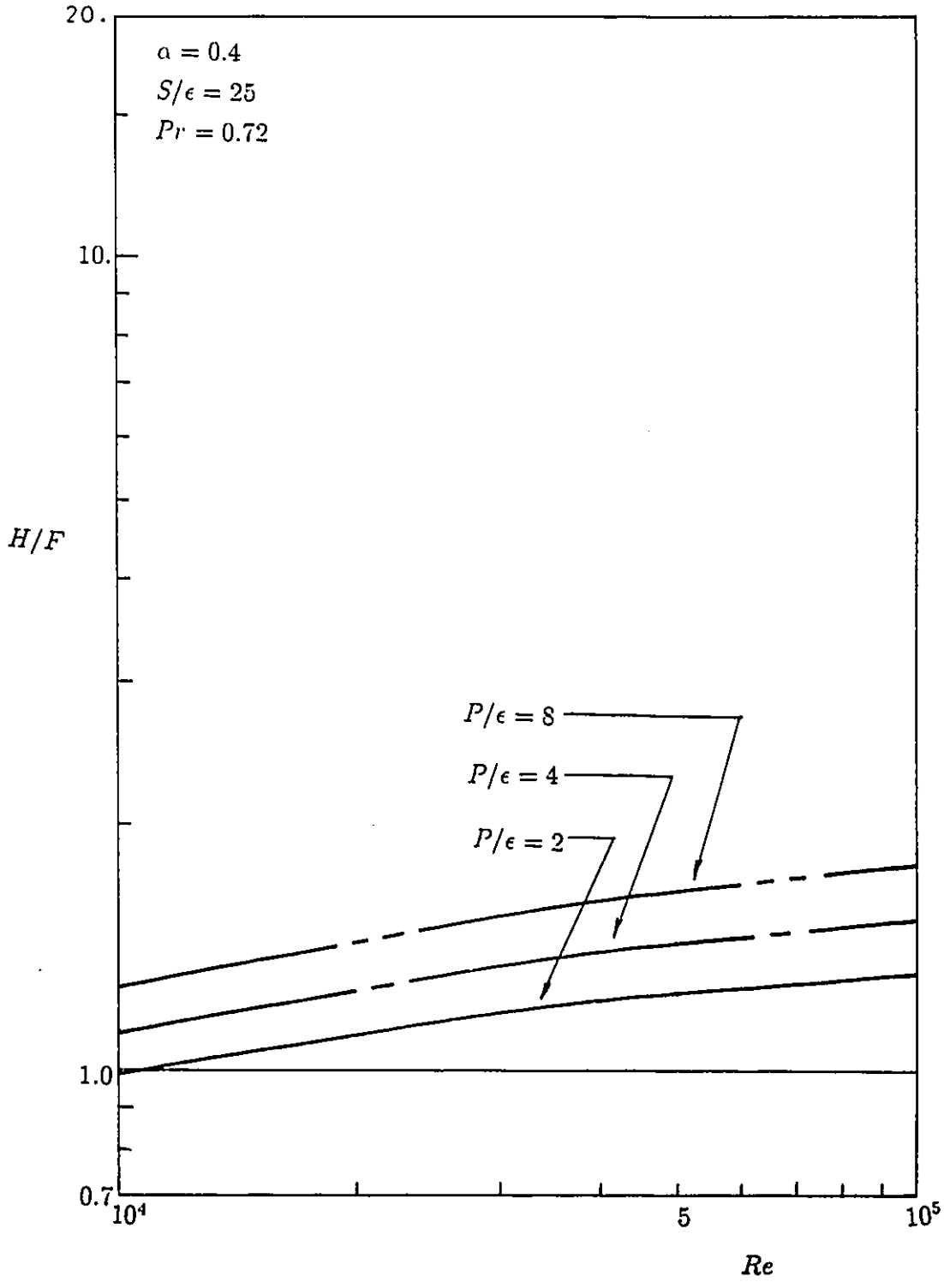

Fig. 5.17 H/F versus Reynolds number

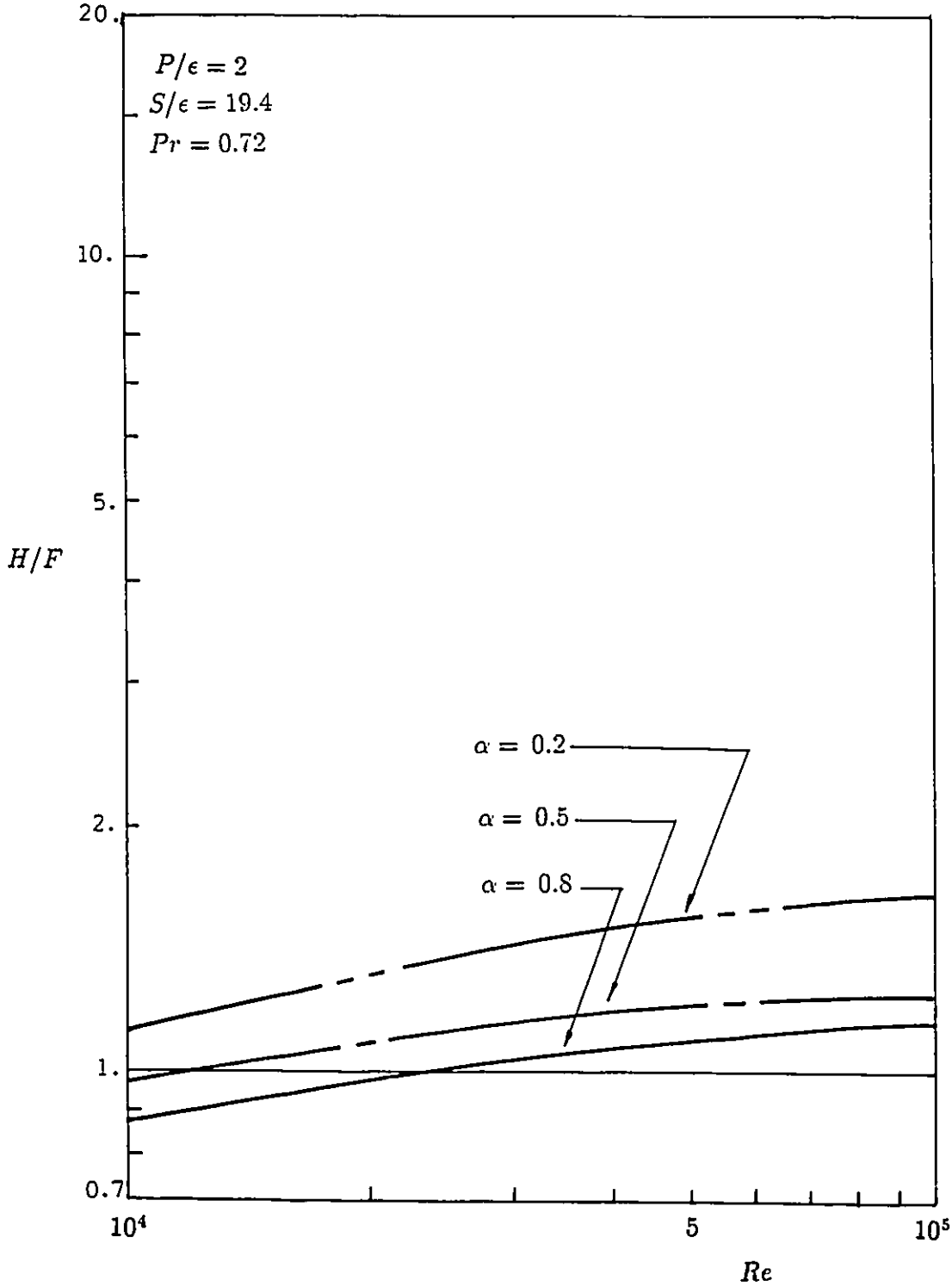

Fig. 5.18 H/F versus Reynolds number

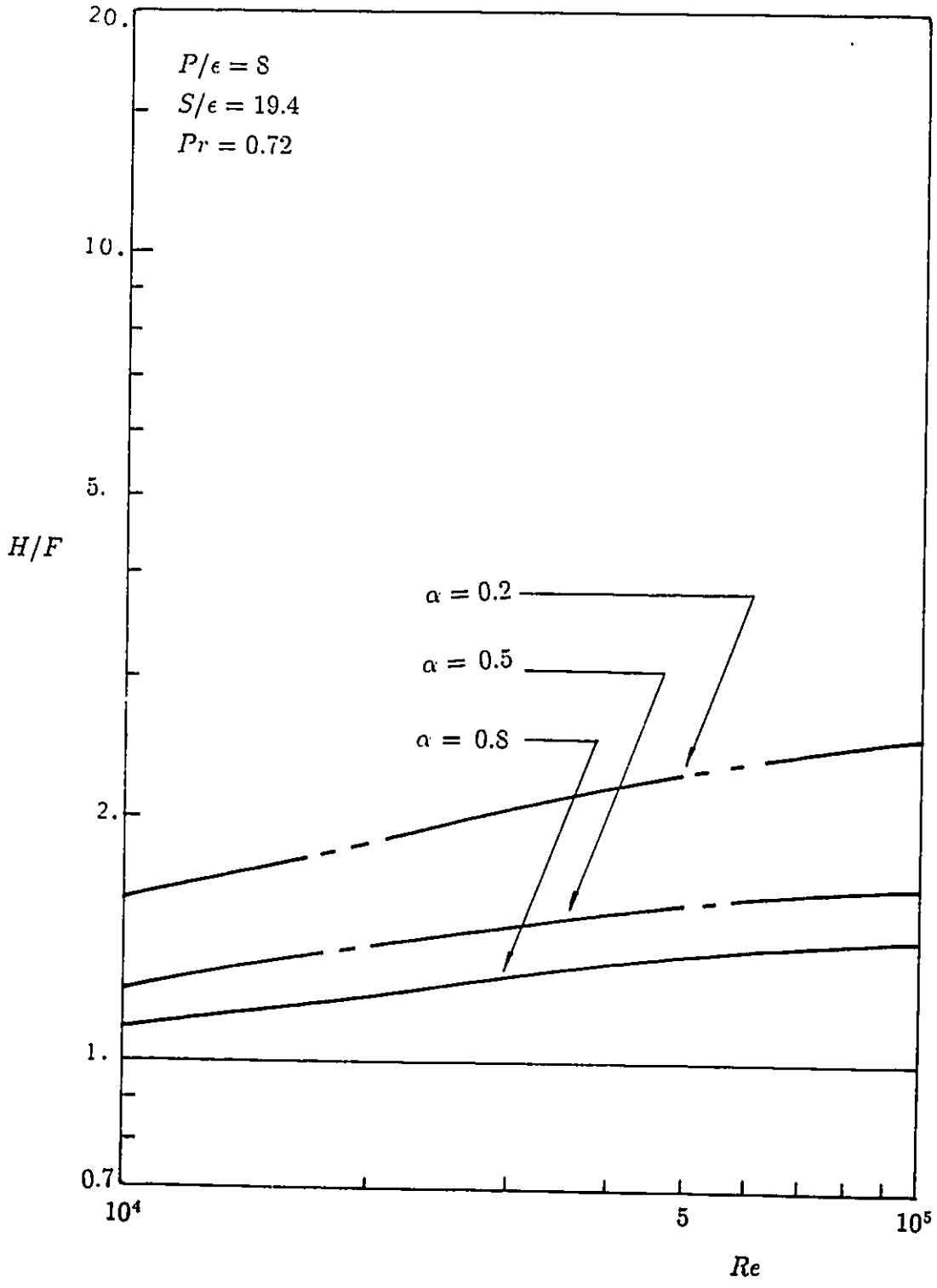

Fig. 5.19 H/F versus Reynolds number

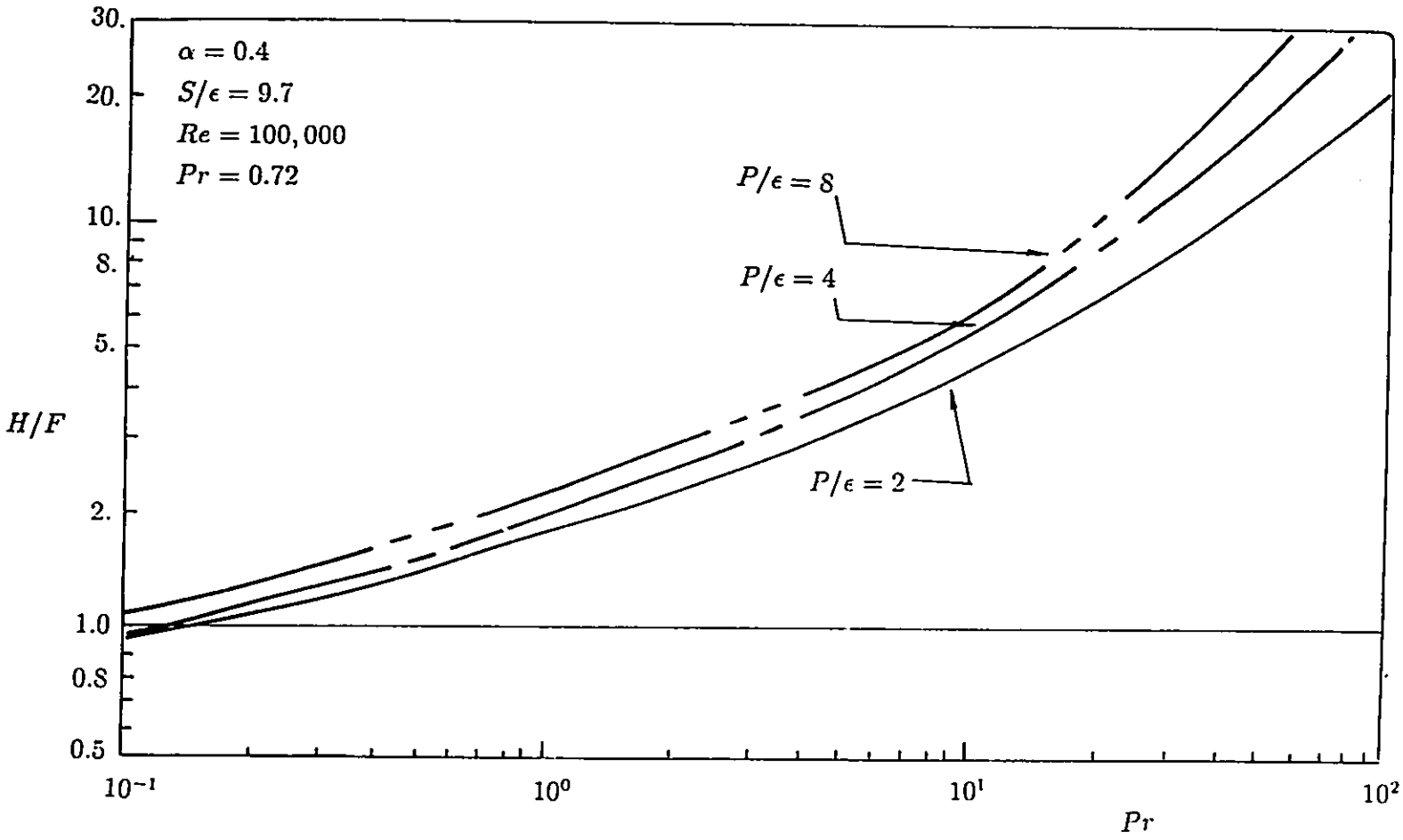

Fig. 5.20 H/F versus Prandtl number

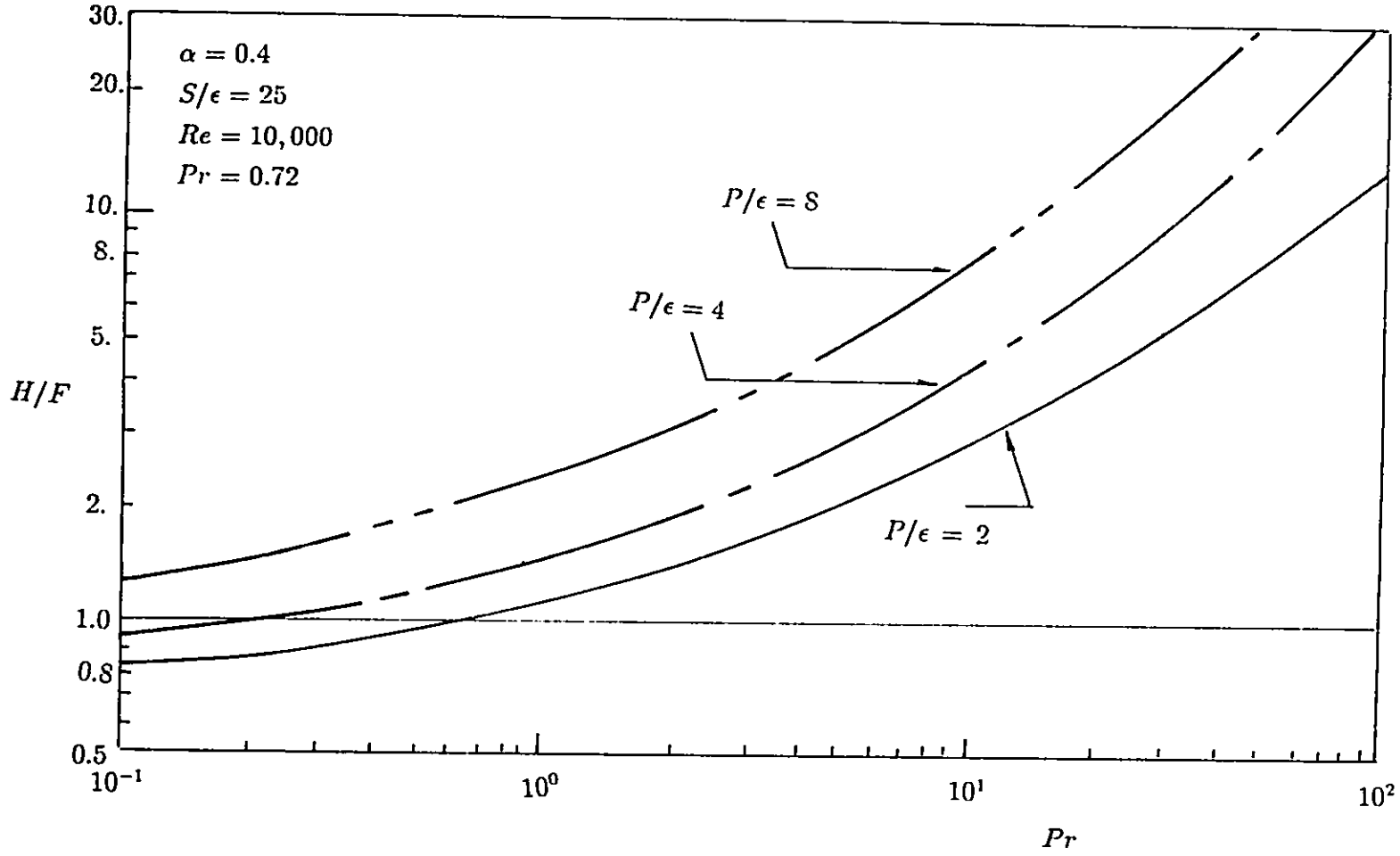

Fig. 5.21 H/F versus Prandtl number

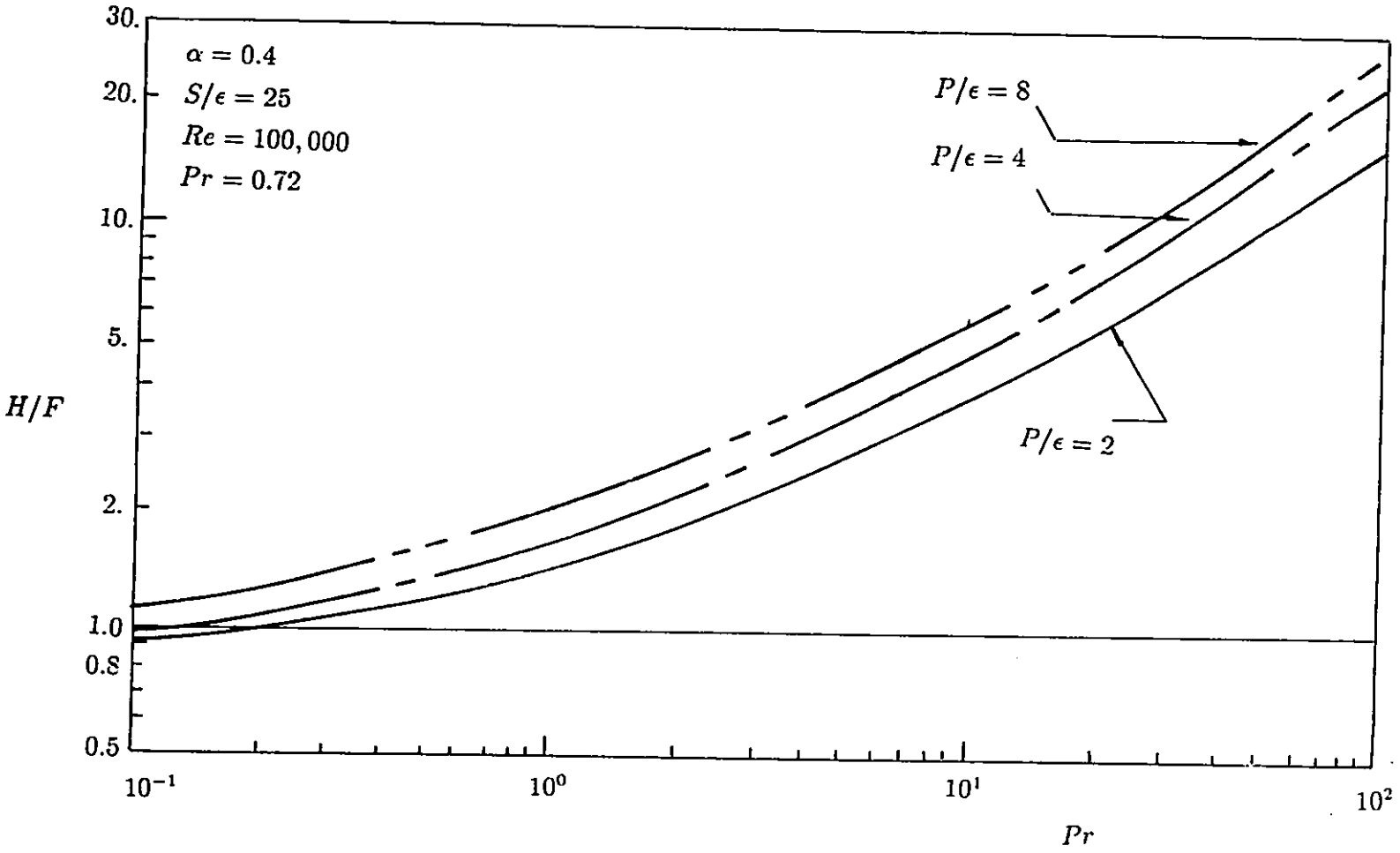

Fig. 5.22 H/F versus Prandtl number